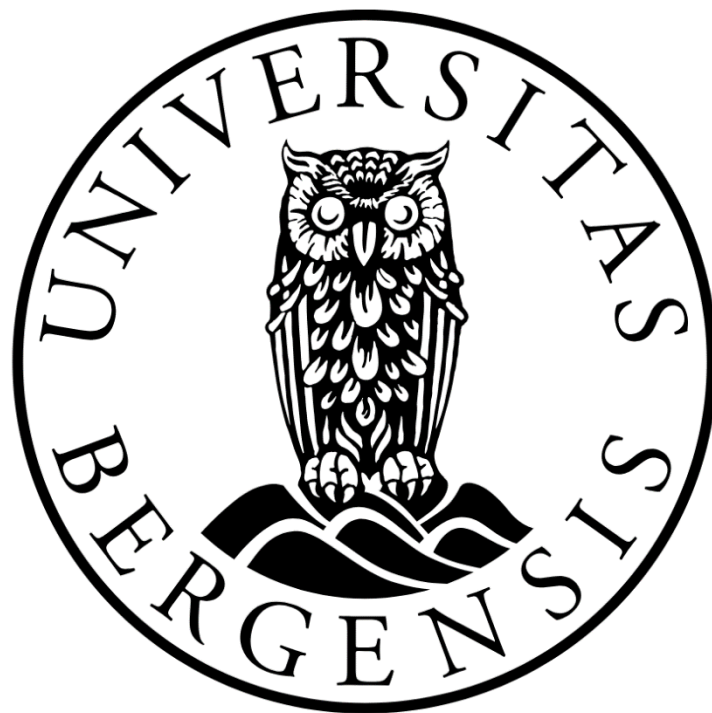


3D seismic investigation of tunnel valleys in  
the Sørliche Nordsjø II offshore wind site:  
morphology, cross-cutting relationships, and  
glacial history

Tonje Sælensminde

Master in Geoscience



Department of Earth Science

University of Bergen

June 2024



# Abstract

Sørlige Nordsjø II (SNII) is an offshore wind site situated in the Southern Norwegian North Sea and is part of the larger goal to decarbonise the energy industry. The shallow geology of the North Sea is highly heterogeneous, partly due to the complex networks of buried tunnel valleys that formed under the extensive glaciation of the middle to late Pleistocene epoch. The understanding of tunnel valleys has potential implications for North Sea glacial history and the determination of sub-seabed conditions for marine infrastructure such as offshore wind turbines and carbon capture and storage. The goal of this thesis is to divide the tunnel valleys at the SNII site into distinct generations based on, firstly, their geomorphological measurements for orientation, maximum incising depth, and the relief of the tunnel-valley thalweg, and secondly, their cross-cutting relationships. Based on the interpretation of 2000 km<sup>2</sup> of 3D seismic data, ~50% (45 tunnel valleys) of the SNII site is covered by detectable tunnel valleys, with widths ranging from 0.5 to 2.8 km, maximum depths of ~400 m, maximum lengths of 41 km, and orientations ranging from NE-SW to NW-SE. All mapped tunnel valleys had undulating thalwegs and slightly sinuous longitudinal shapes, with abrupt start and end slopes when present inside the study area. K-means clustering, a machine learning algorithm, was used to divide the mapped tunnel valleys into five groups based on similarities in morphology. Five levels of relative age were discovered by analysing cross-cutting relationships. The generational analysis concluded that seven events of tunnel valley formation have occurred at the SNII site, including one generation that is composed of a paleo valley with seabed relief. The oldest generation (G1) is of proposed Elsterian age (MIS 12), and the youngest generation (G7) is of probable MIS 2 age, corresponding to the Last Glacial Maximum. Three main types (and two subtypes) of infill were inferred from seismic facies: diamicton/gravels/till deposited subglacially, glaciolacustrine/glaciomarine deposited in a proglacial environment, and dipping ‘clinoform’ packages either deposited created ice-marginally by glaciofluvial backfilling (subtype one) or in a pro-glacial environment (subtype two). This was found to support a time-transgressive formation of tunnel valleys. Potential geohazards and implications for seabed conditions have been reviewed, with the main challenges for the safety and stability of seabed infrastructure being partially filled paleo valleys, buried lake sediments, the potential activity of salt tectonics, and tunnel valleys. Two main geohazards were found related to tunnel valleys: Unstable buried valley shoulders close to the seabed, and the tunnel valleys tendency to act as migration paths for hydrocarbons. The findings of this thesis can be implemented in future offshore wind sites where tunnel valleys make up the dominant facies of the shallow subsurface.

# Acknowledgements

This thesis is part of my master's degree in Quaternary geology and paleoclimate at the University of Bergen, Department of Earth Science, Faculty of Mathematics and Natural Science. In this chapter, I would like to express my gratitude to all who have contributed to this project.

A big thank you goes to all my supervisors for guiding my research and writing process during these two years. Jo Brendryen (University of Bergen) is thanked for introducing me to the project and providing valuable guidance from start to finish. Christian Haug Eide (University of Bergen) is thanked for his great support and creative ideas. Haflidi Haflidason (University of Bergen) is thanked for his dedication to thorough yet quick feedback. Hannah Petrie (Equinor) is thanked for supporting the start-up of this project and answering all my academic and work-related questions. Thank you to Schlumberger for academic access to Petrel used for seismic interpretation.

I would like to thank all who contributed with nice conversations and helpful tips in the 3D seismic interpretation lab. Special thanks to Karianne for motivating me to write at university instead of at home. Special thanks go to Thor Parmentier for great academic and (mostly) non-academic conversations, memes, and, of course, proofreading. I want to thank my whole family for laughs, dinners, and listening to me talking about my thesis. Lastly, the biggest thank you goes to Jonas, my biggest supporter.

# Table of contents

<b>Chapter 1 Introduction .....</b>	<b>1</b>
1.1 Motivation .....	1
1.2 Aims.....	4
<b>Chapter 2 Geological background .....</b>	<b>5</b>
2.1 Study area .....	5
2.2 Tectonic setting.....	5
<b>Chapter 3 Stratigraphical setting .....</b>	<b>8</b>
3.1 Permian: Zechstein Group salt .....	8
3.2 Paleogene: Hordaland Group.....	8
3.3 Neogene: Nordland Group.....	9
3.4 Quaternary glaciations .....	10
3.5 Quaternary tunnel valleys .....	16
<b>Chapter 4 Theoretical background.....</b>	<b>18</b>
4.1 Local and global occurrence of tunnel valleys .....	18
4.2 Tunnel valley formation.....	20
4.3 Tunnel valley morphology.....	21
4.4 Tunnel valley infill.....	24
4.5 Proglacial lakes and outwash fans .....	26
<b>Chapter 5 Data.....</b>	<b>27</b>
5.1 Seismic data .....	27
5.2 Well data .....	30
<b>Chapter 6 Methods.....</b>	<b>31</b>
6.1 Variance and RMS analysis .....	31
6.2 Seismic Interpretation.....	34
6.3 Workflow tunnel valley interpretation.....	35
6.4 Morphology analysis .....	37
6.5 Velocity model.....	38
6.6 K-means clustering .....	40
<b>Chapter 7 Results .....</b>	<b>41</b>
7.1 Surfaces: Seabed and base tunnel valleys.....	41
7.2 Tunnel valley morphology.....	43
7.3 Cross-cutting relationships .....	50

7.4 K-means clustering .....	51
7.5 Tunnel valley generations and icefronts .....	53
<b>Chapter 8 Discussion.....</b>	<b>66</b>
8.1 Tunnel valley mapping and morphology .....	66
8.2 Tunnel valley generations .....	73
8.3 Tunnel valley formation based on infill facies .....	80
8.4 Implications for North Sea glacial history, geohazards and seabed conditions for marine infrastructure.....	83
<b>Chapter 9 Summary and conclusions.....</b>	<b>90</b>
<b>Bibliography .....</b>	<b>92</b>
<b>Appendices .....</b>	<b>105</b>
Appendix 1: K-means Clustering .....	105

# List of Figures

<b>Figure 1.1:</b> Introduction figure.....	2
<b>Figure 2.1:</b> Tectonic evolution of the North Sea basin from the Early Devonian to the Paleocene modified from (Patruno et al., 2022).....	6
<b>Figure 3.1:</b> Synthetic stratigraphy for the North Sea Bason, focused on the Central North Sea modified from (Patruno et al., 2022).....	9
<b>Figure 3.2:</b> Maximum extents of the northern hemisphere glaciation modified from (Batchelor et al., 2019).....	11
<b>Figure 3.3:</b> Overview of marine isotope stages from the Pliocene to present day (Batchelor et al., 2019).....	11
<b>Figure 3.4:</b> Maximum extents of the northern hemisphere glaciation modified from (Batchelor et al., 2019).....	14
<b>Figure 3.5:</b> Seismic line a-a' (Fig. 1.1b).....	17
<b>Figure 4.1:</b> a. map of the North Sea with interpreted tunnel valleys and tunnel valley density where red is high density and blue low density.....	19
<b>Figure 4.2:</b> Schematic showing tunnel valley formation under a receding ice sheet. Modified from (Kristensen et al., 2008).....	20
<b>Figure 4.3:</b> Overview of tunnel valley morphology with measurements from previous works.....	23
<b>Figure 4.4:</b> Schematic of time-transgressive infill of a tunnel valley, modified from (Kristensen et al., 2008).....	25
<b>Figure 5.1:</b> a. Overview of 2D seismic data where black polygon is the SNII area boundary....	28
<b>Figure 5.2:</b> a. Overview of 3D seismic data where black polygon is the SNII area boundary....	29
<b>Figure 6.1:</b> Examples from attribute analysis a. variance surface at -284 ms showing outlines of a complex network of buried tunnel valleys.....	33
<b>Figure 6.2:</b> Summary of morphological measurement method.....	37

<b>Figure 6.3:</b> Velocity model including (from left to right) gamma-ray log, sonic log, layer cake with average velocities and seismic section with well 4/4-1 displayed, TWT in milliseconds and depth in metres correlated for the seabed and the foundation zone (100 m).....	39
<b>Figure 6.4:</b> Step by step how on how k-means clustering divides data into groups.....	40
<b>Figure 7.1:</b> Seabed time depth surfaces from the two seismic datasets MC3D-MDB 2013 and 2008.....	41
<b>Figure 7.2:</b> Overview of the Base Tunnel Valleys surface. a. Time depth surface for the base tunnel valleys.....	42
<b>Figure 7.3:</b> The 45 mapped tunnel valleys within the two seismic datasets MC3D-MDB 2013 and 2008.....	43
<b>Figure 7.4:</b> Summary TV2 time elevation surface and seismic geometries.....	46
<b>Figure 7.5:</b> Mapped tunnel valleys placed in a relative age hierarchy based on cross-cutting relationships where I are the relatively oldest valleys and V are the relatively youngest valleys.....	50
<b>Figure 7.6:</b> Result of the k-means clustering with polygons in respective colours represent the valleys in each cluster, and the means for each morphological measurement and the orientations of the valleys are summarised for each cluster.....	52
<b>Figure 7.7:</b> Comparison of the results of the clustering analysis and cross-cutting relationship analysis.....	54
<b>Figure 7.8:</b> Tunnel valley generations from oldest (G1) to youngest (G6) where the colours of the tunnel valleys correlate to the clustering results in Fig. 7.6.....	55
<b>Figure 7.9:</b> Tunnel valley generations with interpreted ice front placement during formation based on their orientations and occurrence within the SNII site.....	57
<b>Figure 7.10:</b> RMS amplitude time surfaces from MC3D_MDB 2013.....	61
<b>Figure 7.11:</b> RMS amplitude time surfaces from MC3D_MDB 2008 dataset.....	62
<b>Figure 7.12:</b> Seismic section showing examples of unmapped tunnel valleys (stippled white) over TV18 (Fig.7.3) along with the placement of the seabed multiple (red), Base tunnel valleys surface (black) and the seabed (light blue).....	63



<b>Figure 8.1:</b> Map showing the tunnel valleys interpreted by (Huuse & Lykke-Andersen, 2000) in red and (Salomonsen, 1995) in blue.....	67
<b>Figure 8.2:</b> Tunnel valleys mapped by (Hammer et al., 2016) in the Southern Norwegian North Sea.....	69
<b>Figure 8.3:</b> Correlation between mapped tunnel valleys in SNII from this thesis and that of (Kristensen et al., 2007).....	70
<b>Figure 8.4:</b> Mapped tunnel valleys displayed over risk map from Petrie et al. (2024), showing risk of installation challenges for wind turbine foundations.....	87

# List of Tables

<b>Table 5.1:</b> Overview of wells inside study area.....	30
<b>Table 6.1:</b> Overview of all interpreted horizons and their seismic characteristics in interpretation order.....	35
<b>Table 7.1:</b> Morphology measurements from all mapped tunnel valleys summarised with maximum, minimum and mean values for each measurement.....	44
<b>Table 7.2:</b> Overview of all morphological measurements for each mapped tunnel valley.....	48
<b>Table 7.4:</b> Table summarising infill types identified in 3D seismic data in seismic sections along the thalweg of tunnel valleys.....	65
<b>Table 8.1:</b> Summary of a selection of previous studies on tunnel valley generations in the North Sea.....	79

# Chapter 1 Introduction

## 1.1 Motivation

Electricity and fuel are resources we depend on, both of which can be acquired from either wind or the subsurface of the North Sea (Fig. 1.1a). Rising global temperatures have inspired an effort to decarbonise the energy industry by, for example, investing in offshore wind power or carbon capture and storage (CCS) (DNV, 2023). Large ice sheets have eroded and deposited complex networks of landforms, resulting in highly heterogeneous sediments composing the shallow subsurface of the North Sea Plateau (e.g. Ehlers & Wingfield, 1991; Huuse & Lykke-Andersen, 2000; Kristensen et al., 2007; Praeg, 1996; Stewart et al., 2013). Over-consolidated sediments (e.g. Cotterill et al., 2017 a; Emery et al., 2019; Martin et al., 2017) and hydrocarbons trapped in buried glacial landforms are common (e.g. Kirkham et al., 2024; Roy et al., 2023; Van Der Vegt et al., 2012), but knowledge of the landforms' distribution, exact locations, and infill remains largely unknown for many areas of the North Sea (e.g. Ottesen et al., 2020; Stewart et al., 2013). An absence of a comprehensive understanding of buried glacial landforms and their connection to glacial history is a challenge when determining seabed conditions for marine infrastructure. This is due to the buried landforms and adjacent sediments holding potential geohazards for installations such as bottom-fixed wind turbine foundations (e.g. Cotterill et al., 2017 b; Cotterill et al., 2017 a; Petrie et al., 2024).

Tunnel valleys, which are the focus of this thesis, are glacial landforms created underneath a receding ice sheet by over-pressured meltwater, which is accountable for the landform's long valley-like shape and undulating thalweg (the deepest part of the valley) (Ehlers & Linke, 1989; Huuse & Lykke-Andersen, 2000; Lonergan et al., 2006; Praeg, 2003). With widths of 0.5 to 5 km and lengths up to over 100 km, the tunnel valleys cover most of the North Sea Plateau in a complex cross-cutting pattern (e.g. Kirkham et al., 2024; Ottesen et al., 2020; Van Der Vegt et al., 2012). Their infill is diverse, ranging from coarse-grained clinoform structures to finer-grained near-horizontal layering, and is most often examined using seismic data, preferably 3D (e.g. Huuse & Lykke-Andersen, 2000; Praeg, 2003; Van Der Vegt et al., 2012). Tunnel valleys can be hazardous for a variety of reasons, both their heterogeneous infill and their tendency to accumulate hydrocarbons that migrate along faults and salt structures from deeper

buried stratigraphy (e.g. Lohrberg et al., 2020; Ottesen et al., 2020). It is important to monitor hydrocarbon migration to the seabed over carbon capture and storage (CCS) efforts to check for potential leakage from the storage site. Tunnel valley networks should be considered when choosing a storage site and investigating leaks in the North Sea (e.g. Callow et al., 2021; Frahm et al., 2020; Karstens & Berndt, 2015). In recent years, production of hydrocarbons in Quaternary sediments has also received increased attention, with an example being the Peon field located west of western Norway further strengthening the relevance of the shallow subsurface (Equinor, 2009).

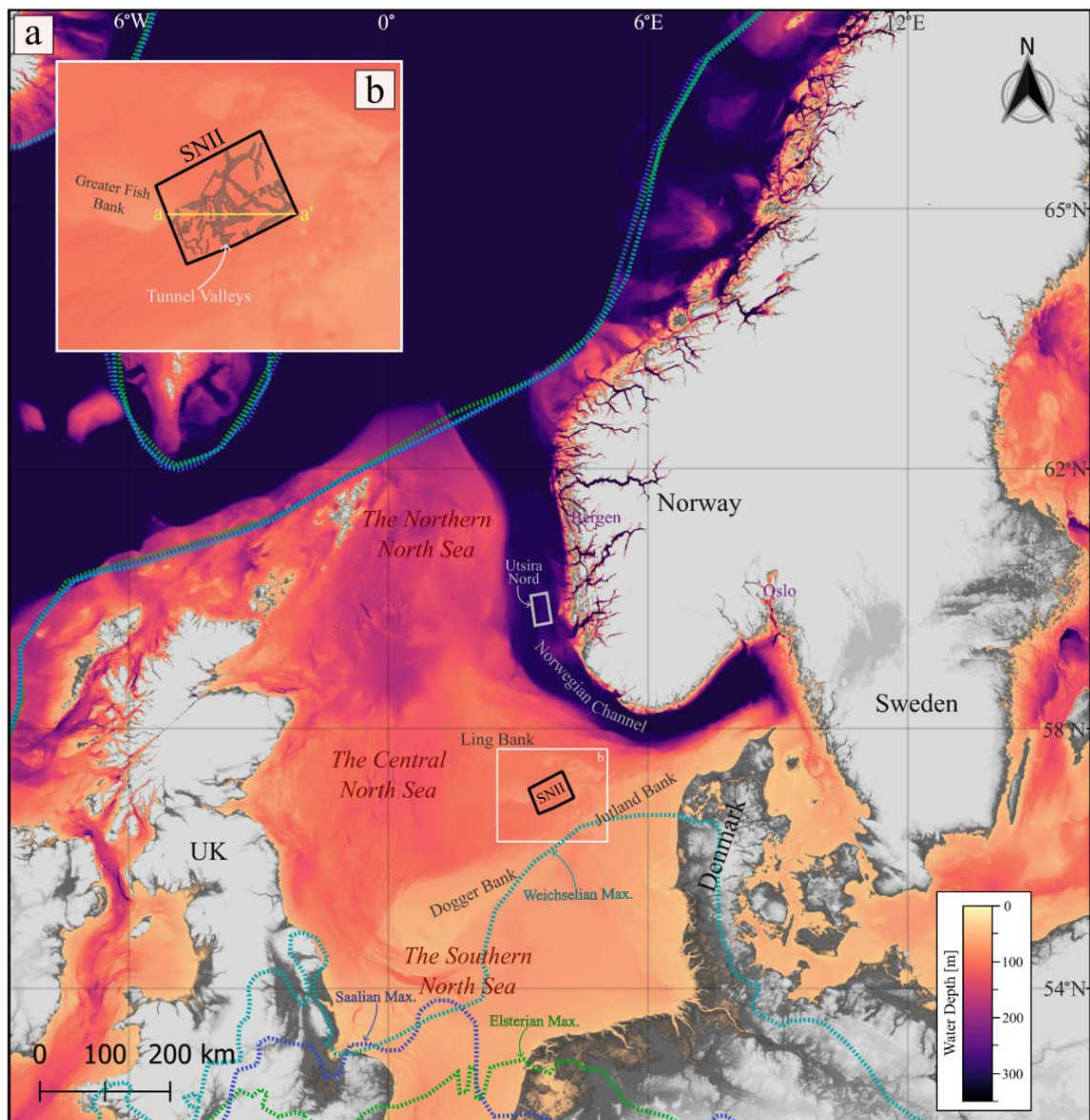


**Figure 1.1:** Introduction figure **a.** Bathymetric hill-shaded map of the North Sea and surrounding landmasses (GEBCO 2023) and the two offshore wind sites Sørlige Nordsjø II and Utsira Nord. The maximum extents of the middle to late Pleistocene ice sheets; Elsterian (MIS 12), Saalian (MIS 10-6) and the Weichselian (MIS 5d-2) (Batchelor et al., 2019). **b.** Bathymetric map of the SNII site including the mapped tunnel valleys from this thesis (grey polygons).

Three well known glaciations advanced into the North Sea during the Middle to Late Pleistocene: the Elsterian, the Saalian, and the Weichselian (Fig. 1.1a; Cameron et al., 1987; Praeg, 2003; Shackleton, 1969; Wingfield, 1989). Tunnel alleys are formed perpendicular to the ice sheet's front; thus, their orientations are indicative of the movements of the paleo ice sheets (e.g. Cameron et al., 1987; Ehlers & Wingfield, 1991; Praeg, 2003; Wingfield, 1989). However, the three-stage model has become outdated as a result of studies on tunnel valley generations that reveal more than three glacial advances into the North Sea (e.g. Kirkham et al., 2024; Kristensen et al., 2007; Ottesen et al., 2020; Stewart et al., 2013; Stewart & Lonergan, 2011). The method by which tunnel valleys are divided into generations often includes both the analysis of tunnel valley morphology and cross-cutting relationships to interpret relative ages (Stewart, 2009). A consensus on tunnel valley formation and the glacial history of the Southern Norwegian North Sea has not yet been reached, though an agreement has been made about the glacial landforms being a product of several erosional and depositional processes (e.g. Kehew et al., 2012; Kristensen et al., 2008).

In 2020, two sites in the Norwegian North Sea were proposed for offshore wind farm development by the Norwegian government: Sørlige Nordsjø II (SNII) and Utsira Nord (Fig. 1.1a; Norwegian Government, 2022). Currently, a detailed mapping of tunnel valleys and their geomorphology in the SNII area is absent. The study site's specific placement in relation to the maximum extent of the Last Glacial Maximum (LGM) and the coalescence of the British-Irish and Fennoscandian ice sheets makes it particularly well-suited for research on the Middle to Late Pleistocene ice sheets (e.g. Hjelstuen et al., 2018; Sejrup et al., 2016). The tunnel valleys in and around the SNII area incise into Neogene and Quaternary sediments to time depths of ~500 ms and have a general orientation of N-S (Fig. 1.1b; Kristensen et al., 2007). Fault systems and salt diapirs are present in the underlying stratigraphy of the study site and enable hydrocarbons to migrate to the seabed and occasionally into tunnel-valley infill (e.g. Petrie et al., 2024). 3D seismic data originating from the oil and gas industry covers most of the SNII area and has a resolution that captures the large geometries of tunnel valleys. From the 3D seismic data, time-depth surfaces, in addition to variance and RMS attributes, will be generated to investigate the morphology and infill of the tunnel valleys in the SNII area, as well as illuminate other potential geohazards. These results will, in conjunction with the tunnel valley's cross-cutting relationships, aid in the interpretation of tunnel valley generations and, further, the nature of the paleo ice sheets within the SNII area. Comparing results with previous work

on tunnel valley morphology, generations, and geohazards will aid in the implementation of the results at future sites for seabed instalments and subsurface operations on the North Sea Plateau.

## 1.2 Aims

The primary aim of this thesis is to map the tunnel valleys at the SNII site, assign them to distinct generations using tunnel-valley geomorphology analysis, and place the identified generations in the context of North Sea glacial history from the middle to late Pleistocene epoch.

The objectives set to achieve the aim stated above are as follows:

1. Perform a detailed interpretation of tunnel valleys and their geometries in 3D seismic data and generate time depth surfaces.
2. Group tunnel valleys based on their general orientation, maximum depth of thalweg in two-way time (ms), and relief of thalweg in two-way time (ms) and combine results with cross-cutting relationships to propose tunnel valley generations.
3. Investigate what the examined geometries imply for glacial and environmental conditions when they were formed.
4. Investigate possible implications for North Sea glacial history, geohazards, and seabed conditions for marine infrastructure.
5. Compare the results of this thesis to previous studies on tunnel valleys in the surrounding areas.

# Chapter 2 Geological background

## 2.1 Study area

The area studied in this thesis is the SNII offshore wind site in the southern Norwegian North Sea (Fig. 1.1a). It is located on the shallow North Sea Plateau, more specifically on the Ling Bank, and has water depths of c. 50-70 meters. The area lies 140 km SW off Norway, is 40 km wide and 60 km long (Fig. 1.1b). Bordering directly to the south is the Danish sector of the North Sea.

## 2.2 Tectonic setting

The North Sea Basin has since the Devonian period been shaped by lithospheric movement, resulting in several episodes of rifting and ensuing subsidence and uplift (e.g. Faleide et al., 2015; Patruno et al., 2022; Underhill & Richardson, 2022), centred around the axis of what is now the present-day shallow epicontinental North Sea (Fig. 2.1; e.g. Anell et al., 2012; Faleide et al., 2002; Ziegler, 1975). After the Caledonian orogeny's rise and successive collapse, the intracratonic North Sea basin was formed, in which the first of two rifting phases took place during the Permian to earliest Triassic (Fig. 2.1; e.g. Faleide et al., 2002, 2015; Underhill & Richardson, 2022). The second rifting phase started in the late Middle Jurassic, and movement slowed during the earliest Cretaceous time when both the Central and Viking grabens were completed (Fig. 2.1; Anell et al., 2012; Faleide et al., 2002; Ziegler, 1975).

Of the two subsequent post-rift stages, the latter had the largest impact on the North Sea Basin's paleogeographic setting, as the tectonic subsidence is proven to have been the most prominent after the Jurassic (Fig. 2.1; e.g. Faleide et al., 2002, 2015; Ziegler, 1975). Regional subsidence during the Cenozoic was focused on the axis of the grabens, and as a result, large amounts of sediment accumulated in the central part of the basin (e.g. Anell et al., 2012; Faleide et al., 2002, 2015; Ziegler, 1975). The Cenozoic deposits have a maximum thickness of c. 3000 metres, including the Quaternary succession (e.g. Doré, 1992; Dowdeswell & Ottesen, 2013; Huuse et al., 2001; Lamb et al., 2018). Accommodation-dominated deposition is suggested to have been the main infill process of the basin, however, other types of deposition are present, including large submarine fans and slope/delta systems (e.g. Anell et al., 2012; Lamb et al., 2018).

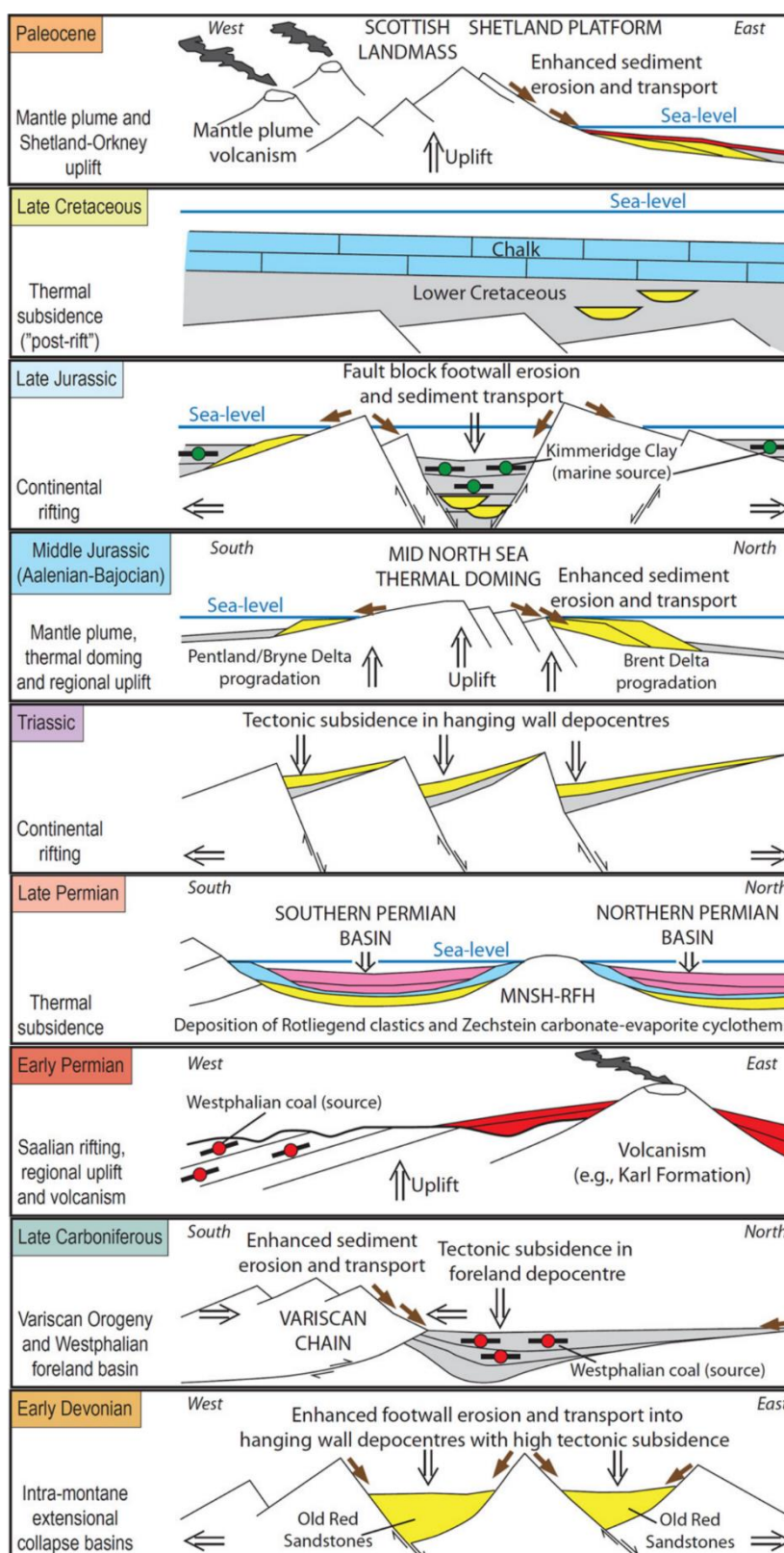


**Figure 2.1:** Tectonic evolution of the North Sea basin from the Early Devonian to the Paleocene modified from (Patruno et al., 2022). Mid North Sea High (MNSH), Ringkøbing-Flyn High (RFH), sandstones (yellow), mudrocks (grey), carbonates (light blue), evaporites (pink), volcanic rocks (brown), source rock (green circle black line).



Sediment loading generated by several kilometres of Cenozoic deposition caused underlying Permian and Mesozoic sediments to react, although differentially depending on lithology. Evaporites deposited during the Permian of the Zechstein Group (Fig. 2.1; Ziegler, 1975) reacted by flowing into diapir and pillow structures piercing both Mesozoic and, in some places, Cenozoic stratigraphy (e.g. Jackson & Stewart, 2017). Underlying marine rocks deposited during the Jurassic with a high concentration of organic material were sufficiently buried to produce hydrocarbons (Fig. 2.1; e.g. Kubala et al., 2003), which started to migrate towards the seabed along faults and salt tectonic structures (e.g. Underhill & Richardson, 2022; Ziegler, 1975).

During the Cenozoic, two major events of uplift occurred, one in the early Paleogene and another in the Late Neogene (Fig. 2.1; e.g. Faleide et al., 2002, 2015; Patruno et al., 2022). The second of two major uplift events occurred shortly before the Quaternary period and was caused by widespread glacial erosion that removed large masses of sediment from the basin, resulting in an isostatic response (e.g. Anell et al., 2012; Faleide et al., 2002, 2015). Following the Late Neogene uplift, c. 1000 metres of sediment were deposited, containing essential information about the Quaternary ice sheets (e.g. Dowdeswell & Ottesen, 2013; Lamb et al., 2018).

## Chapter 3 Stratigraphical setting

### 3.1 Permian: Zechstein Group salt

The Zechstein Group was deposited in a marine environment during the Late Permian and is mainly composed of evaporites and carbonates, although some local occurrences of clastic rocks appear (Fig. 3.1; e.g. Patruno et al., 2022; Underhill & Richardson, 2022; Ziegler, 1990). Along the centre of the North Sea basin, halites are present within the Zechstein Group, and along the basin margin, anhydrites and dolomites can be found (Bjørlykke, 2015; Deegan & Scull, 1977). The Zechstein Group is overlain by Triassic rocks and underlain by the Rotliegend Group and in some places basement (Fig. 3.1; Underhill & Richardson, 2022). The rocks present above the Zechstein Group will vary dependent on the level of salt-tectonic activity, as some salt structures penetrate close to the seabed. These structures make the Zechstein Group Salt relevant for the study interval in this thesis.

### 3.2 Paleogene: Hordaland Group

The Hordaland Group was deposited during the Eocene and Oligocene and is mainly composed of fine-grained mudstones with interbedded sandstones (Fig. 3.1; Deegan & Scull, 1977; Patruno et al., 2022). The mudstones have a high porosity, low permeability, small grain size, and exhibit ductile behaviour due to being rich with smectite (Løseth et al., 2003). This results in a mudstone with high water contents. Its low permeability inhibits pore-fluid drainage during burial, meaning that they are effective seals (Løseth et al., 2003). The Hordaland Group mudstones are largely under-compacted for this reason and have a high chance of being remobilized (Løseth et al., 2003). Underlying the group, with no breaks in the stratigraphy, are turbiditic sands and clays deposited during the Palaeocene (Fig.3.1). Above lies the Nordland Group, separated from the Hordaland Group by an unconformity along which velocity and density inversions are common because of the latter group's high water content (Fig. 3.1; Deegan & Scull, 1977; Løseth et al., 2003).

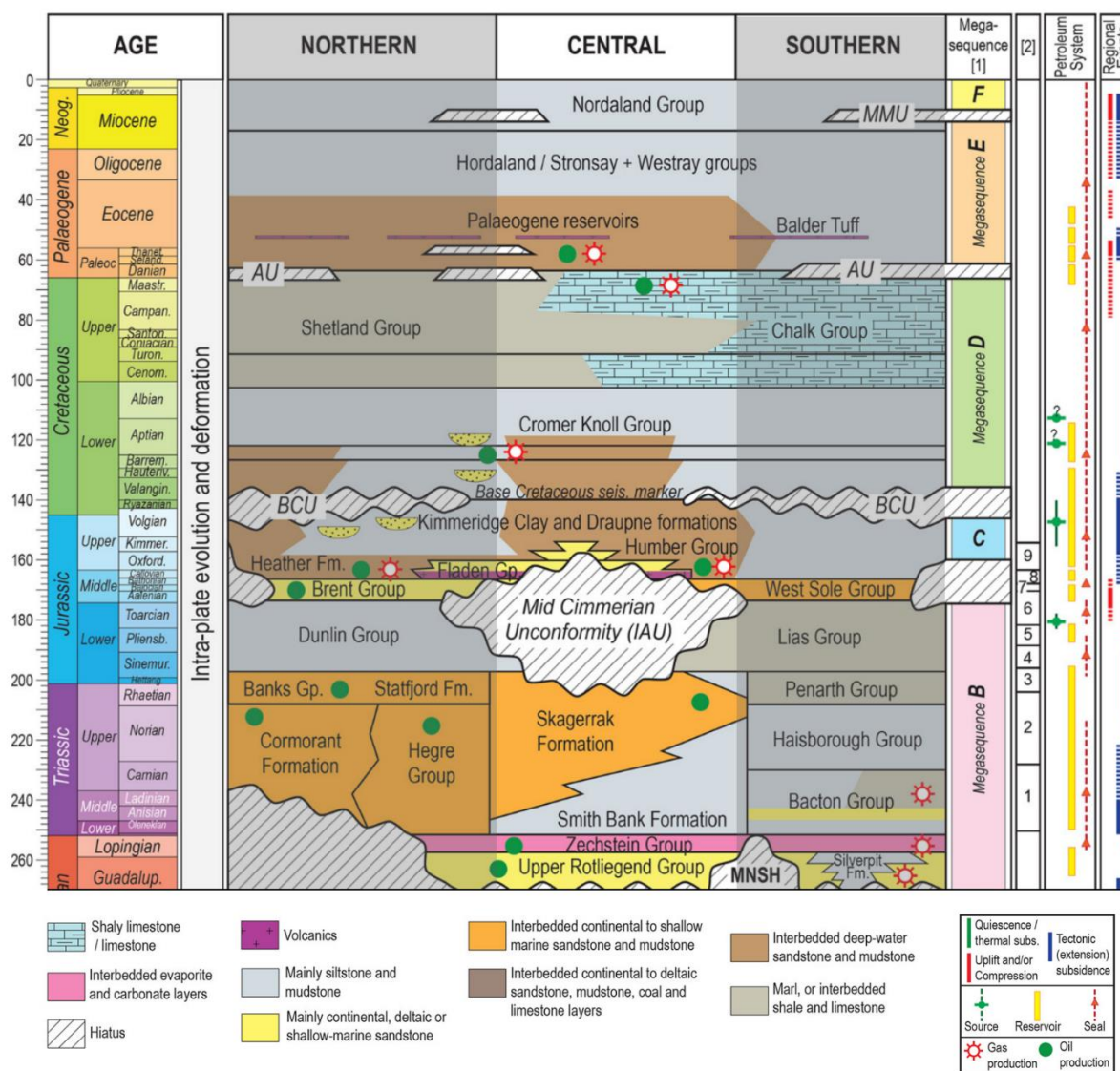


**Figure 3.1:** Synthetic stratigraphy for the North Sea Basin, focused on the Central North Sea modified from (Patruno et al., 2022). Base Cretaceous Unconformity (BCU), Atlantean Unconformity (AU), Mid Miocene Unconformity (MMU).

### 3.3 Neogene: Nordland Group

The Nordland Group is mainly composed of marine claystones that are soft and sometimes micaceous and/or silty, deposited during the Middle Miocene and Lower Pliocene (Fig. 3.1; Deegan & Scull, 1977; Patruno et al., 2022; Worsley et al., 1988). During the Lower Miocene there was a hiatus, thus the base of the Nordland group corresponds to the Oligocene/Miocene unconformity (Fig. 3.1; Patruno et al., 2022; Worsley et al., 1988). The Nordland Group includes the Utsira formation in the North Sea, but the group extends north to the western part of the Barents Sea without the Utsira Formation (Deegan & Scull, 1977). On the mid-Norwegian continental shelf the Nordland Group corresponds to the Naust formation (e.g. Ottesen et al., 2009). The upper part of the Nordland Group consists of unconsolidated sediment

with an upwards increase in glacial influence with open marine and glacial deposits at the top where the group ends at the seabed (e.g. Eidvin et al., 2000).

### 3.4 Quaternary glaciations

The Quaternary period started c. 2.6 million years ago and marked a significant change in the paleoenvironment of the Northern Hemisphere (e.g. Cameron et al., 1987; Ehlers, 1990; Ottesen et al., 2014; Rea et al., 2018; Sejrup et al., 1996, 2005). In the Northern North Sea, ice-rafted debris from icebergs found in sediment cores are dated to the start of the Quaternary period (e.g. Eidvin & Rundberg, 2001; Ottesen et al., 2009). However, the earliest documentation for grounded ice in the North Sea is dated to c. 2.00 Ma and presents as iceberg plough-marks on buried surfaces found in seismic data (e.g. Dowdeswell & Ottesen, 2013; Rea et al., 2018).

#### Early Pleistocene

During the earliest Quaternary, the Fennoscandian Ice Sheet is said to have advanced into the northern North Sea (Fig. 3.2A), all the way to the paleo-shelf break, and later into the central North Sea, but the infill of the North Sea Basin was what later made the confluence of the Fennoscandian and British-Irish ice sheet possible (Ehlers, 1990; Sejrup et al., 1995). This occurred around the same time as what is thought to be the initiation of the Norwegian Channel Ice Stream at c. 1.1 Ma (Batchelor et al., 2017; Ottesen et al., 2014; Sejrup et al., 1995), though the exact chronology is disputed, with some suggesting it occurred as late as c. 350 ka (Løseth et al., 2022). In either case, the Norwegian Channel Ice Stream eroded early Quaternary sediments from the North Sea Basin and deposited them in the North Sea trough-mouth fan to the north (e.g. Hjelstuen et al., 2012; Ottesen et al., 2016). As a result, much of the continental shelf has an Upper Regional Unconformity (e.g. Løseth et al., 2022; Nygård et al., 2005). The middle Pleistocene transition occurred from 1.25 Ma to 700 ka (Fig. 3.2B, C), changing the climate system fundamentally when the dominant cycle switched from a low-amplitude 41-ka cycle to a high-amplitude 100-ka cycle, causing an increase in intensity of North Sea glacial influence (e.g. Clark et al., 2006). As a result, the most extensive ice sheets are associated with the last c. 900 ka (e.g. Ehlers et al., 2018), specifically the British-Irish ice sheet and Fennoscandian Ice Sheet over the North Sea Basin (Ehlers, 1990; Lee et al., 2012; Løseth et al., 2022; Nygård et al., 2005; Sejrup et al., 1994, 1995). The 100-ka cycle includes colder (glacial) and warmer (interglacial) periods, and dating glaciogenic sediments makes it possible to assign glaciations to stages in the pattern of cooling and warming, called Marine Isotope Stages (Fig. 3.3; e.g. Ehlers & Gibbard, 2004).

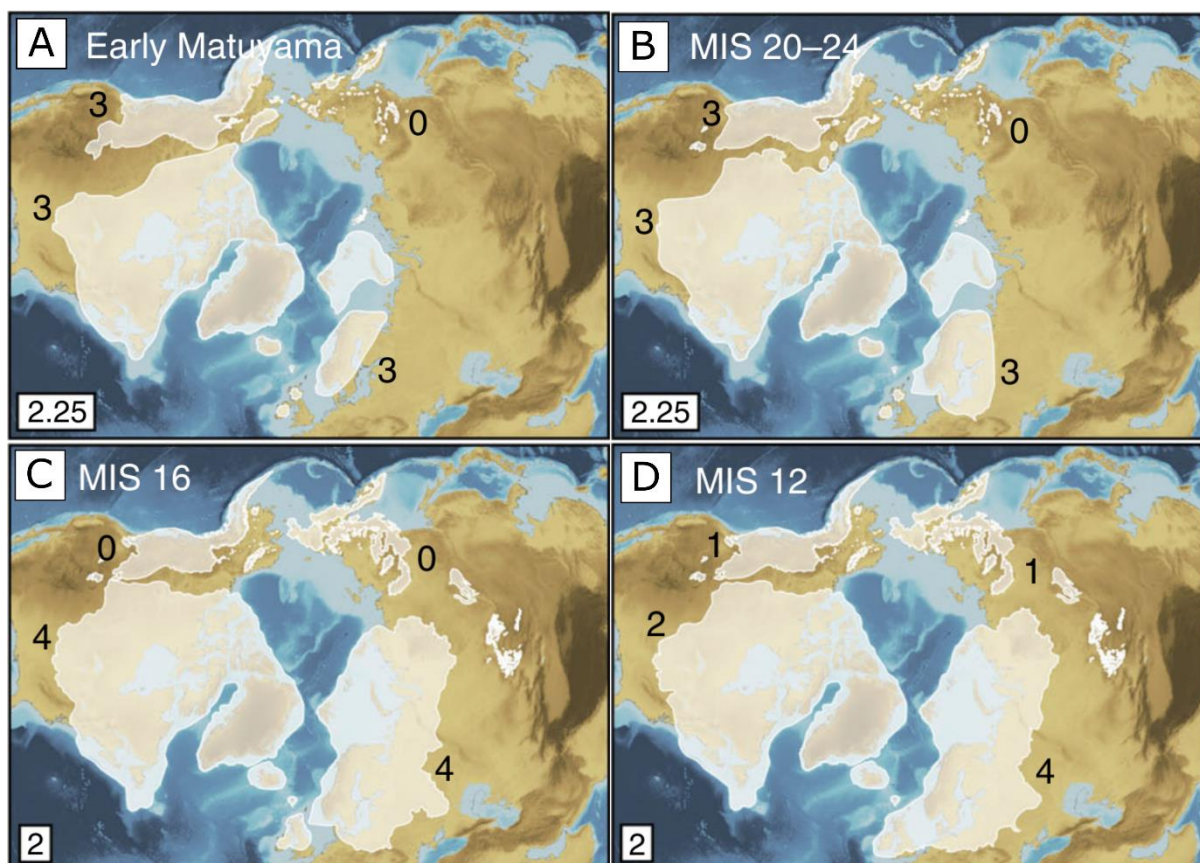


**Figure 3.2:** Maximum extents of the northern hemisphere glaciation modified from (Batchelor et al., 2019). A. Early Matuyama, B. MIS 20–24, C. MIS 16, D. MIS 12. Numbers in bottom left corners and on the maps are robustness scores.

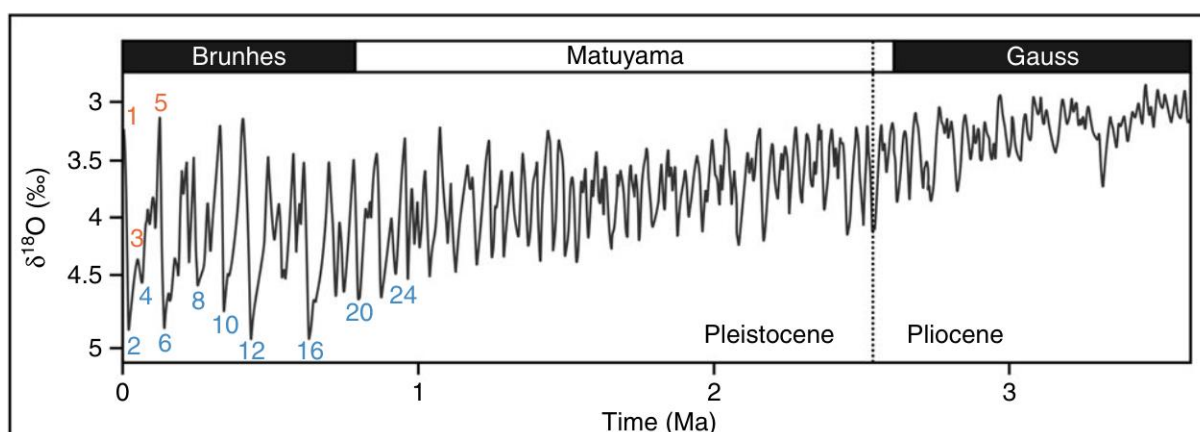


**Figure 3.3:** Overview of marine isotope stages from the Pliocene to present day (Batchelor et al., 2019).

### Middle- to Late Pleistocene

The glaciations of the North Sea are commonly divided into three: the Elsterian, Saalian, and Weichselian, dated to MIS 12 (480–410 ka), MIS 10–6 (370–135 ka), and MIS 5d–2 (115–12 ka), respectively (Fig. 3.3; Cameron et al., 1987; Praeg, 2003; Shackleton, 1969; Wingfield,

1989). During these glaciations, the Fennoscandian and British-Irish ice sheets coalesced, and the first two glaciations extended as far as the present-day coast of NW Europe (Fig. 1.1; e.g. Ehlers, 1990; Nygård et al., 2005; Sejrup et al., 1994, 1995). The last of the three major glaciations was less extensive and is thought to have reached just south of the SNII area during the Last Glacial Maximum in MIS 2 (Fig. 1.1; Ehlers, 1990; Ehlers & Wingfield, 1991; Hjelstuen et al., 2018; Sejrup et al., 2016). However, recent studies on buried glacial landforms in the North Sea Basin suggest that the notion of three major glaciations may be overly simplified (Ottesen et al., 2020; Stewart et al., 2013; Stewart & Lonergan, 2011).

### The Elsterian

The Elsterian (MIS 12) marks the largest glacial advance in northwestern Europe during the Pleistocene epoch, and the beginning of the cyclic shelf-edge glaciations that followed (Fig. 3.2D; e.g. Sejrup et al., 2005; Stoker et al., 1993, 1994, 2011). During the Elsterian, the sedimentation patterns in the North Sea changed drastically and is clearly visible in the stratigraphy as a change from non-glacial to glacial sediment (e.g. Cameron et al., 1987; Graham et al., 2011). In the south, the coalesced ice-sheet border reached as far as  $\sim 53^{\circ}\text{N}$  based on tunnel valleys with a north-south direction and similar geomorphologies (e.g. Graham et al., 2011; Praeg, 1996). Deformation and till structures that are buried also aid in discerning the Pleistocene ice-sheet borders both onshore and offshore (e.g. Graham et al., 2011; Praeg, 2003). Another reliable indicator of southerly ice-sheet extent is the redirection of European paleo-rivers towards the south (e.g. Toucanne et al., 2009). The northern maximum extent of the Elsterian ice-sheet reached the shelf-break, evidenced by large sedimentary fans containing glacial sediment situated on the Atlantic continental margin (e.g. Rise, 2004; Sejrup et al., 2005; Stoker et al., 1994).

In the central and southern North Sea there is a network of tunnel valleys with varying morphology, where similar tunnel valleys have been assumed to be of the same generation. The oldest of the generations in this area could be related to the Elsterian glacial stage and, as mentioned above, possibly correlates to the southern margin of the most extensive ice-sheet of this glacial stage (Huuse & Lykke-Andersen, 2000). There have been no direct dating of presumed Elsterian tunnel valleys (Graham et al., 2011), however, they have been cross-correlated to NW European and UK features and stratigraphy (e.g. Kluiving et al., 2003; Lutz et al., 2009). A distinct unconformity is visible in seismic data along with the Elsterian tunnel valleys (e.g. Cameron et al., 1987; Huuse & Lykke-Andersen, 2000; Stoker et al., 2011). In the southern North Sea this unconformity incises deltaic units, and farther north, it incises the

deltaic sediments' lateral equivalents (Cameron et al., 1987, 1992; Gatliff et al., 1994; Johnson et al., 1993; Scourse et al., 1998; Stoker et al., 2011; Stoker & Bent, 1985). As the tunnel valleys accompanying the unconformity are of proposed Elsterian age, the unconformity is assumed to be from the same glacial stage (e.g. Graham et al., 2011). Both Lonergan et al. (2006) and Stewart & Lonergan (2011) mapped a large number of tunnel valleys across the North Sea and found that there has likely been more than one glacial advance during the Elsterian stage. This was due to finding several distinguishable and cross-cutting tunnel valley generations, more than one per glacial stage, meaning the Elsterian could be more complex than previously thought. This is also supported by the findings of Lutz et al. (2009), where three of the interpreted tunnel valleys are of proposed Elsterian age.

### The Saalian

The Saalian glacial stage (Fig. 3.3; MIS 10-6) has left clues that indicate at least three phases of glacial activity starting in MIS 10 (Fig. 3.4A; e.g. Ehlers, 1990; Ehlers & Gibbard, 2004; Ottesen et al., 2020). In the southern North Sea, a till was dated to MIS 8, indicating ice coverage during this time (Rappol et al., 1989). From the same borehole, a shallow marine sand laying above the till was dated to MIS 7, thought to represent a warm period after the MIS 8 colder period (e.g. Beets et al., 2005). The extent of the MIS 8 Saalian glacial phase is not known for certain, but it is thought to be a result of the British-Irish Ice-sheet extending into the North Sea and southwards (Fig. 3.4B; e.g. Graham et al., 2011). On the other hand, the last glacial phase of the Saalian, MIS 6, has left behind a glacial erosion surface that show a minimum southward ice-sheet extent of  $\sim 56^{\circ}\text{N}$  and northward extent to the shelf edge (Fig. 3.4C; e.g. Carr, 2004; Holmes, 1997). In the southern North Sea, tills (Carr, 2004) and tunnel valleys of presumed late Saalian age (e.g. Kluiving et al., 2003; Kristensen et al., 2007) increase the minimum extent of the MIS 6 ice-sheet to  $\sim 54^{\circ}\text{N}$ , making it clear that the last phase was the most extensive (e.g. Graham et al., 2011).

Like the Elsterian tunnel valleys, the Saalian tunnel valleys have not been directly dated but rather divided into generations and correlated to different marine isotope stages (MIS) (e.g. Cameron et al., 1987; Graham et al., 2011; Huuse & Lykke-Andersen, 2000; Wingfield, 1989). Stewart & Lonergan (2011) mapped tunnel valley generations in the central North Sea correlated to the Elsterian, but also linked several generations to the three glacial stages of the Saalian (MIS 10, 8, and 6). The complex network of cross-cutting tunnel valley generations in the North Sea supports that the three-stage model for the middle to late Pleistocene glaciations is too simplistic (e.g. Graham et al., 2011).

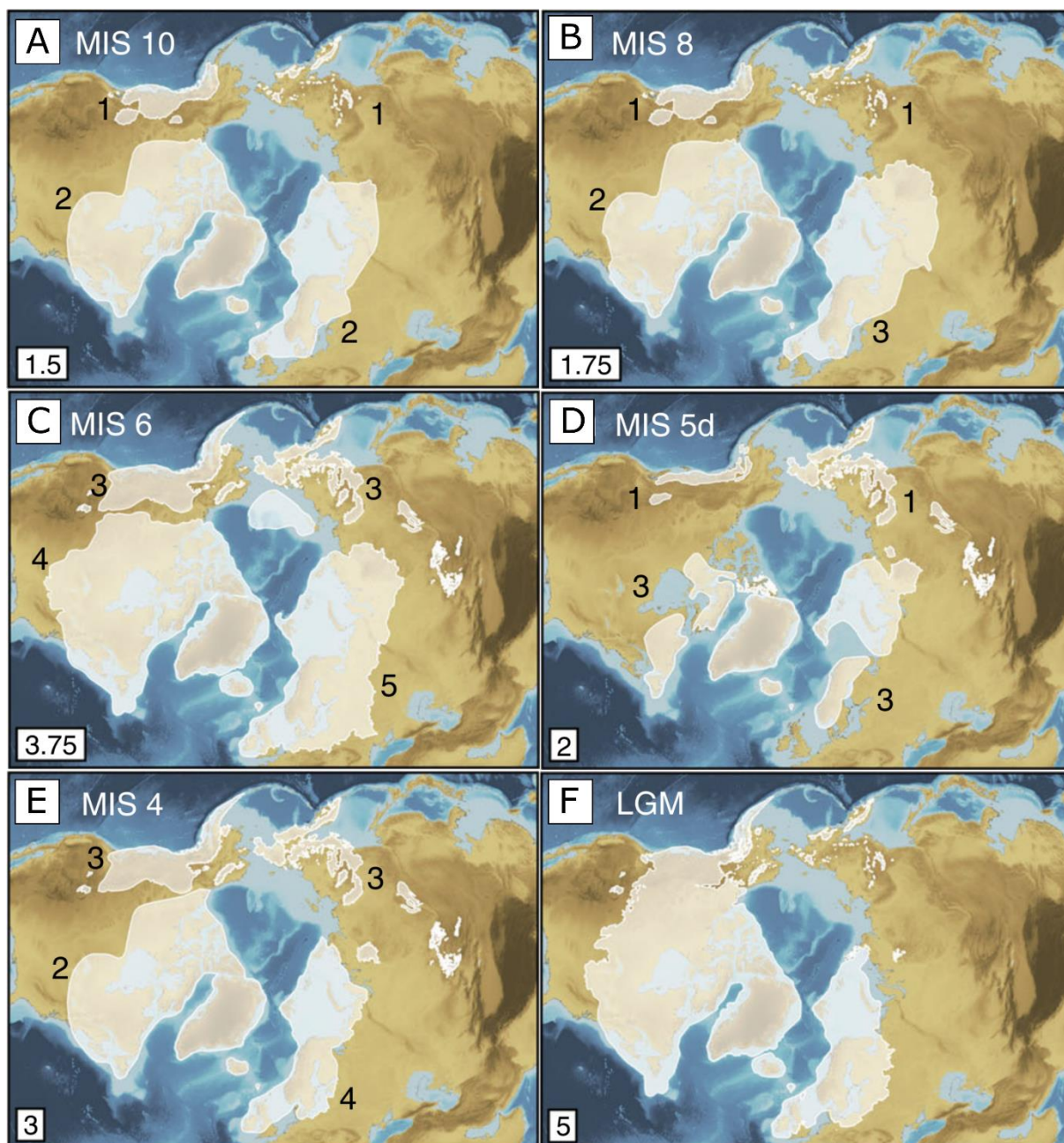


**Figure 3.4:** Maximum extents of the northern hemisphere glaciation modified from (Batchelor et al., 2019). A. MIS 10, B. MIS 8, C. MIS 6, D. MIS 5d, E. MIS 4, F. Last Glacial Maximum (LGM). Numbers in bottom left corners and on the maps are robustness scores.

### The Weichselian and the Last Glacial Maximum

The Weichselian (Fig. 3.3; MIS 5d-2) is the last of the three major glaciations, but also the one with the most uncertainty regarding maximum ice-sheet extent towards the south of the North Sea. During the Weichselian, two phases of extensive ice-sheet growth are recorded, one dated to MIS 4 and one to MIS 2, Early and Late Weichselian, respectively (Fig. 3.4E, F; e.g. Carr et al., 2006; Graham et al., 2007). For the Early Weichselian glacial phase, a till is present in the northern North Sea as evidence for grounded ice at that time. This till was deposited on top of



Eemian interglacial deposits as well as glacial marine sediment and the underlying Eemian deposits are proven to include the Blake magnetic event, dating them to c. 115 ka (e.g. Carr, 2004; Carr et al., 2006; Johnson et al., 1993; Stoker et al., 1985). Also correlated to the Early Weichselian stage are a network of buried tunnel valleys as further evidence for ice-sheets extending into the North Sea (e.g. Huuse & Lykke-Andersen, 2000).

Sediments from the Atlantic margin, the northern North Sea, and the Norwegian Channel show extensive ice coverage and an assumed northerly limit is said to be the shelf break (e.g. Mangerud, 2004; Sejrup et al., 2003). Also supporting this northerly extent are North Atlantic continental margin fans that indicate an increase in sediment supply during the Early Weichselian (e.g. Elverhøi et al., 1998; Mangerud, 2004; Sejrup et al., 2003, 2005). Towards the south there is less evidence, and a maximum extent is assumed from onshore records of the Baltic and Scandinavian ice-sheets reaching central Denmark (e.g. Graham et al., 2011). Although the extents of the MIS 4 ice-sheet are challenging to define, proof for grounded ice coverage in the North Sea is plentiful, including paleo-ice-stream activity corresponding to this time by Graham et al. (2007). In Scotland, to the west, a two-tiered till sequence created a general agreement for two extensive glacial phases during the Weichselian (Brown et al., 2007).

Like the Early Weichselian phase, the maximum limits for the Late Weichselian ice have been, and still are, a debated topic. Sejrup et al. (1987) proposed an ice-free North Sea during the Late Weichselian, based on borehole studies, but this hypothesis has later been disproven by the discovery of buried paleo-ice-streams (e.g. the Witch Ground Ice Stream) and subglacial tills in the North Sea showing extensive ice coverage during this phase (e.g. Bradwell et al., 2008; Carr et al., 2006; Graham et al., 2007; Rise & Rokoengen, 1984; Sejrup et al., 1994, 2000, 2005, 2009). A northern extent to shelf break is supported by a wide range of evidence including geomorphological, chrono-stratigraphical, and micromorphological studies on deposits from the North Sea and surrounding onshore areas (Fig. 3.4F). Examples of this are both tills and moraines to the northwest of Shetland (e.g. Bradwell et al., 2008; Davison, 2004; Stoker & Holmes, 1991) as well as actual patterns from ice-flow in the Isles (Golledge et al., 2008).

The location of the southern maximum ice margin in the North Sea is not widely agreed on, but by combining a patchwork of information, a preliminary border can be interpreted. The Norwegian Channel and the Skagerrak were both filled by ice during the last Glacial Maximum, which is assumed to correlate with the Late Weichselian, indicating the minimum eastward extent (e.g. Sejrup et al., 2003). Baltic ice is known to have extended as far south as onshore

Denmark, and in the North Sea basin, the Dogger Bank might delimit a southerly extent, as it is theorized to be a terminal moraine from the Weichselian ice sheet (e.g. Davison, 2004; Sejrup et al., 2005; Stewart, 2009; Stoker et al., 1993; Stoker, 1995). Deformation structures found in seismic data, geomorphological mapping, and sediment provenance done on cores all indicate a southerly ice movement over the Dogger Bank area, revealing a southward deflection of ice streams originating from the northern United Kingdom due to ice-cover in the central North Sea originating from Scandinavia (Fig. 3.4F; e.g. Davies et al., 2011; Everest et al., 2005).

The coalescence of the Fennoscandian and the British-Irish ice-sheets is broadly accepted to lie between the Dogger bank and Denmark (e.g. Bradwell et al., 2008; Graham et al., 2007; Sejrup et al., 1994, 2000, 2009). Building on this knowledge in addition to mapped tunnel valleys that are visible on the sea floor, the Late Weichselian phase's maximum extent is proposed at  $\sim 56^{\circ}\text{N}$  (e.g. Davison, 2004; Sejrup et al., 2005; Stewart, 2009; Stoker et al., 1993; Stoker, 1995). The global Last Glacial Maximum is defined by sea-level records (e.g. Mix, 2001), but data from the North Sea basin and certain formations indicate that the late Weichselian maxima predate this by several thousand years (e.g. Peck et al., 2006; Scourse et al., 2009; Sejrup et al., 2009). What matches with the timing of the global LGM, however, is the Dimlington Stadial that correlates to two prominent moraines east of Britain, but was likely a readvance during the period of ice-sheet collapse after the Late Weichselian (Hall & Bent, 1990; Stewart, 1991). The Dimlington Stadial is also theorized to have further shaped the Dogger Bank when a land-based lobe advanced into the basin from the British-Irish ice sheet (e.g. Davies, 2008; Davies et al., 2011; Sejrup et al., 2009). Following the British-Irish and Fennoscandian ice sheet collapses, sea-levels rose drastically and inundated previously dry coastal areas (e.g. Boulton & Hagdorn, 2006; Bradwell et al., 2008; Graham et al., 2009; Hubbard et al., 2009; Sejrup et al., 2009).

### 3.5 Quaternary tunnel valleys

Within the study area, tunnel valleys are abundant and incise into the unconsolidated, well layered sediment of the Nordland Group (Fig. 3.5; e.g. Huuse & Lykke-Andersen, 2000; Petrie et al., 2024). The tunnel valleys were created during the Pleistocene glaciations and are filled in with glacial deposits belonging to the upper part of the Nordland group (e.g. Huuse & Lykke-Andersen, 2000; Kristensen et al., 2008; Ottesen et al., 2014). This results in well layered and largely undisturbed strata below and around the tunnel valleys, and chaotic and/or complex patterns within the tunnel valleys and above (Fig. 3.5).

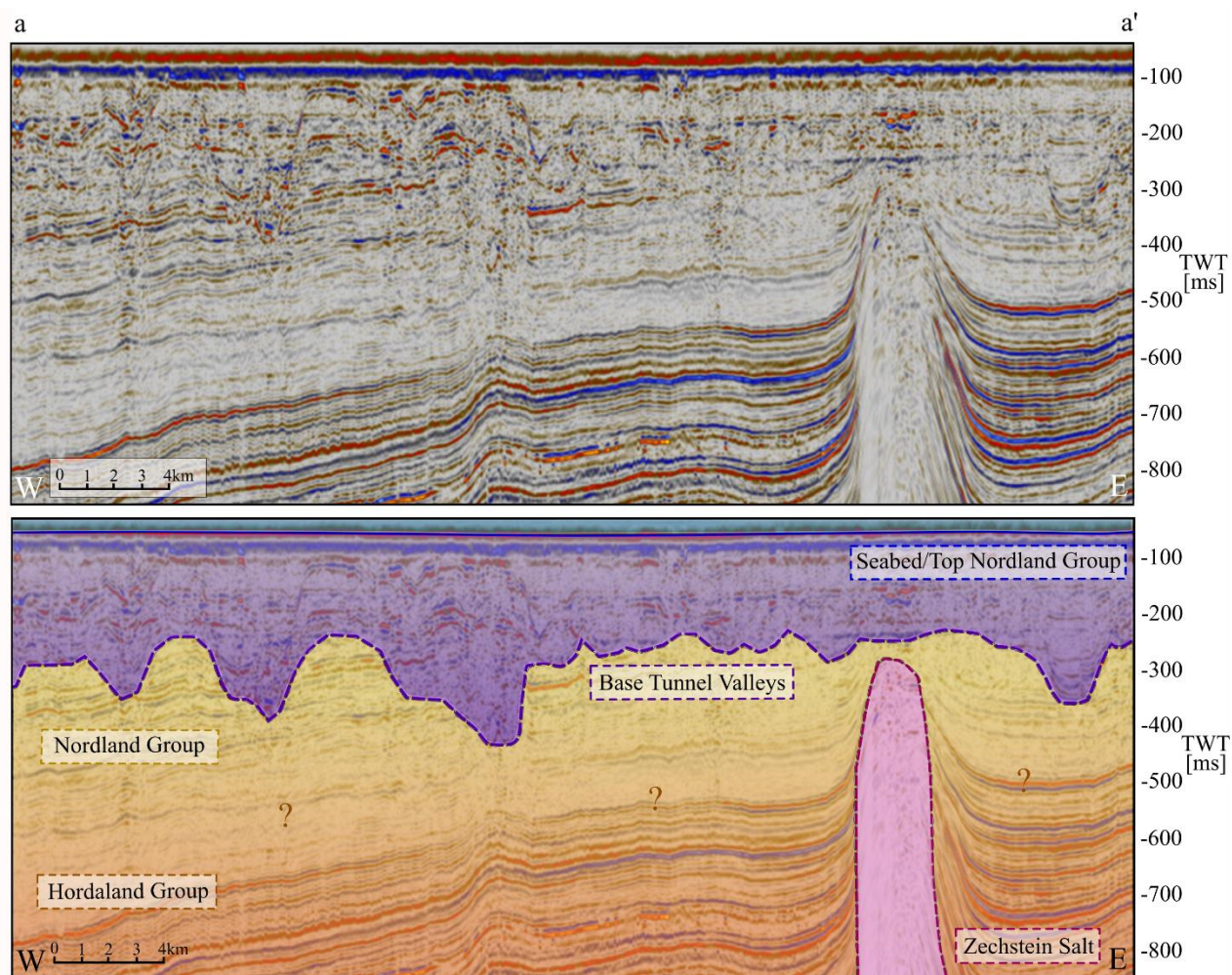


**Figure 3.5:** Seismic line a-a' (Fig. 1.1b). Stratigraphical setting interpreted on seismic including the Zechstein Group Salt (pink), the Hordaland Group (orange), the Nordland group (yellow), base of all tunnel valleys to the seabed (purple), and the seabed/top Nordland Group (blue).

## Chapter 4 Theoretical background

As early as the late nineteenth century, authors like Jentzsch (1884), Gottsche (1897), and Ussing (1903) described valleys with a subglacial origin and later, Madsen (1921) was the first to call them ‘tunnel valleys’.

### 4.1 Local and global occurrence of tunnel valleys

Complex networks of tunnel valleys have been mapped across much of the North Sea and the surrounding landmasses. For example, Bradwell et al. (2008) mapped tunnel valleys in the Northern North Sea, Moreau et al. (2012) in the Southern North Sea, and Stewart (2009) in the Central North Sea. Both Kristensen et al. (2007) and Huuse & Lykke-Andersen (2000) mapped tunnel valleys in the Danish North Sea, Fichler et al. (2005) in the Norwegian Central North Sea, and (Lutz et al., 2009) in the German North Sea. On land, tunnel valleys have been mapped in, for example, Switzerland, Germany, Denmark, Sweden, and Poland (Dürst Stucki et al., 2010; Galon, 1965; Jørgensen & Sandersen, 2006; Lidmar-Bergström et al., 1991; Stackebrandt, 2009).

Ottesen et al. (2020) mapped tunnel valleys from both 3D seismic and aeromagnetic data across much of the central and northern North Sea (Fig. 4.2a). The SNII is situated in a section of the North Sea with a moderate density of tunnel valleys, and a thin package of quaternary sediments compared to the thickest areas to the west (Fig. 4.2a, b). The area with the highest density of tunnel valleys is located along the border dividing the Norwegian and UK sector of the North Sea, between Scotland and Western Norway (Fig. 4.2a). Tunnel valleys are most often found in substrates that are easy to erode (Wingfield, 1990), and as the North Sea basin is filled with large amounts of Quaternary sediment (Fig. 4.1a), it is a favourable environment.

Tunnel valleys have been observed not only in the North Sea and adjacent regions, but also on the African continent and in the Middle East. These valleys were proposed to have formed in the Ordovician period by similar processes to those in the North Sea and are summarised by Van Der Vegt et al. (2012). On the American continent, Atlantic Canada is known to have been covered by enormous ice sheets during the Pleistocene, resulting in the development of tunnel valleys (e.g. Boyd et al., 1988; King, 2001; Shaw et al., 2006).

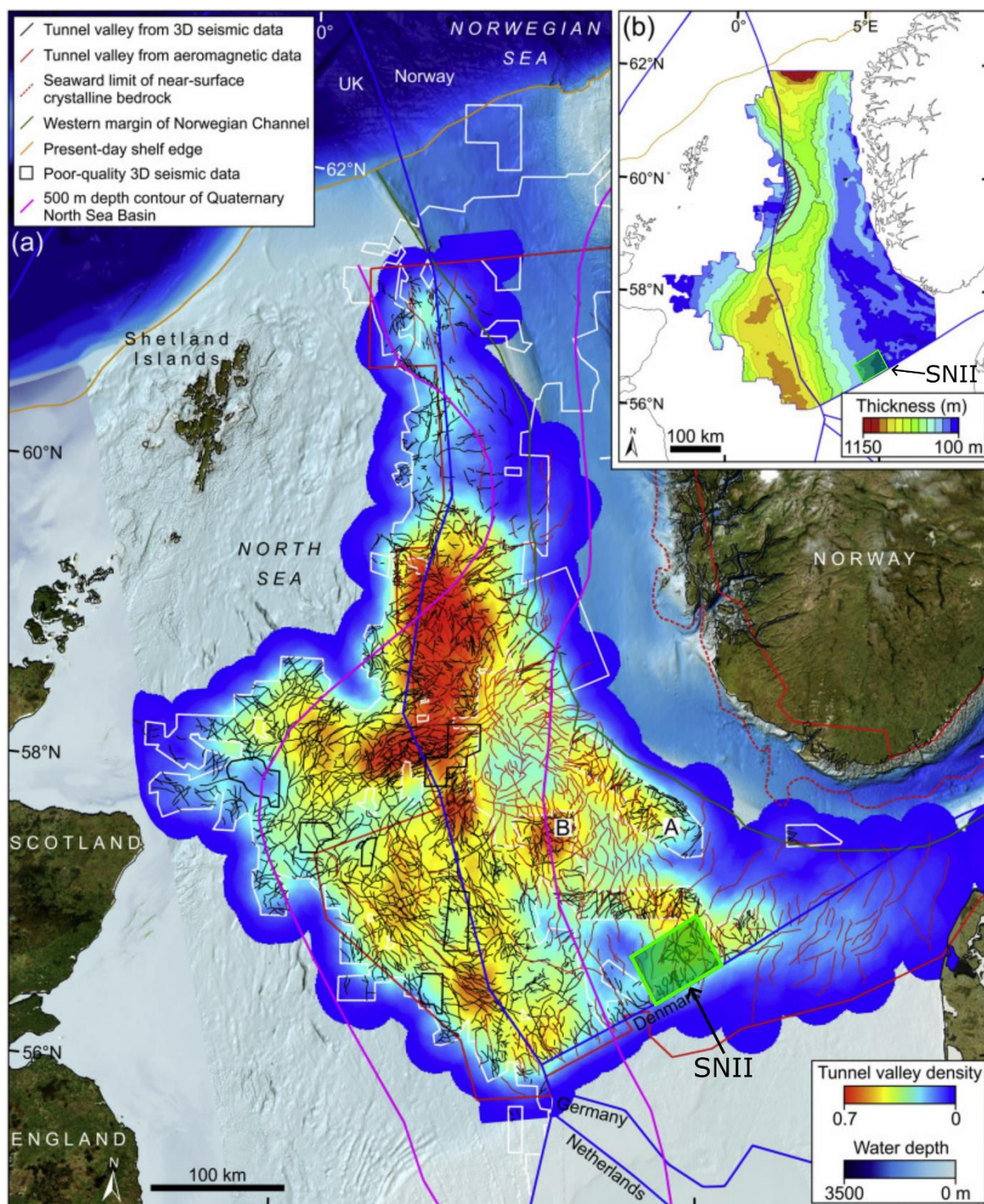


**Figure 4.1:** *a.* map of the North Sea with interpreted tunnel valleys and tunnel valley density where red is high density and blue low density. The position of the SNII site is shown as a green polygon. *b.* Quaternary sediment thickness in the North Sea. Figure modified from (Ottesen et al., 2020).

## 4.2 Tunnel valley formation

A general agreement of how tunnel valleys are made was not reached until recently. Woodland (1970) proposed formation by meltwater erosion under large ice sheet covers. Later, Wingfield (1990) argued that the glacial incisions he analysed were of other origin than the tunnel valleys (Woodland, 1970) described, and proposed that his ‘major incisions’ were created by a sudden breach of a subglacial lake (Jökulhlaup). Now, most describe tunnel valleys as an incision created underneath the outermost boundaries of a receding ice-sheet with an undulating thalweg (Fig. 4.2; e.g. Hammer et al., 2016; Huuse & Lykke-Andersen, 2000; Lonergan et al., 2006; Praeg, 1996, 2003). The consensus is that tunnel valley formation is of a time-transgressive nature, meaning they form over time rather than instantly (e.g. Lonergan et al., 2006; Praeg, 2003) and is a result of a combination of more than one sub-glacial erosional process (e.g. Huuse & Lykke-Andersen, 2000; Lonergan et al., 2006; Praeg, 1996).

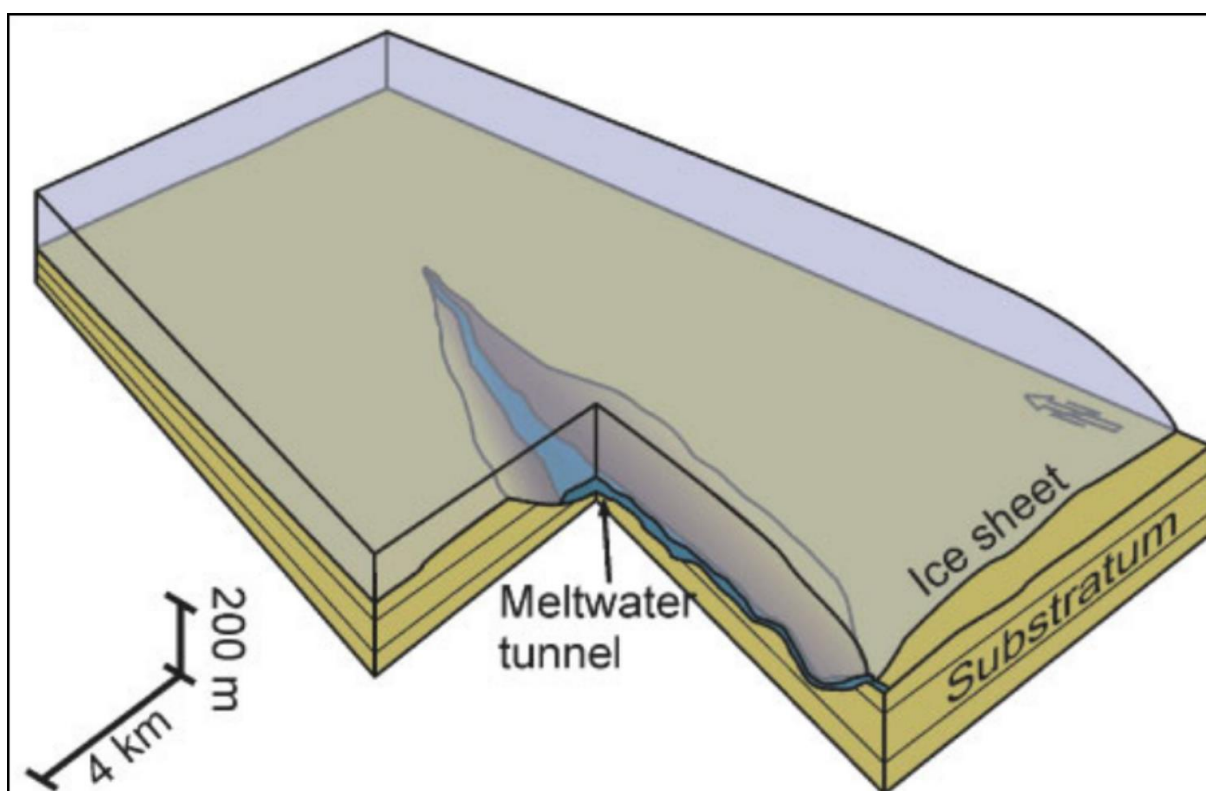


**Figure 4.2:** Schematic showing tunnel valley formation under a receding ice sheet. Modified from (Kristensen et al., 2008).

When an ice sheet recedes, large amounts of meltwater are transported sub-glacially and can create over-pressured meltwater channels that evolve into tunnel valleys (Fig. 4.2; e.g. Huuse & Lykke-Andersen, 2000; Lonergan et al., 2006; Praeg, 2003). After c. 430 ka BP, the interglacials increased in intensity and the atmosphere had a higher concentration of CO<sub>2</sub> than

previously (e.g. Kirkham et al., 2024; Yin & Berger, 2010). This is called the Mid-Brunhes Transition (MBT) and increased the amplitude of the glacial/interglacial cycle (Fig. 3.3; e.g. Yin & Berger, 2010). Kirkham et al. (2024) speculated that this transition resulted in the formation of more tunnel valleys than before, caused by higher quantities of meltwater being produced during glacial terminations because of the higher temperatures.

Larger outbursts of meltwater, like when a sub-glacial lake is breached, can also contribute to the incision of tunnel valleys, either continuing an existing valley, or initiating the formation of a new one (e.g. Huuse & Lykke-Andersen, 2000; Kehew et al., 2012; Van Der Vegt et al., 2012). Some tunnel valleys are wide and shallow, suggesting that glacial erosion played a significant role in their formation, as opposed to narrow and deep tunnel valleys, which are more likely mainly eroded by meltwater (e.g. Huuse & Lykke-Andersen, 2000). The exact location of tunnel valleys under the ice-sheet border is determined by where erosional forces can easily incise, which is influenced by previously existing rivers, the permeability of the substrate in the area, shallow salt diapir structures, and faulting (e.g. Huuse & Lykke-Andersen, 2000; Praeg, 1996; Salomonsen & Jensen, 1994). Lonergan et al. (2006) observed that tunnel valleys close to the ice sheet margin formed simpler patterns compared to those far away from the margin, which displayed complicated anastomosing patterns. Thus, the valleys close to the former margins of large ice sheets might have the most reliable clues to the direction of ice retreat.

Tunnel valleys are created with the longitudinal profile perpendicular to the overlying ice sheet's border, thus being an important indicator for the maximum extents of paleo ice masses (Fig. 4.2; e.g. Huuse & Lykke-Andersen, 2000; Lohrberg et al., 2020; Lonergan et al., 2006; Praeg, 2003; Woldstedt, 1922). The ice sheet borders are dynamic and would likely have gone through several cycles of smaller re-advances during recession, resulting in a comparably dynamic nature of tunnel valley systems. As several generations of tunnel valleys can be formed during a single glaciation, reconstructing them could contribute to a better understanding of paleo ice sheet positions and movements (e.g. Kirkham et al., 2024; Kristensen et al., 2008; Stewart et al., 2013).

### 4.3 Tunnel valley morphology

Tunnel valleys in the North Sea can be described as buried, elongated depressions with base to shoulder relief of c. 30–400 m, widths of c. 250–5000 m, and lengths up to several tens of kilometres (Fig. 4.3; e.g. Huuse & Lykke-Andersen, 2000; Lonergan et al., 2006; Praeg, 1996, 2003; Van Der Vegt et al., 2012). Incisions wider than 5 km are likely either cross-shelf troughs

or ice streams (e.g. Ghienne et al., 2007). In cross-section, the base of the valleys varies between a U- or V-shape with generally steep, sloping sides (Fig. 4.3; e.g. Huuse & Lykke-Andersen, 2000; Jørgensen & Sandersen, 2006; Stewart et al., 2013). Kirkham et al. (2021, 2024) have observed both eskers and crevasse-squeeze ridges within the tunnel valleys using high resolution 3D seismic data.

The longitudinal profile of the tunnel valleys can be defined as undulating due to distinctive over-deepening and internal sills up to 200 m above the deepest section of the valley (Fig. 4.3; e.g. Huuse & Lykke-Andersen, 2000; Lonergan et al., 2006; Praeg, 2003). Both the start and end of tunnel valleys are described as abrupt (e.g. Huuse & Lykke-Andersen, 2000), and the valleys exhibit varying degrees of sinuosity in plan-view. Tunnel valleys of the same generation, created by the same ice-sheet and formed around the same time, are largely parallel to each other (Praeg, 2003). However, large valleys branch out and form anastomosing systems where smaller tunnel valleys diverge and converge (e.g. Huuse & Lykke-Andersen, 2000; Lonergan et al., 2006; Praeg, 2003). When multiple generations of tunnel valleys coexist in a single location, younger generations incise into older tunnel valleys, forming a cross-cutting relationship (e.g. Kristensen et al., 2008; Praeg, 2003; Stewart et al., 2013; Van Der Vegt et al., 2012).

Huuse & Lykke-Andersen (2000) proposed a series of diagnostic features for tunnel valleys, namely: i) partially or completely buried valleys that ii) incise into the substrate, forming elongate depressions with iii) widths of c. 1-5 km and iv) lengths up to several tens of kilometres, v) the thalweg of the valley has an abrupt beginning and end, and vi) is over-deepened with shallower sections often accompanied by internal sills. Lastly, vii) the valleys exist within the borders of known large ice sheets with viii) orientations often perpendicular to the ice front.



## Tunnel valley morphology

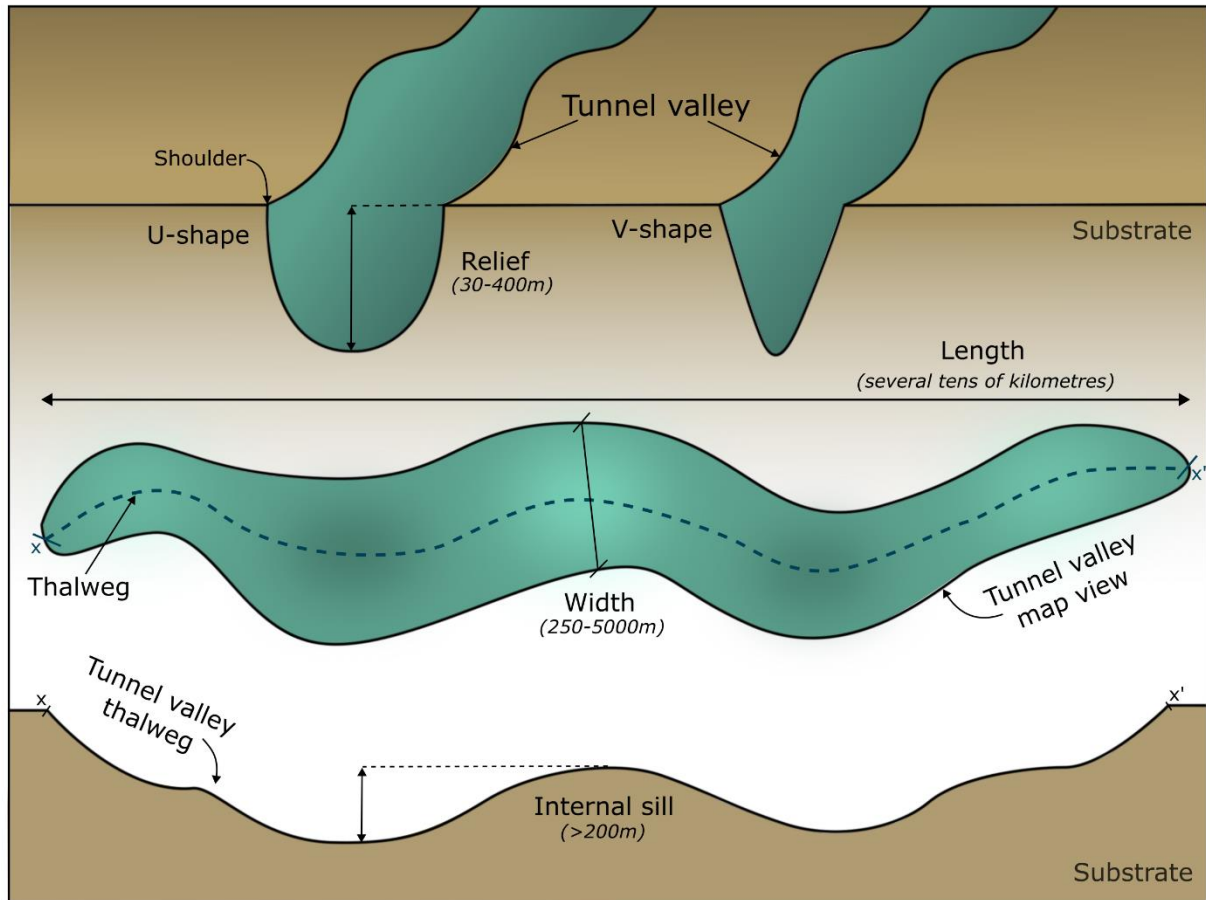


**Figure 4.3:** Overview of tunnel valley morphology with measurements from previous works. Tunnel valley (turquoise) and substrate (brown).

## 4.4 Tunnel valley infill

There is a general pattern for tunnel valley infill that includes an upward decrease in glacial influence and a variety of sedimentary and erosional processes (e.g. Huuse & Lykke-Andersen, 2000; Krohn et al., 2009; Le Heron et al., 2004; Smith, 2004). For that reason, it is possible to subdivide tunnel valley infill depending on its relation to the base erosional surface. Primary infill is genetically related to the erosional surface, while secondary infill is genetically unrelated, and may include non-glacial processes in its depositional history (e.g. Van Der Vegt et al., 2012).

Primary infill of tunnel valleys can include diamicton, massive gravels and sands, coarse-gravel deposits, and massive sands and silts in 'clinoform' structures. Diamicton is frequently found along the base of tunnel valleys (e.g. Ehlers & Linke, 1989; Kluiving et al., 2003; Moscariello, 1996; Piotrowski, 1994). This could be a basal till, and a result of a readvancing ice-sheet or the next glaciation eroding down into an already existing tunnel valley (e.g. Le Heron et al., 2004; Le Heron, 2007; Moscariello et al., 2008). Similar are the coarse-gravel deposits also found at the base of tunnel valleys, which form a variety of subglacial landforms, like eskers and channels, and, as a result, are interpreted as subglacial deposits (e.g. Jørgensen & Sandersen, 2006; Moreau et al., 2005; Moscariello et al., 2008). Another type of primary infill is massive gravels and sands, which are theorised to be a result of ice-proximal sub-aquatic fans in the form of debris-flows (e.g. Ghienne & Deynoux, 1998; Le Heron et al., 2004; Le Heron, 2007).

The fourth and final type of primary infill is massive sands and silts deposited in large packages comparable to clinoforms that may stretch across the entirety of the valley (Fig. 4.4a; Kluiving et al., 2003; Kristensen et al., 2008; Praeg, 1996). One common theory for their deposition is time-transgressive backfilling, where meltwater erodes into the underlying strata of a receding ice sheet and the sediment is deposited at the ice margin along the terminal slope Praeg (1996). This theory is strengthened further by the suggestion of glaciohydraulic supercooling, the fact that the clinoforms slope towards the former ice sheet centre, and that borehole data indicate locally derived sediment (Kristensen et al., 2008).

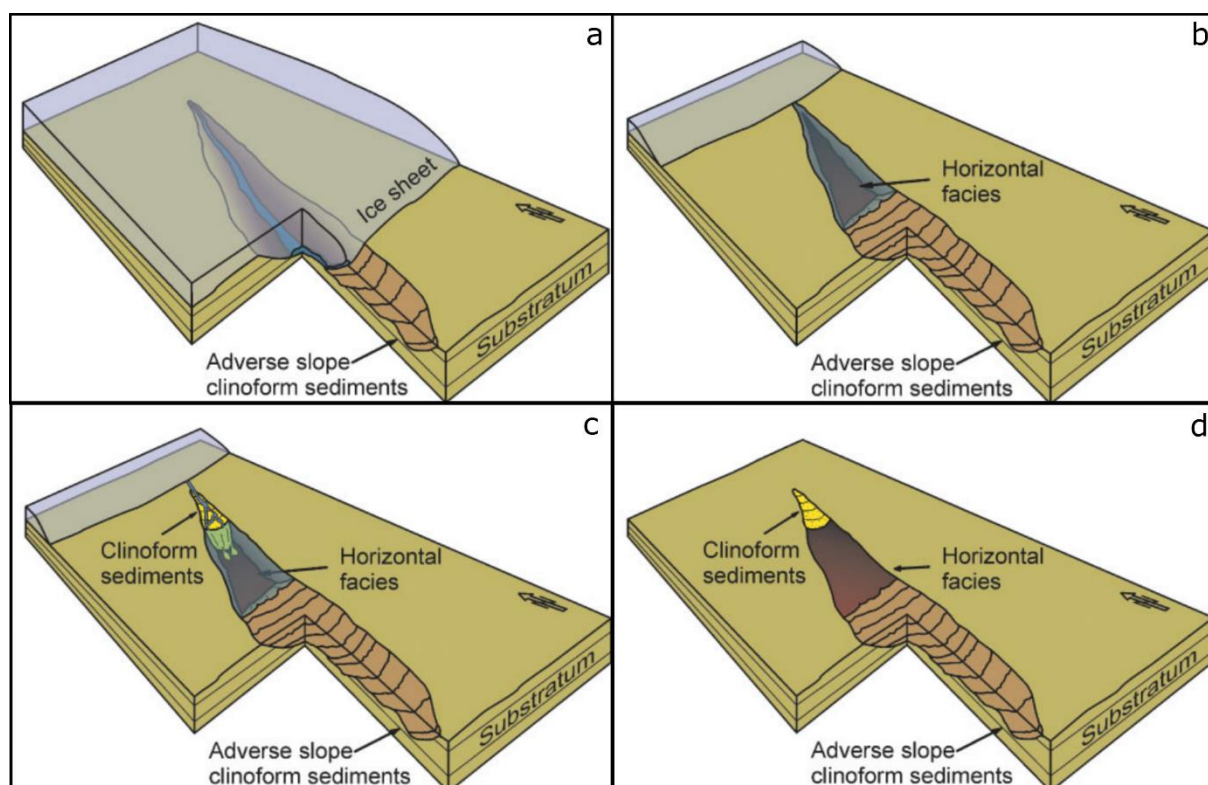


**Figure 4.4:** *Schematic of time-transgressive infill of a tunnel valley, modified from (Kristensen et al., 2008). a. adverse slope clinoform sediments, b. horizontal facies, c. clinoform sediments, and d. fully filled inn tunnel valley.*

Secondary infill can include all types of sediment derived from a wide range of erosional and depositional processes, either during or after ice-sheet retreat. The distal parts of outwash fans might reach the tunnel valleys, as well as other types of deposits of glaciofluvial nature (Fig. 4.4c; e.g. Ehlers & Linke, 1989; Jørgensen & Sandersen, 2006; Le Heron et al., 2004; Piotrowski, 1994). Diamictons can also present as secondary infill when formed by processes like slumping of valley sides, melt out from stagnant ice, or settling from sediment plumes or ice-rafting (e.g. Ehlers & Linke, 1989; Eschard et al., 2005; Hirst et al., 2002; Van Der Vegt et al., 2012).

Several secondary infill types originate from marine or lacustrine environments, both glacial-related and not. One example is sediment from turbidites or underflows, which is commonly represented by well-sorted sands (e.g. Hirst et al., 2002; Le Heron et al., 2004; Moscariello, 1996). Another type of infill, which is regularly found in tunnel valleys, consists of laminated clays and silts that appear to have been deposited in calm conditions (Fig. 4.2b; e.g. Cameron et al., 1987; Huuse & Lykke-Andersen, 2000; Kluiving et al., 2003; Krohn et al., 2009; Piotrowski, 1994; Praeg, 2003). Tunnel valleys, particularly those with greater widths and

depths, are frequently left underfilled, allowing a variety of depositional systems to fill up the remaining depression (e.g. Bradwell et al., 2008).

#### 4.5 Proglacial lakes and outwash fans

During deglaciation, proglacial lakes can form in front the ice sheet margin (e.g. Carrivick & Tweed, 2013). These are common features related to large ice sheets that have advanced into the North Sea (e.g. Clark et al., 2012; Emery et al., 2019; Livingstone et al., 2010). The formation of proglacial lakes is greatly impacted by glacier dynamics and the surrounding environment, since they are frequently located in depressions in the terrain or dammed by ice and/or moraines, therefore they come in an extensive array of sizes (e.g. Carrivick & Tweed, 2013). Proglacial lake deposits are characterised by laminated fine-grained sediments with the occasional dropstone (e.g. Emery et al., 2019).

Outwash fans are glacial landforms that form in front of an ice sheet by meltwater carrying sediment from up-ice and depositing them at the glacier margin (e.g. Boulton, 1986; Emery et al., 2019). They have a recognisable shape with a narrow apex that fans out gradually away from the ice margin, and the sediments deposited are characterised by well sorted sands with decreasing grain-size away from the ice margin (e.g. Cartelle et al., 2021; Emery et al., 2019).

## Chapter 5 Data

### 5.1 Seismic data

The SNII site is covered by a grid of 2D seismic lines from the NSR 04/05 (Fig. 5.1a; TGS, available through DISKOS) 2D seismic survey. The seismic data is zero-phase and reverse polarity, with lines spaced between 4-10 km stretching across the site from southwest to northeast and northwest to southeast. The 2D seismic survey was originally acquired for exploration purposes and is for that reason poorly suited for seismic interpretation in the shallow most section (top 500 ms TWT) where the signal-to-noise ratio is significantly lower than in the deeper sections (Fig. 5.1b).

Almost the entirety (90%) of the SNII site is covered by 3D seismic data of varying quality (Fig. 5.2a). This includes four surveys: MC3D-NDB 2008 (PGS), MC3D-MDB 2013 (PGS), ST99M01 and DG15001, which all are available through DISKOS. These, like the 2D survey, were originally obtained to search for hydrocarbons in deep stratigraphy, forfeiting the quality of the seismic data irrelevant to exploration. As a result, all four 3D seismic surveys have strong acquisition-line imprints that make seismic interpretation near the seabed challenging. Also equivalent to the 2D seismic survey, the data is zero-phase and reverse polarity, and has a vertical resolution of about 10 metres in the top c. 500 ms TWT (Fig. 5.2b).

The MC3D-NDB 2013 offers the highest quality data, and because it covers most of the southern section of the SNII area, this survey will be the starting point for a lot of interpretation. Covering the northeastern part of the SNII site, the MC3D-NDB 2008 and DG15001 surveys are good for shallow seismic interpretation. Finally, the ST99M01 survey has the strongest acquisition-line imprints, making the shallow seismic data nearly unusable, resulting in this seismic survey being used primarily for deeper stratigraphy.

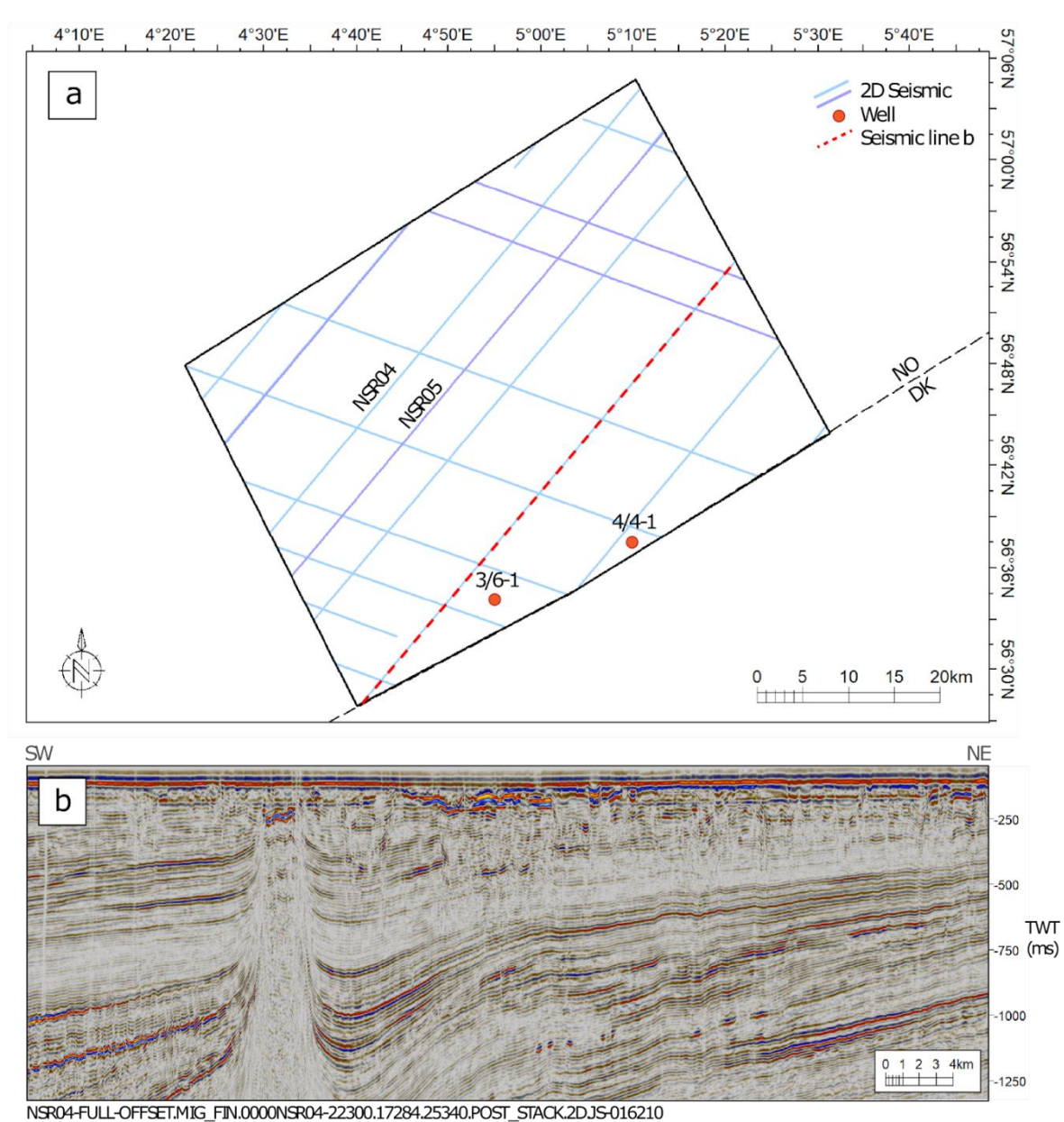


**Figure 5.1:** *a.* Overview of 2D seismic data where black polygon is the SNII area boundary. *b.* Seismic line shown in *a.* with red dashed line.

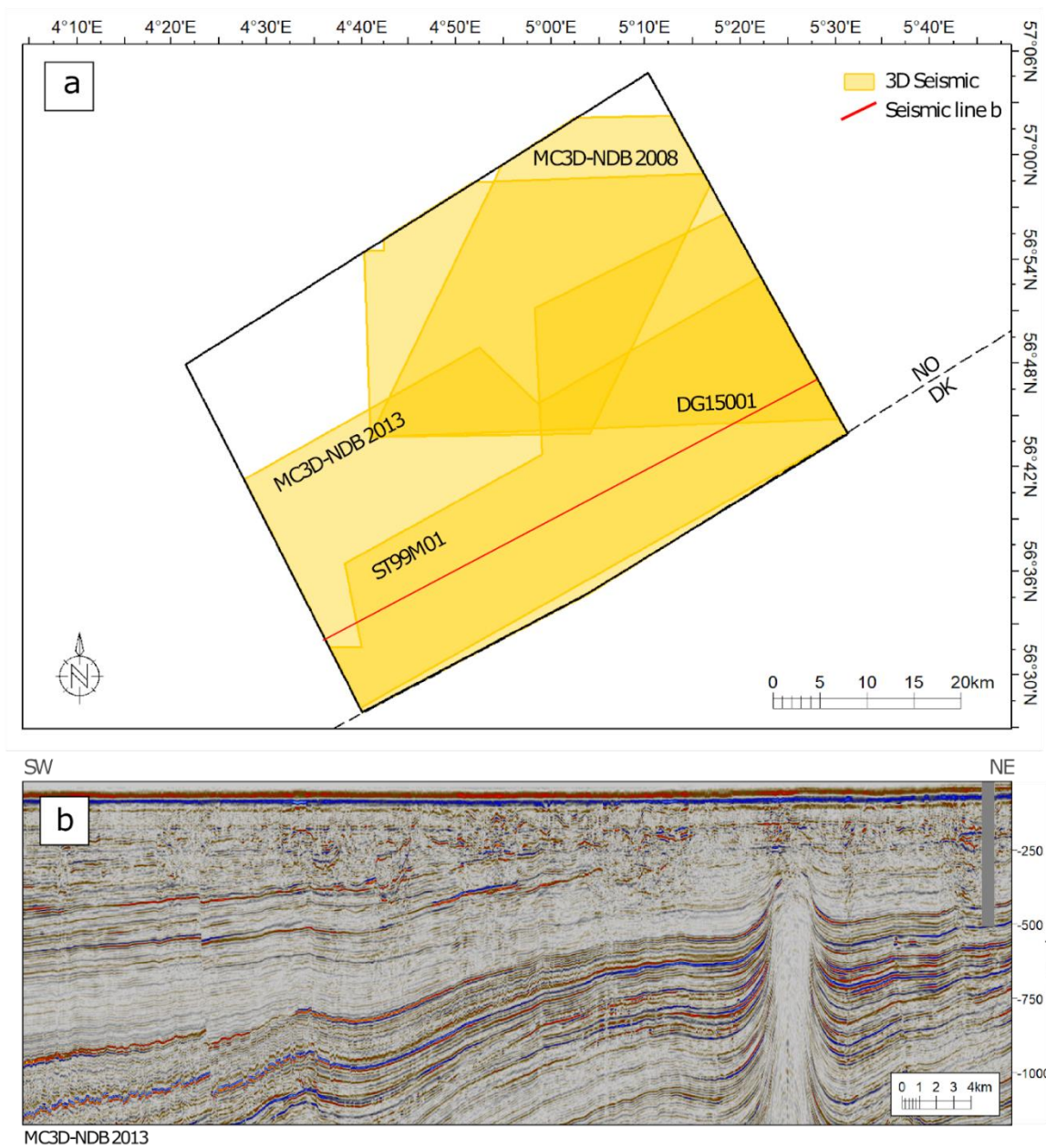


**Figure 5.2:** *a.* Overview of 3D seismic data where black polygon is the SNII area boundary. *b.* Seismic line shown in *a.* with red line.

## 5.2 Well data

Two wells are present in the southern part of the SNII site, 3/6-1 and 4/4-1 (Fig. 5.1a), both are exploration wells, and both are dry. Well 3/6-1 has a total vertical depth of 2167 metres, with the oldest penetrated age being Late Cretaceous Tor formation. The Nordland group is found at 90 metre depth, and the next group down is the Hordaland at 791 metres. The total vertical depth for well 4/4-1 is 2012 metres but has the same oldest penetrated age and formation as the previously mentioned well. The 4/4-1 does however penetrate the Norland group marginally deeper at 105 metres and the Hordaland group slightly shallower at 541 metres. Information on the two exploration wells is summarised in Table 5.1.

*Table 5.1: Overview of wells inside study area.*

Well name	3/6-1	4/4-1
NS degrees	56° 35' 0.14" N	56° 38' 8.65" N
EW degrees	4° 53' 30.35" E	5° 8' 11.53" E
Completion date	10.07.2000	13.10.2013
Type	EXPLORATION	EXPLORATION
Status	P&A	P&A
Content	DRY	DRY
Top Nordland Gp. (mMD RKB)	90	105
Total depth (mMD)	2167.0	2012.0



# Chapter 6 Methods

## 6.1 Variance and RMS analysis

In this thesis, seismic attribute analysis is performed on 3D seismic data to extract information that is not originally clear in seismic data. This information is in the form of seismic attributes, which can be obtained by performing computations or measuring the data's components. It is possible to extract a variety of attributes from seismic data, each with its own unique ability to highlight specific features, especially when combined with the effective application of colour maps. The attributes used in this thesis are variance and RMS amplitude, all analysis performed in Petrel.

For variance attribute analysis, the similarity/dissimilarity of adjacent seismic traces is measured on a scale of 0 to 1, with the former signifying total similarity and the latter signifying total dissimilarity. This attribute is known as an edge method, and it is useful for recognising significant lateral and vertical changes in seismic data, such as faulting or channel edges (Fig. 6.1a). In this thesis, variance attribute analysis is applied to 3D seismic data to image tunnel valley limits and other features that may be relevant to understanding the study site's shallow geology. A variation of extraction window lengths is used, as the resolution can be customised through adjusting the length, for example, longer extraction windows are more suitable when working with low quality data. Variance values are extracted from seismic volumes and surfaces using the following parameters: Inline range: 3, Crossline range: 3, Vertical smoothing: 20.

To visualise variance volumes or surfaces, an appropriate colormap must be selected and customised to fit the data. The minimum and maximum variance values are zero and one, respectively, however in most circumstances, the true distribution of variance values falls somewhere in between. To enhance clarity and display the variability in variance attributes, the colour scales of the maps was adjusted to capture the true distribution of variance values. This was done separately for each variance extraction due to the maximum and minimum values varied.

RMS amplitude, which stands for Root Means Squared, is calculated by substituting trace values  $x$  and window values  $w$  and  $n$  into equation 1, where  $N$  is the number of samples.

**Equation 1:**

$$x_{rms} = \sqrt{\frac{1}{N} \sum_{n=1}^N w_n x_n^2}$$

RMS amplitude extraction creates a smoothed version of the reflection strength, which is commonly used to identify amplitude anomalies, potential depositional environments and landforms (Fig. 6.1b). As the equation is squared, there are no negative values. The extraction window is adjusted depending on the amount of detail needed. For regional surfaces, large extraction window where used, and for the insides of tunnel valleys, smaller extraction windows. The RMS attribute is useful when looking for discontinuities and coarse facies, hence it is helpful for identifying tunnel valleys and their infill within the study site. High RMS values can be sands and/or gravel, while very low RMS amplitudes can be silts and/or clays. This is caused by the respective sediment's acoustic impedance in comparison to the underlying substrate. Occurrences of shallow hydrocarbons can also be interpreted from RMS amplitudes but must be confirmed by a 'soft-kick' in the seismic data. Similarly to variance attribute analysis, applying a colormap and modifying it to the data is important. In this thesis, lighter hues have been assigned to higher values which suggest coarser grained facies inside tunnel valleys, as well as probable occurrences of shallow gas. RMS amplitude volumes are extracted from seismic datasets using the following parameters: Window: 9. For horizons, the extraction window is defined and 'interval average' is chosen to show the average RMS amplitudes for the chosen window.

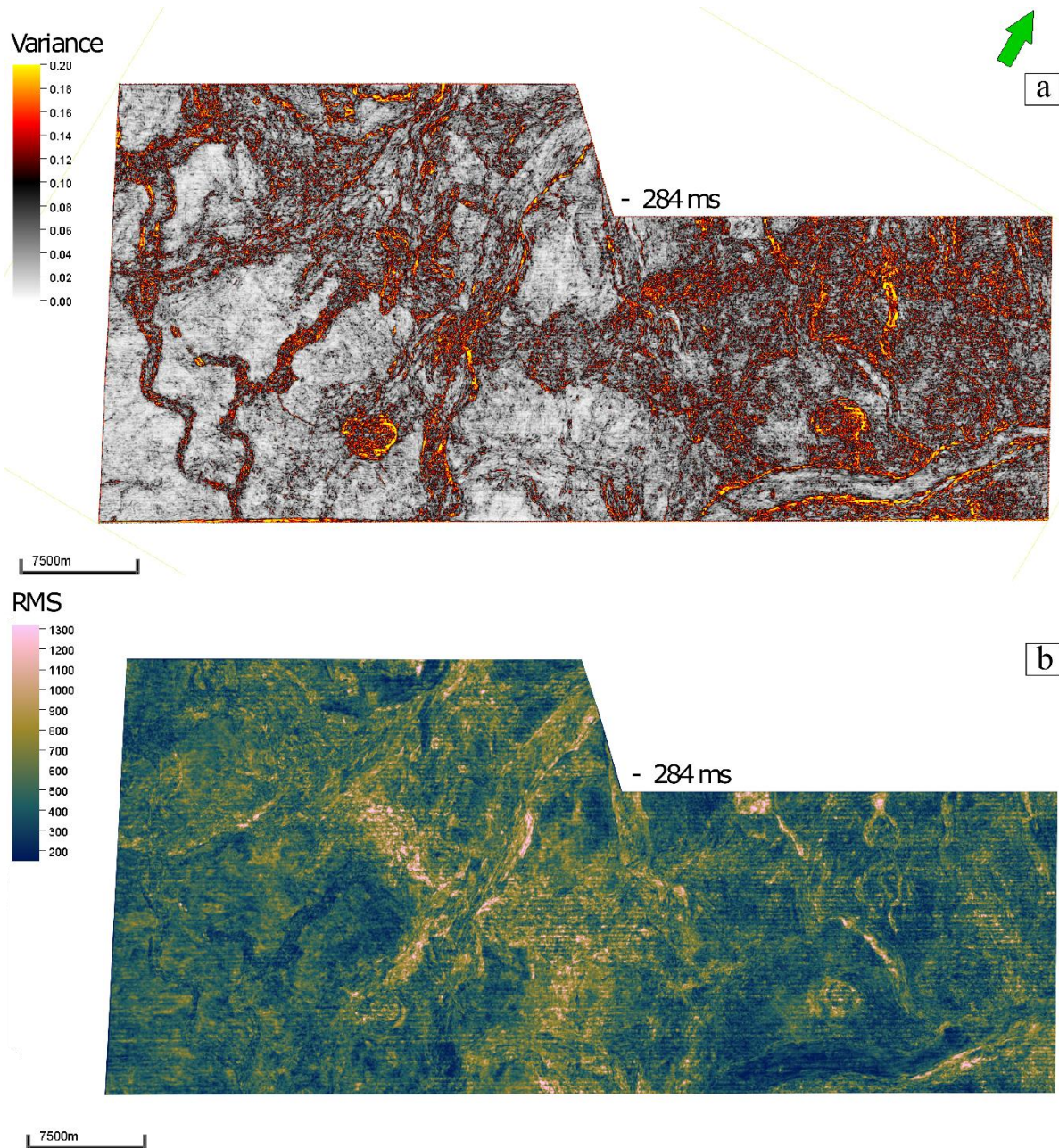


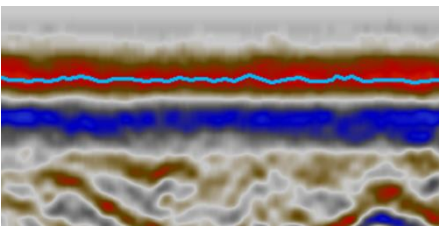
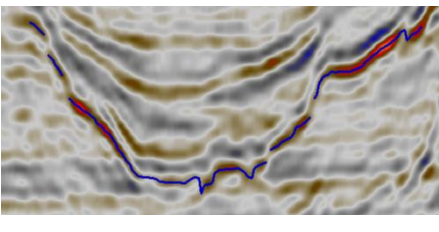
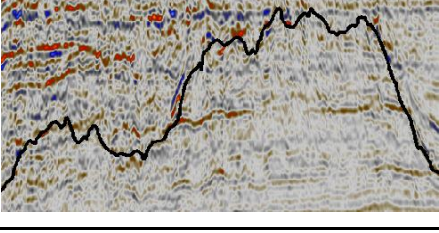
**Figure 6.1:** Examples from attribute analysis **a.** variance surface at -284 ms showing outlines of a complex network of buried tunnel valleys. **b.** RMS amplitude surface at -284 ms showing a variation of high and low amplitudes within and around tunnel valleys.

## 6.2 Seismic interpretation

The horizons interpreted in this thesis are the seabed, individual tunnel valleys, and the base of all tunnel valleys (Table 6.1). The seabed reflector is highly continuous throughout the area and was interpreted using 3D autotracking in two 3D seismic datasets (MC3D-NDB 2013 and 2008). The seabed reflector is expected to be the first seismic signal and a peak because there is a significant positive change in acoustic impedance from seawater to sediments. The base of the individual tunnel valleys was primarily interpreted using manual 2D tracking with snapping and interpretation increments ranging from 2-16 lines in a minimum of two orientations, using the same 3D seismic datasets as the seabed. The smaller tunnel valleys proved challenging to interpret, with several sharing the same horizon as they were difficult to separate. Each tunnel valley horizon was given the label "TV#", and when there were several tunnel valleys per horizon, the letters a-e were used to distinguish them. A sudden change from sub-parallel reflectors to chaotic and/or sub-horizontal facies separated by a peak in a U- or V-shape was used as criteria when interpreting the tunnel valleys.

The base of the tunnel valleys is assumed to broadly correspond to a peak in the seismic data due to younger sediments overlying more compacted older sediments as the valleys are erosive in nature, and this commonly presents as a positive impedance contrast. The horizon corresponding to the base of all tunnel valleys was again interpreted using manual 2D tracking with snapping, but on a much wider grid of 64 by 64 lines, as less accuracy was required for the bigger area. Each direction of the grid's lines began at a random polyline intersection that was oriented to cross the tunnel valleys in the area as perpendicular to strike as possible and align with the study area's boundaries. This horizon was exclusively interpreted using the MC3D-NDB 2013 3D seismic dataset. Similar criterium as for the individual valleys were used when interpreting this surface, with the addition of having to interpret between the clear tunnel valley incisions. Here the horizon was interpreted above seemingly undisturbed/less chaotic seismic facies, making sure to consider the multiples below large valleys and gas chimneys where relevant. Table 6.1 summarises the interpreted horizons.

**Table 6.1:** Overview of all interpreted horizons and their seismic characteristics in interpretation order.

Horizon	Seismic phase	Amplitude	Tracking method	Seismic signature
Seabed	Positive amplitude (peak)	High	3D Autotracking	
Tunnel valley	Positive amplitude (peak)	Moderate to low	Manual 2D tracking with snapping	
Base tunnel valleys	Peak/through	Varied	Manual 2D tracking with snapping	

### 6.3 Workflow tunnel valley interpretation

Step by step workflow on how tunnel valleys have been interpreted from 3D seismic data.

1. The 3D seismic dataset is imported to Petrel, checked for artefacts, and parameters modified as needed. The seismic volume initially had data at far deeper depths in TWT than is reasonable to analyse in this thesis as tunnel valleys only exist at maximum c. 500 ms TWT in this area; therefore, it has been cropped at 1000 ms TWT for faster processing times.
2. To decrease the effect of seabed relief on future attribute time slices, the 3D volume is flattened with a volume-specific seabed surface as input.
3. The flattened volume is used to create a variance attribute volume and an RMS attribute volume, which is covered in chapters 5.2.1 and 5.2.2. Polygons are created for the tunnel valleys observed on time slices, first in the variance volume, that features the most

evident valley edges. The RMS volume is used to both check the shape and dimensions of existing polygons and make new ones.

4. To begin interpreting horizons for each tunnel valley, the polygon, in addition to any of the two attribute volumes, is used to guide the placement of random polyline intersections within the original flattened volume. The intersections are perpendicular to the tunnel valley thalweg, and the base of the tunnel valley is interpreted along it using manual 2D with snapping and increments ranging from 2 to 32.
5. A colormap is added to the grid to visualise the thalweg, and a new random polyline intersection is traced throughout the entire length of the tunnel valley. The gridding is completed by interpreting along the thalweg and to each side in the same increments as before, stopping at the valley shoulders.
6. 3D auto-tracking is used to extend the interpretation to a complete 3D interpretation of the tunnel valley, using 90% certainty when the data is excellent and 80% when the data is poor. During the 3D auto-tracking process, complex areas occur; these are addressed by erasing and re-gridding sections of the interpretation. The tunnel valley polygon is adjusted to fit the 3D horizon.
7. The tunnel valley horizon is used as the main input to create a surface, with the polygon acting as the boundary. The grid size and position are set based on the original seismic dataset, and the grid increment is 12.5 for X and 12.5 for Y. The final surface is fitted with a suitable colour map and smoothed when needed.
8. Smaller tunnel valleys might not appear on attribute time slices, so the interpretation workflow changes slightly. Instead of knowing the tunnel valley's trajectory ahead of time, it is discovered by trial and error when interpreting the tunnel valley base. This method requires shifting between interpreting perpendicular to and along the thalweg, as well as interpreting a few tunnel valleys at the same time due to their occasional anastomosing nature.

## 6.4 Morphology analysis

Morphological analysis of tunnel valley time depth surfaces is an important part of the objectives of this thesis and includes eight morphological measurements. Tunnel valley length is measured along the shortest path through the tunnel valley and orientation is measured along the same line (Fig. 6.2a). The thalweg length is measured along the deepest part of the tunnel valley (Fig. 6.2a), and sinuosity (quantitative index of meandering) is calculated by dividing thalweg length by total length. Maximum width is measured at the widest point of the tunnel valley (Fig. 6.2a). Maximum and minimum depth is measured in two-way time depth [ms] from top of seismic, and thalweg relief is the difference between these two (Fig. 6.2b).

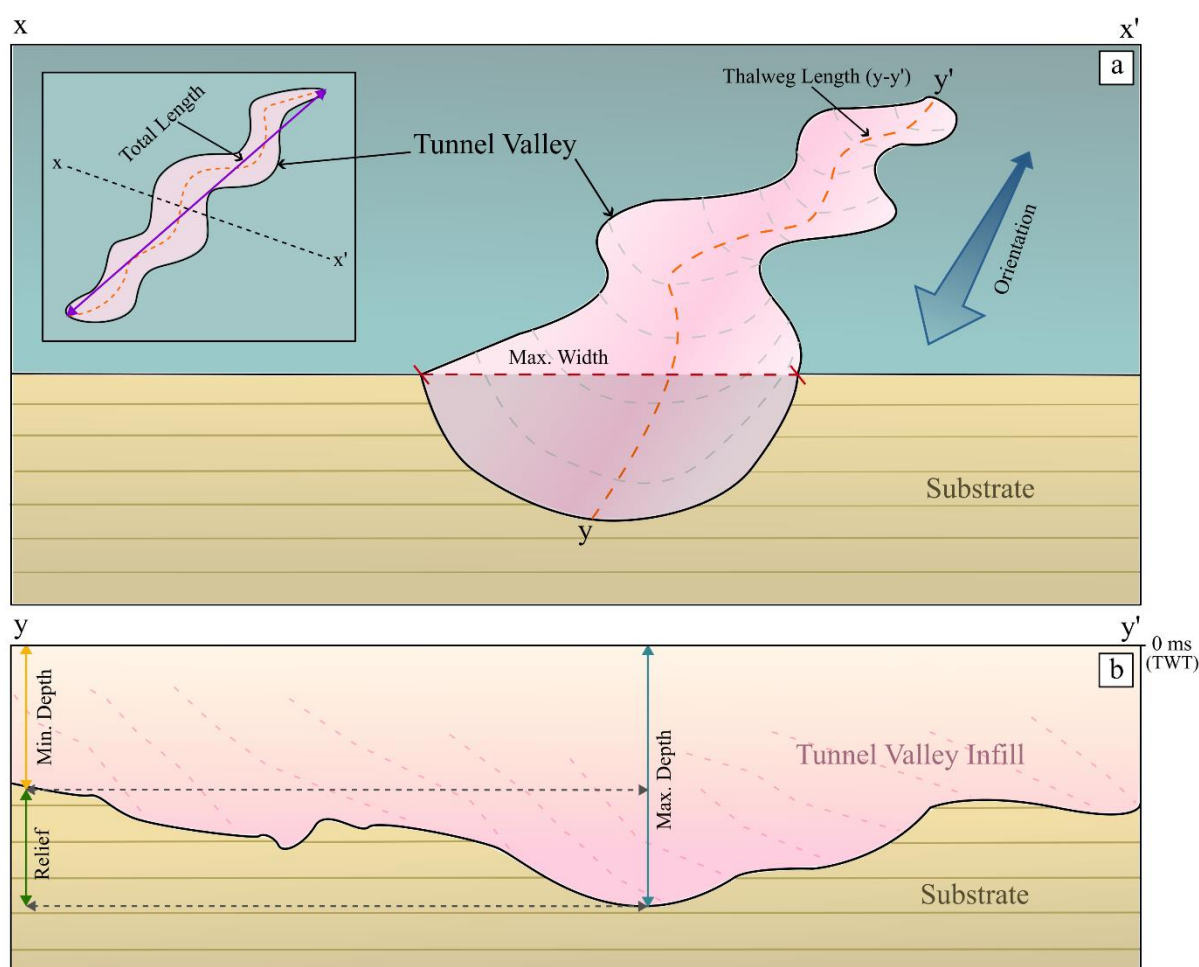


**Figure 6.2:** Summary of morphological measurement method **a**. Illustrative figure of a tunnel valley in cross-section and in map view showing where the morphological data is measured and how orientation is read. **b**. cross-section of tunnel valley along the thalweg showing the different morphological measurements regarding depths and reliefs.

## 6.5 Velocity model

To better understand the size of and relationship between tunnel valleys, it is necessary to create a velocity model to convert two-way time depth [TWT ms] to depth [m]. A ‘layer-cake’ velocity model was created using a sonic log from the 4/4-1 well (Fig. 6.3). The model was divided into layers where the velocities changed drastically, with more attention to detail in the shallow section as it is the focus of this thesis. Unfortunately, the data quality in the shallow section is poor, thus an average velocity of 1800 m/s is assigned to the top 100 metres. This is justified by the likely high water-content of the unconsolidated sediments in this section in addition to similar studies on the shallow subsurface in the North Sea (e.g. Huuse & Lykke-Andersen, 2000; Kirkham et al., 2024b). A velocity of 1500 m/s is used for the water column.

To use the velocity model to calculate time depth in milliseconds (TWT) to depth in metres (d) the following Equation 2 is applied where  $v$  is the average velocity of the interval in metres per second.

**Equation 2:**

$$TWT = \frac{d * 2}{v} * 1000$$

The water column has a thickness of 62 metres at the well position and measurement time (though the thickness of the water column will vary across the site), and by using the formula above, the resulting TWT depth is -82 ms (Fig. 6.3). An important term in offshore wind is the foundation zone which spans 100 meters below the seabed (Fig. 6.3). By using this velocity model, the base of the foundation zone can be found at -194 ms TWT and is applied in this thesis to visualise geology in the shallow subsurface that might be problematic for seabed installations.



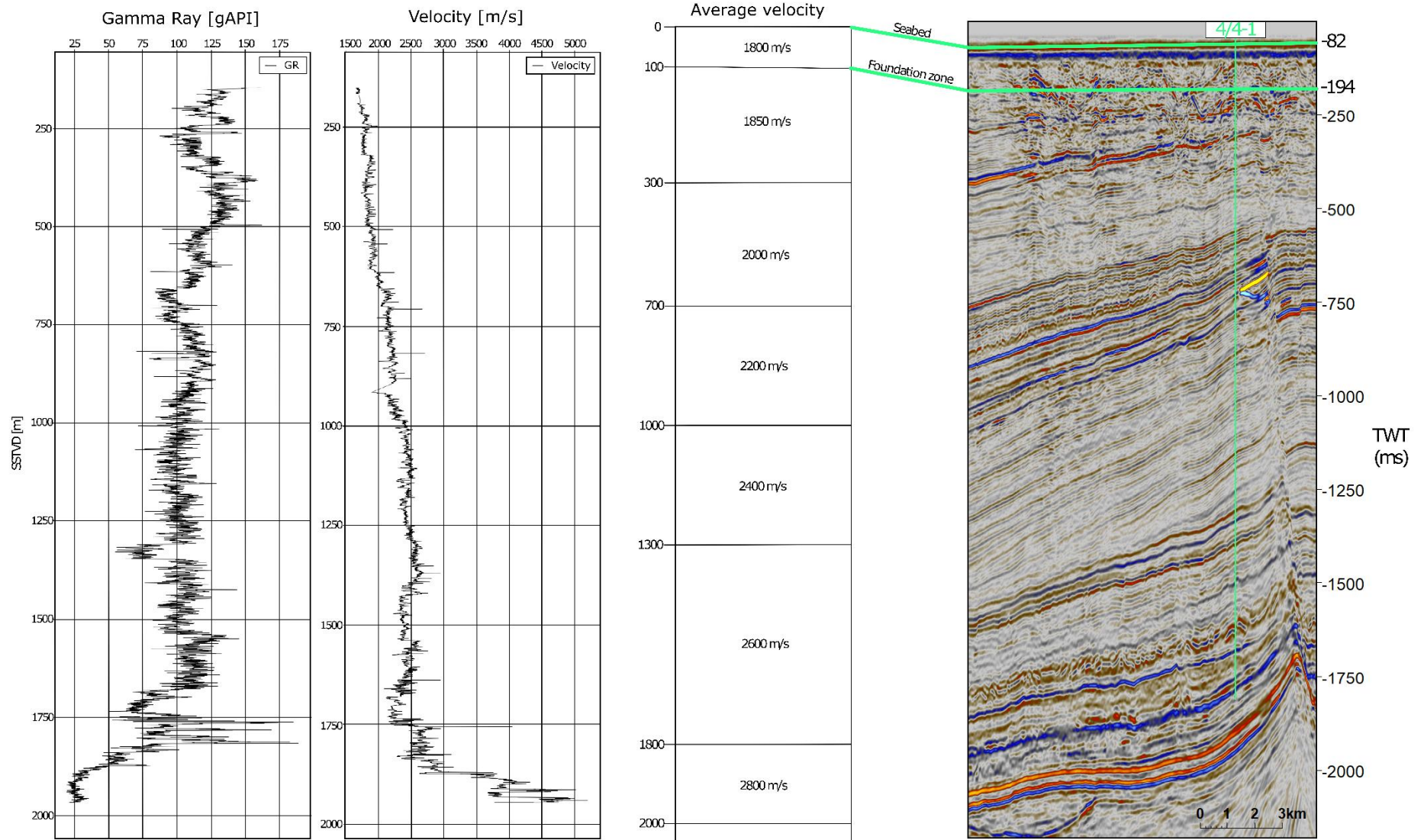


**Figure 6.3:** Velocity model including (from left to right) gamma-ray log, sonic log, layer cake with average velocities and seismic section with well 4/4-1 displayed, TWT in milliseconds and depth in metres correlated for the seabed and the foundation zone (100 m).

## 6.6 K-means clustering

The K-means clustering algorithm is used to uncover groupings in the geomorphological data collected on tunnel valleys to minimise the amount of personal bias on tunnel-valley generations. Some authors believe that tunnel valleys of the same generations share some of the same characteristics, like orientation and depth (e.g. Stewart et al., 2013). Thus, the k-means clustering algorithm is tasked with dividing the mapped tunnel valleys into groups based on these characteristics. The algorithm is a type of machine learning and can be executed using the Python programming language and the Spyder 5.2.2. environment. The full code can be found in Appendix 1. Step 1 is to import the Python libraries, which in this case are Pandas, StandardScaler, Numpy, Matplotlib, and KMeans. The first three are for reading the excel file, standardising the data, carrying out computations, and plotting the data, respectively, while the KMeans library has the algorithm used for the analysis. Step 2 is to import the data (Fig. 6.4a), which in this case are the numerical columns ‘Relief’, ‘Orientation’ and ‘MaxDepth’, that are described in detail in chapter 6.4. After importation, the data is standardised using the StandardScaler library. In Step 3 Scikit-Learn is used to perform the k-means analysis by first choosing the number of clusters, then fitting the model to the data. The number of clusters chosen in this thesis is 5 based on the number of levels in the relative age hierarchy described in the results chapter. Step 4 consists of extracting the centroid (centre of cluster) for each cluster (Fig. 6.4b, c, d) to use in Step 5 where the results of the k-means analysis is visualised. In Step 5 mainly the Matplotlib library is used to plot a scatterplot where each tunnel valley is assigned a colour indicating clusters and their centroids. The resulting plot can be found in the results chapter.

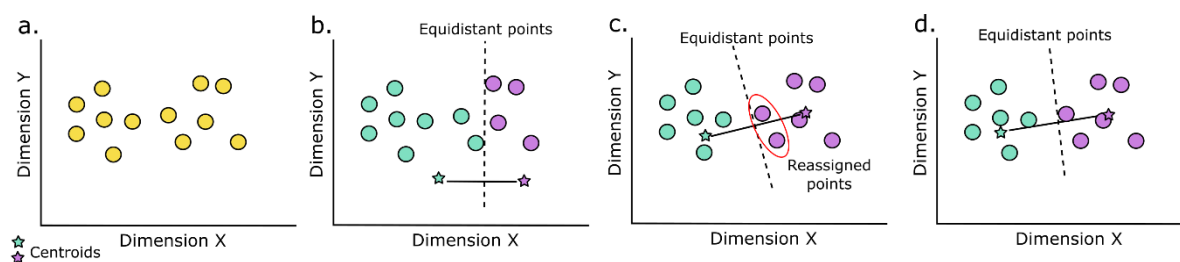


**Figure 6.4:** Step by step how on how k-means clustering divides data into groups. **a.** loading of data. **b.** choosing random centroids and fitting them to the data. **c.** reassigning points based on how they relate to the centroids. **d.** result of k-means clustering. Figure modified from (Muzhingi, 2020).

## Chapter 7 Results

The findings of this thesis will be described in the following order: the seabed and ‘base tunnel valleys’ surfaces, tunnel valley morphology analysis, cross-cutting relationships, k-means clustering, and finally the tunnel valley generations and proposed ice fronts.

### 7.1 Surfaces: Seabed and base tunnel valleys

The seabed in the study area ranges from time depths of c. -45 ms to c. -90 ms (c. 34-68 m) in the MC3D-MDB 2013 dataset and c. -50 ms to c. -120 ms (c. 38-90 m) in the MC3D-MDB 2008 dataset (Fig. 7.1). The change in maximum time depth thickness is mainly due to the incised structures shown with black arrows (Fig. 7.1). Overall, the seabed surface is shallower along the western and eastern perimeters of the study area, and deeper along the middle. In the 2013 dataset, the shallow area to the very west is the Greater Fish Bank (Fig. 7.1). The incised structures on the seabed are morphologically similar to tunnel valleys (see Fig. 4.3 on tunnel valley morphology), c. 0.5 km wide, and show signs of over-deepening; thus, they could be valleys from the last cold stage that are not yet filled.

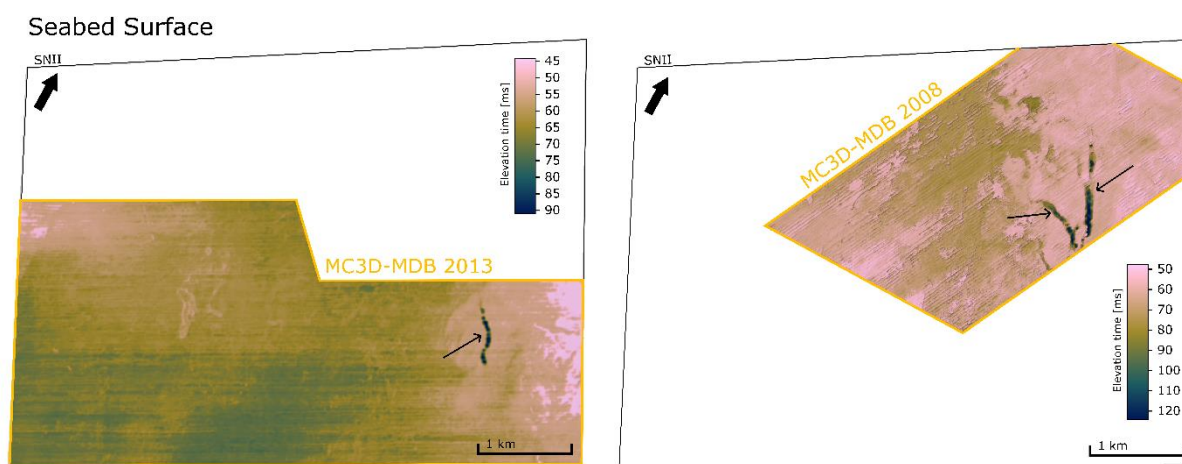


**Figure 7.1:** Seabed time depth surfaces from the two seismic datasets MC3D-MDB 2013 and 2008. Greater Fish bank is visible as a shallow area to the west in the 2013 dataset. 2-3 unfilled paleo valleys are visible on the seabed surface. Vertical exaggeration of 5.

The base of the tunnel valley surfaces ranges from c. -500 ms to c. 100 ms and corresponds to the mid-Pleistocene unconformity (Fig. 7.2a). This surface is only interpreted for the MC3D-MDB 2013 dataset due to its higher resolution of the shallow subsurface compared to the 2008 dataset. Most of the surface is covered in incised features that could represent either tunnel valleys or fluvial systems. Particularly shallow areas where the Base Tunnel Valleys surface comes close to the seabed can be found along the tunnel valleys TV4, TV2, and TV7 (Fig. 7.2a).

Along the southeastern border of the SNII site, between TV2 and TV1, there is a relatively deep section of the surface that shows signs of channel-like features striking northwest to southeast (Fig. 7.2a). The northeastern section of the surface is without deeply incising valleys except for TV1 (Fig. 7.2a). In seismic section b-b', the surface of the base tunnel valleys is frequently shallower than the 100-metre foundation zone, especially where there are valley shoulders of larger tunnel valleys (Fig. 7.2b). Seismic anomalies can be seen between and over TV16 and TV36c, with a pull-down-zone disturbing the seismic imaging below (Fig. 7.2). Multiples are present below several of the valleys in the seismic section, one example being below TV4 (Fig. 7.2b).

Base Tunnel Valleys Surface

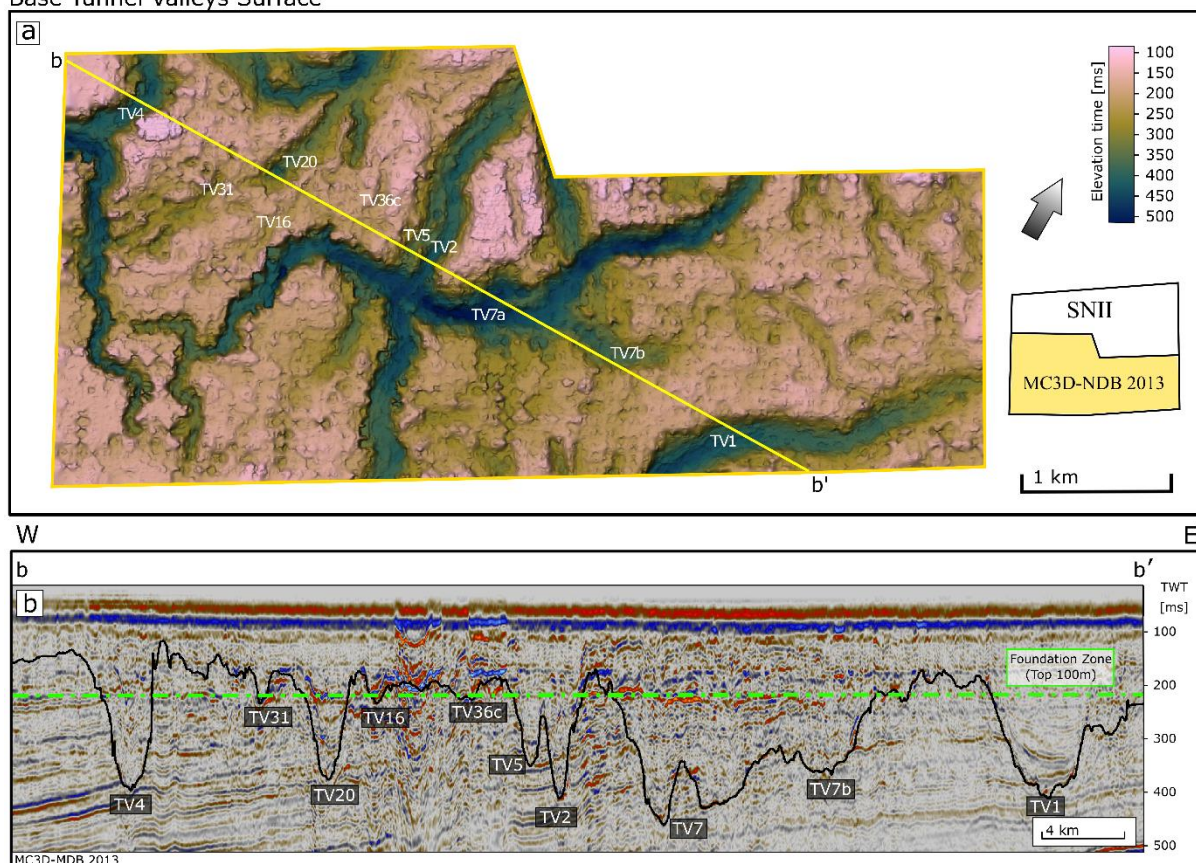


**Figure 7.2:** Overview of the Base Tunnel Valleys surface. **a.** Time depth surface for the base tunnel valleys. **b.** Seismic line b-b' where black line is the base tunnel valley surface. (Edit colour and placement of foundation zone line)

## 7.2 Tunnel valley morphology

A total of 45 potential tunnel valleys are identified inside the borders of the study site using 3D seismic data and seismic 3D interpretation. 3D time depth surfaces are created for each tunnel valley, and they are named from TV1 through TV37 (Fig. 7.3). The colormap for each tunnel valley is adjusted individually, with darker colours indicating deeper areas on the time-depth surfaces and lighter colours indicating shallower areas. The colormaps are adjusted individually for each tunnel valley, so they are not comparable to each other.

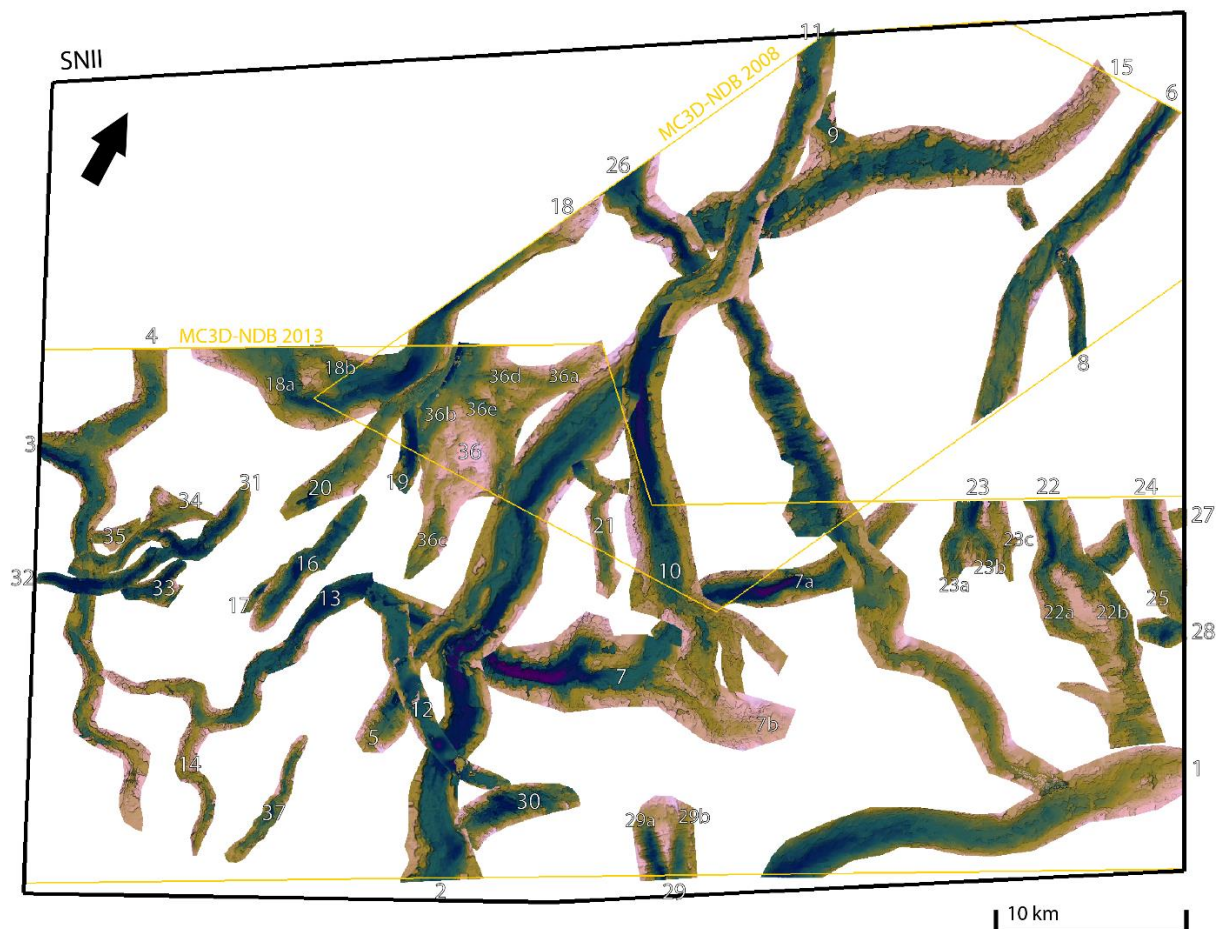


**Figure 7.3:** The 45 mapped tunnel valleys within the two seismic datasets MC3D-MDB 2013 and 2008. Study area SNII framed in black.

In this chapter, all interpreted tunnel valleys are compared to the list of diagnostic features proposed in Chapter 4.3 (Tunnel valley morphology) to investigate whether they fit the criteria and to describe their morphology. Firstly, all 3D-interpreted tunnel valleys are completely buried and incise into underlying stratigraphy at time depths ranging from 200 to 522 ms TWT (180 to 483 mbsl) at the deepest points of the valleys (Table 7.1). TV7 (a and b) incises the deepest of the valleys, with TV3 and TV15 coming second and third (Table 7.2 found at the end

of this sub chapter). TV21 has the shallowest maximum depth of the interpreted valleys, but interpretation became increasingly difficult closer to the seabed (top c. 200 ms TWT), meaning that just as shallow or shallower valleys likely are more common. The widths measured at the widest part of each valley range from c. 0.5 to 2.85 km (Table 7.1), where 14 valleys are narrower than 1 km. Of these 14 valleys, five are narrower than 0.8 km (measured at their widest part). The widest of all the interpreted tunnel valleys is TV2, and the narrowest valley is TV17 (Table 7.2).

**Table 7.1:** Morphology measurements from all mapped tunnel valleys summarised with maximum, minimum and mean values for each measurement.

Measurement	Minimum	Maximum	Mean
Max. Depth (Thalweg) [ms TWT]	200	522	330
Max. Width [km]	0.50	2.85	1.36
Total Length [km]	2.35	38	10.84
Thalweg Length [km]	2.30	41	11.75
Sinuosity	1.003	1.264	1.077
Min. Depth (Thalweg) [ms TWT]	156	358	247
Relief (Thalweg) [ms TWT]	24	233	84
Orientation [°]	87	240	174

Many interpreted valleys in this thesis are limited by the extents of the 3D seismic datasets, which especially impact the measured lengths for each valley. The maximum measured length of an interpreted valley (straight line from a to b) is c. 38 km (TV26), but the valley is cut off in the north of the site. All interpreted tunnel valleys that are limited by data are marked with an asterisk (\*) in Table 7.2. The shortest interpreted tunnel valley is measured at 2.3 km, which is TV35. In addition to the total length of each valley, the length of the thalwegs is measured and ranges from 2.3 km to 41 km (Table 7.1), where all thalweg lengths are either equal to or longer than the total length of the valleys. This is reflected by the sinuosity values that range from 1.003 to 1.264 (Table 7.1), because sinuosity is calculated by dividing the thalweg length by the total length for each valley, meaning that all numbers above 1 indicate some sinuosity (curving of the valley). The least sinuous valleys are TV20 and TV23c, and the most sinuous valley is TV18.

Possibly the most frequently mentioned diagnostic feature of a tunnel valley is the nature of the thalweg. Most of the interpreted tunnel valleys show some degree of over-deepening, and a good example of this is TV2, where the thalweg is significantly deeper in the middle of the valley than up- and down-valley (Fig. 7.4). The difference in ms between the minimum and maximum measured depths of the thalwegs shows how much internal relief each valley interpretation has and ranges from 24 to 233 ms TWT (22-216 m) (Table 7.1), where shorter and narrower valleys have less internal relief than the larger valleys. TV7b and TV18 both have internal relief of the thalweg of over 200 ms TWT (185 m) and are also two of the widest and deepest incising valleys. The shallower incising valleys that are generally shorter and narrower also have the smallest internal relief, which includes valleys like TV36 (a, b, c, d, e) and TV12.

All interpreted tunnel valleys are within what is believed to be the limits of the last three glaciations, Elsterian, Saalian, and Weichselian, and they have orientations plausible to have been perpendicular to the icefronts during ice sheet retreat. The orientations of the interpreted valleys could have been measured generally south-easterly or north-westerly, whereas the latter was chosen so the orientation arrows could point in the drainage direction. The interpreted valleys have measured orientations from 87 to 240°, meaning they span between south-easterly and south-westerly extremes, with the mean direction of the valleys almost exactly south (174°). The orientations of the valleys, in addition to the maximum widths, maximum depths, and internal relief of the thalweg, are chosen to be the most defining measured features of the tunnel valleys interpreted. The thalweg length and total length for each tunnel valley (and, as a result, sinuosity) are strongly limited by the extent of available data and would skew comparisons between the valley measurements.

Several of the valleys split into two, and a few merge back together after splitting. Common to the larger valleys that diverge is that one of the branches is much shallower than the other, indicating that one is the main valley and the other could have been created later and/or is cutting into the first. There are several examples of this in the interpreted tunnel valleys, one of which is where TV5 branches out from TV2. In this case, TV5 is smaller and shallower and can be followed into TV2 as a shelf along the western side of the valley (Fig. 7.4a, d). This could indicate that TV5 was created after TV2 was partly filled with sediment by a readvance of ice with less erosive power. A different example of a tunnel valley splitting but also re-merging is in TV 18, where an internal sill splits the valley into TV18a and TV18b before they shortly merge again after c. 4 km (Fig. 7.3). The internal sill could be harder to erode than the surrounding strata. The third way is when two similarly sized valleys emerge from one with

only a slight sill that indicates which one is a “different” valley. Examples of this are TV13 and TV14, and TV22a and TV22b, where TV14 and TV22 are slightly shallower and likely created secondarily to TV13 and TV22a, though likely not by much (Fig. 7.3). Anastomosing patterns are present where valleys diverge and re-merge again in a complex pattern, which is true for TV31 - TV34 (Fig. 7.3). It is not possible to see this type of pattern in the larger valleys that are interpreted, but data limitations could be the cause.

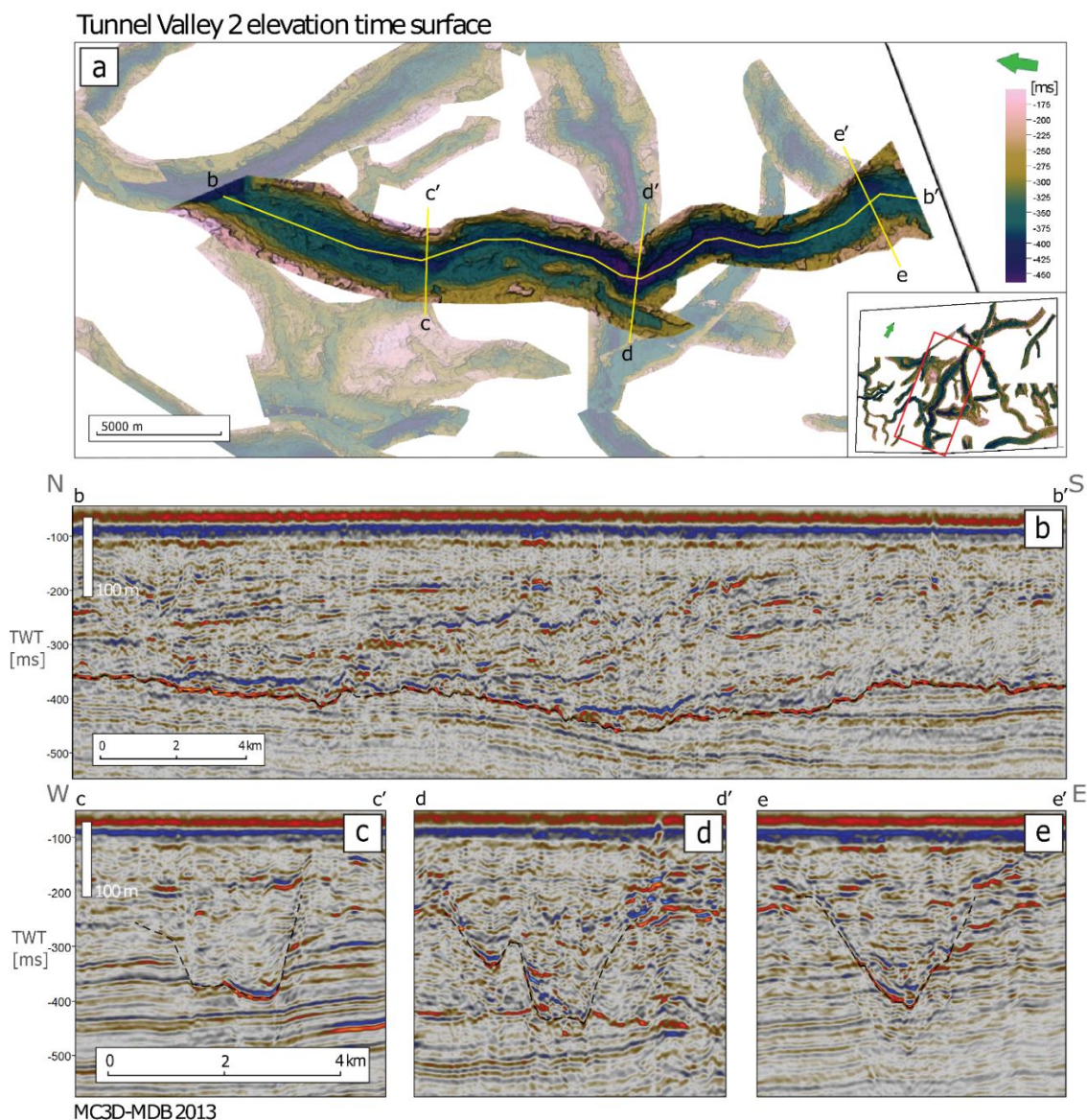


**Figure 7.4:** Summary TV2 time elevation surface and seismic geometries **a.** Map view of TV2 and surrounding mapped valleys showing the placement of the cross-section both along and perpendicular to the valley thalweg. **b.** Seismic line b-b' along the deepest part of the valley thalweg. Black stippled line marking the base of the valley. **c.** Seismic cross-section c-c' perpendicular to the thalweg. **d.** Seismic cross-section d-d' perpendicular to the thalweg. **e.** Seismic cross-section e-e' perpendicular to the thalweg.



To the west of TV2, the valleys are generally smaller, with higher sinuosity that shows a general drainage direction towards the south (Fig. 7.3). The valleys in this section also show two cases where a valley with a general orientation of c.  $200^\circ$  (TV4 and TV13) is cut or cuts into a valley with a general orientation of c.  $150^\circ$  (TV3 and TV14). To the east of, and including, TV2, the pattern of valleys shows several different drainage directions of the larger valleys (Fig. 7.3). Wide and deep valleys like TV1, TV7 (a and b), and TV 15 are oriented more towards the west than the others in the section and are also frequently cut into by other valleys. Another set of wide and deep valleys is oriented towards the south, including TV2, TV10, TV11, and TV6, and the remaining slightly smaller and slightly shallower valleys have a general orientation towards the south-east. To summarise, the interpreted tunnel valleys can be divided into five sets depending on the general drainage patterns and directions. Where tunnel valley terminations are present within the study area, they are abrupt and difficult to map as they are closer to the seabed.

**Table 7.2:** Overview of all morphological measurements for each mapped tunnel valley.

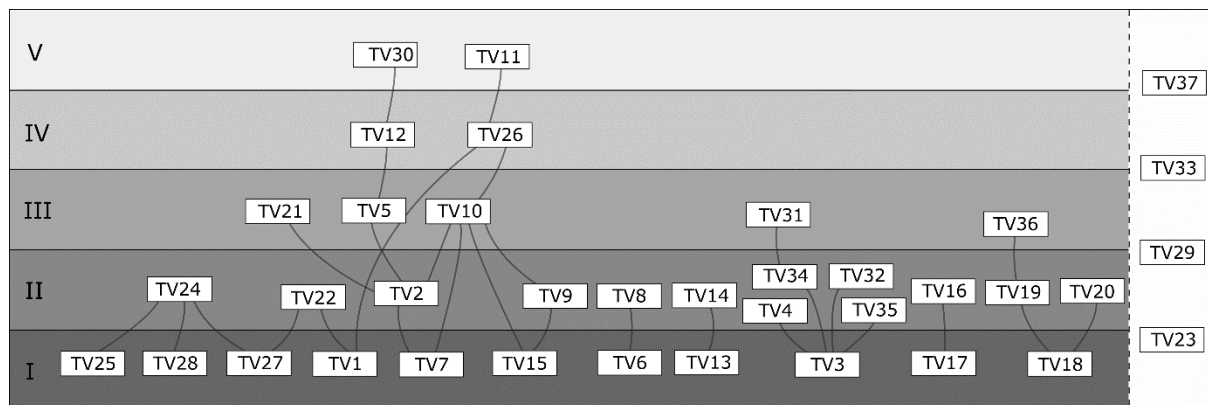
<b>TV</b>	<b>Thalweg Length [km]</b>	<b>Total Length [km]</b>	<b>Max. Width [km]</b>	<b>Min.Depth [ms TWT]</b>	<b>Max.Depth [ms TWT]</b>	<b>Sinuosity</b>	<b>Relief [ms TWT]</b>	<b>Orientation [°]</b>
TV1*	21.8	21.4	2.3	262	447	1.024	185	225
TV2*	28.7	27	2.85	355	459	1.063	104	180
TV3*	23	20	1.35	310	477	1.15	167	145
TV4*	7.4	6.4	1.7	355	424	1.156	69	200
TV5	14.2	13.8	1.15	277	363	1.03	86	195
TV6*	18.6	18	1.63	331	402	1.031	71	185
TV7*	32.1	27.7	2.2	358	522	1.157	164	225
TV8*	9.4	9.1	0.9	246	383	1.041	137	135
TV9	3.6	3.3	1.8	342	389	1.1	47	130
TV10*	38.4	33.9	2.2	261	447	1.13	186	150
TV11*	17.1	16.4	1.4	246	319	1.045	73	177
TV12	11.5	11.1	1.2	236	270	1.036	34	115
TV13	17.3	13.9	1	279	427	1.25	148	205
TV14	7.7	6.5	0.85	316	359	1.179	43	155
TV15*	24.2	23.5	2.5	298	464	1.028	166	230
TV16	8.5	8.4	1.2	182	252	1.006	70	200
TV17	3.3	3.1	0.5	194	240	1.08	46	210
TV18*	21.1	16.7	1.9	230	447	1.264	217	225
TV19*	8.3	7.9	1	298	359	1.046	61	165
TV20*	12.1	12.1	1.4	292	345	1.003	53	200
TV21	7.1	6.6	0.9	156	200	1.078	44	150
TV22a*	9.3	8.7	1.5	201	307	1.075	106	140

Table 7.2 continued:

<i>TV</i>	<i>Thalweg Length [km]</i>	<i>Total Length [km]</i>	<i>Max. Width [km]</i>	<i>Min.Depth [ms TWT]</i>	<i>Max.Depth [ms TWT]</i>	<i>Sinuosity</i>	<i>Relief [ms TWT]</i>	<i>Orientation [°]</i>
<i>TV22b*</i>	11.3	10.7	1	215	271	1.055	56	132
<i>TV23a*</i>	3.9	3.7	1.25	255	323	1.047	68	165
<i>TV23b*</i>	3.6	3.5	1.25	250	321	1.035	71	145
<i>TV23c*</i>	4.1	4.1	0.8	207	254	1.003	47	150
<i>TV24*</i>	5.9	5.7	1.95	208	253	1.025	45	132
<i>TV25</i>	3.5	3.2	1.4	224	270	1.079	46	140
<i>TV26*</i>	41.2	38.1	2.4	223	362	1.082	139	115
<i>TV27*</i>	5.4	5.1	1.5	213	262	1.06	49	225
<i>TV28*</i>	2.4	2.3	1.4	217	258	1.014	41	240
<i>TV29a*</i>	2.8	2.8	1.8	242	309	1.011	67	135
<i>TV29b*</i>	3.4	3.3	0.9	208	279	1.008	71	155
<i>TV30</i>	6.4	6.3	1.7	230	289	1.012	59	225
<i>TV31</i>	7	5.7	1	224	313	1.239	89	205
<i>TV32</i>	8.1	7.2	0.75	272	329	1.119	57	235
<i>TV33</i>	4.2	3.5	0.7	274	320	1.199	46	225
<i>TV34</i>	7.2	7	0.8	218	278	1.04	60	205
<i>TV35</i>	2.5	2.3	0.6	226	261	1.073	35	225
<i>TV36a*</i>	10	9	1.1	179	245	1.103	66	185
<i>TV36b*</i>	6.5	6.5	0.9	219	243	1.009	24	195
<i>TV36c</i>	8	7.8	1.1	170	235	1.035	65	180
<i>TV36d</i>	8.5	8.3	0.8	184	253	1.02	69	90
<i>TV36e</i>	9.3	7.6	0.9	185	240	1.211	55	90
<i>TV37</i>	7.7	7.2	0.7	183	218	1.068	35	180

### 7.3 Cross-cutting relationships

The tunnel valley surfaces in Figure 7.3 are interpreted in three dimensions, making it possible to discern cross-cutting relationships between certain valleys. A relative age hierarchy can be achieved by systematically noting which valley cuts into or overlies another valley. The result is shown in Figure 7.5, where five levels of relative age are shown, with ‘I’ being the oldest and ‘V’ being the youngest. The four valleys in the right column are without any cross-cutting relationships (Fig. 7.5). The valleys without any cross-cutting or overlying valleys constraining their age are assumed to be younger than all valleys on the levels below that are connected with black lines (Fig. 7.5). Using only the valley’s cross-cutting relationships limits any relative age prediction to the valleys that are in the same network. For this instance, it means that TV6 is older than TV8 based on the latter cutting into the former. The two valleys’ relative age to all the other valleys in the area is unknown. The valleys on level ‘I’ are all older than all the connected valleys on the levels above (Fig. 7.5), but it is important to note that TV27, TV1, TV7, and TV15 are not necessarily the same age. This is true for the valleys at all levels of the relative age hierarchy.



**Figure 7.5:** Mapped tunnel valleys placed in a relative age hierarchy based on cross-cutting relationships where I are the relatively oldest valleys and V are the relatively youngest valleys. In the column to the far right are tunnel valleys without cross-cutting relationships. The lines connecting the valleys show which valleys cut into which.

## 7.4 K-means clustering

The goal of the k-means clustering is to divide the interpreted tunnel valleys into groups (clusters) of valleys that are similar to each other (Fig. 7.6a). It is useful to know which valleys have similar geomorphological features because valleys of the same generation often look alike and are largely oriented in the same direction (Praeg, 2003). A wide range of data is collected from the tunnel valley surfaces, but some measurements have more potential limitations than others, making them less suitable for analysis. Most of the tunnel valleys interpreted are limited by the extent of the data used to interpret them, and their real length is likely much longer than what is measured. For this reason, both length measurements and sinuosity (a product of the length measurements) are removed from the k-means clustering.

The depths measured in TWT are also limited by data extent, but the maximum incision depths of the valleys are important to differentiate between the valleys, so both the maximum depth and the thalweg relief are included in the clustering analysis. The minimum depth data are excluded because several of the smaller valleys as well as the larger valleys that terminate within the study area have the shallowest sections of the thalweg limited by the resolution of the seismic data, thus the measurements are less reliable than those of the maximum depths, where the base erosive reflectors in the deepest parts of the valleys have high amplitudes. The last type of data included in the clustering analysis is orientation, which is an important characteristic for dividing tunnel valleys into generations as orientation is perpendicular to the ice front (Praeg, 2003).

The result of the clustering analysis is five clusters of tunnel valleys that have similar maximum depths, thalweg reliefs, and orientations. The clusters are shown in Figure 7.6, with the mean measurements summarised for each. Cluster 1 (C1) includes five tunnel valleys that are wide, incise deeply, and have a general direction towards the southwest (Fig. 7.6b). C1 has the highest mean thalweg relief, meaning it is the cluster of valleys with the most prominent over-deepening. The shape of the valleys in this cluster is relatively straight, with long, softly bending valley walls, except for TV13, which has a higher sinuosity. All the tunnel valleys in C1 exceed the limits of the 3D seismic data, except for TV13. Cluster 2 (C2) includes 10 valleys of various sizes, with orientations generally towards the south (Fig. 7.6c). Compared to the valleys in C1, the C2 valleys are narrower and have less internal relief of the thalweg.

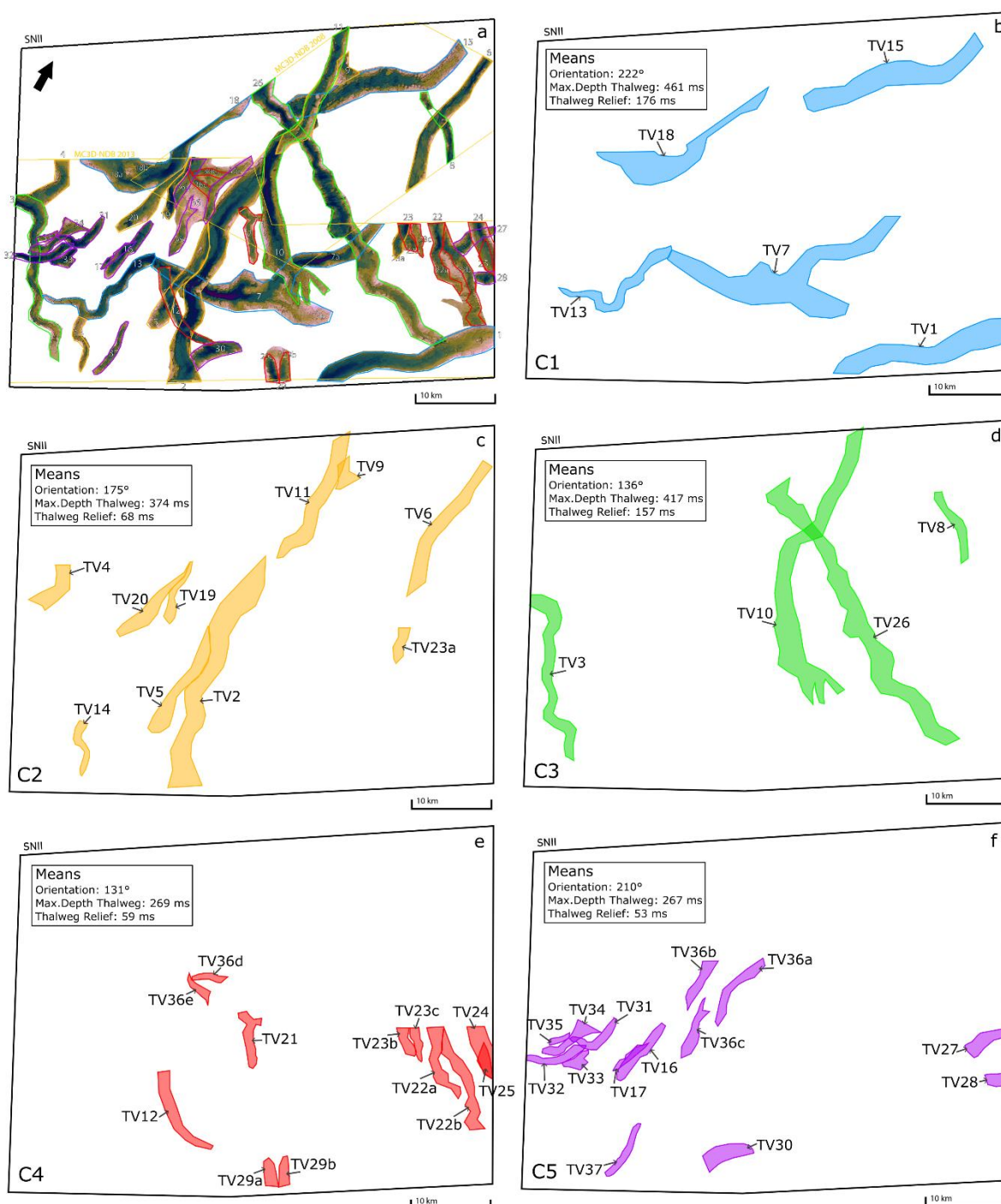


**Figure 7.6:** Result of the *k*-means clustering with polygons in respective colours represent the valleys in each cluster, and the means for each morphological measurement and the orientations of the valleys are summarised for each cluster.

Cluster 3 (C3) includes four tunnel valleys that are oriented towards the east-southeast (Fig. 7.6d). All exceed the limits of the data, but TV11 and TV3 both terminate towards the southern end of the valleys. The valleys in C3 are the second deepest incising after C1 and have the second largest mean internal relief of their thalwegs. Cluster 4 (C4) includes 12 tunnel valleys

that are significantly shallower than the tunnel valleys in C1, C2, and C3 (Fig. 7.6e). C4 has valleys oriented towards the east-southeast, and several of the valleys come in pairs, either merging or separating from each other. The last cluster is cluster 5 (C5) and includes 14 tunnel valleys that incise to the same depth as those of C4 (Fig. 7.6f). There is an 80° difference between the valleys in C4 and C5, with the latter having a mean orientation towards the southwest. The valleys in C5 are relatively straight and short, and the highest density of C5 valleys is in the southwestern section of the study area. On the contrary, the C4 valleys are most common in the southeastern section.

## 7.5 Tunnel valley generations and icefronts

Tunnel valleys that are created at the same time by the same ice sheet are called a generation, and by combining the results from the k-means clustering and the cross-cutting relationships (Fig. 7.7), six generations can be proposed for the mapped valleys in the study area, where G1 is the oldest and G6 is the youngest (Fig. 7.8). The clusters were used as a starting point for each generation and adjusted to fit the cross-cutting relationships of the valleys. Each of the generations shown in Figure 7.8 is made up of tunnel valleys with similar orientations. Three of the generations only have tunnel valleys from the same cluster (G1, G2, and G6), while the rest have a mix of two to three clusters. C2 has tunnel valleys in three of the six generations, but none in the oldest or youngest. The proposed ice front placement based on the orientation of tunnel valleys in each generation is shown in Figure 7.9.

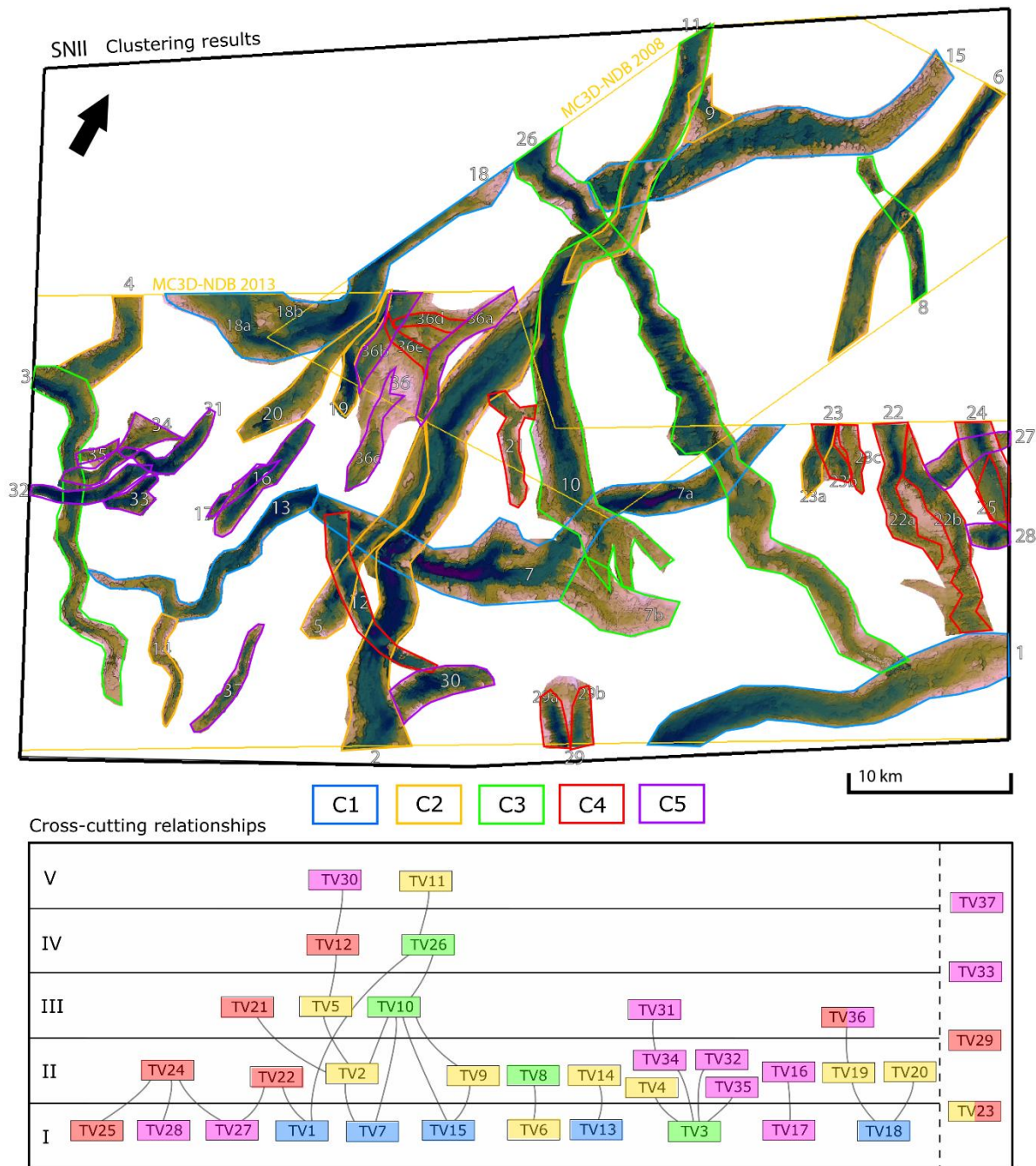
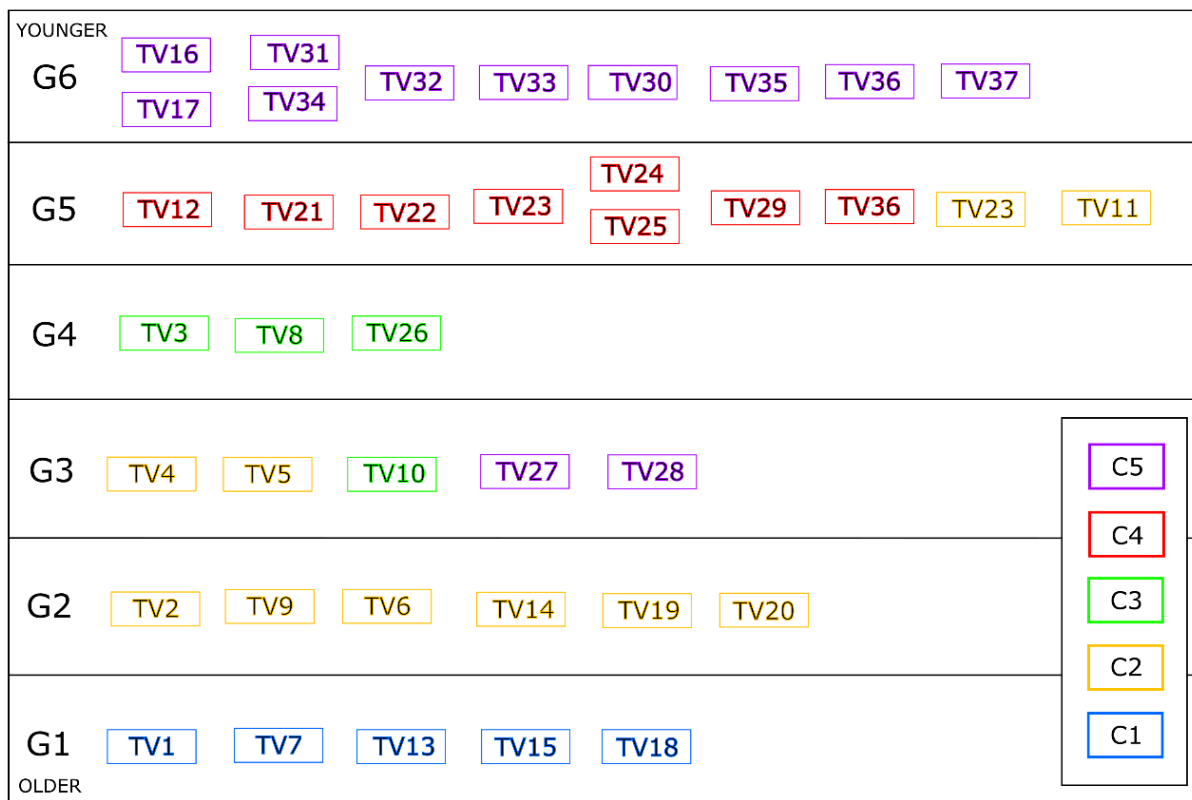


Figure 7.7: Comparison of the results of the clustering analysis and cross-cutting relationship analysis.





**Figure 7.8:** Tunnel valley generations from oldest (G1) to youngest (G6) where the colours of the tunnel valleys correlate to the clustering results in Fig. 7.6. The tunnel valleys are ordered from smallest numbers starting to the left in each generation, and for each cluster within a generation. Cross-cutting relationships within one generation is present where valleys are stacked.

Generation 1 (G1) is the oldest generation of tunnel valleys, including all C1 valleys, and is cut by and/or overlain by all younger generations except for G6 (Figs. 7.7, 7.8). The valleys in G6 do not exist over G1 valleys, so no direct relationship can be observed (Fig. 7.7). G1 has a mean orientation towards the southeast and is the most easterly-oriented generation. It also included the deepest incising and widest valleys with the highest sinuosity. They are not the longest valleys measured inside the SNII area, though as they are limited by the available data, it is plausible that they are much longer than what is mapped. G1 is present across the whole of the study area and does not prefer certain sectors more than others. The proposed ice front for G1 indicates ice retreat towards the northeast based on the mean orientation of the tunnel valleys (Fig. 7.9).

Generation 2 (G2) is the second-to-oldest generation of tunnel valleys and only includes valleys from C2, though not all C2 valleys are in G2 (Figs. 7.7, 7.8). The G2 valleys are either cut or overlain by all younger generations, and several of the valleys in G2 are branching out from or

into the G1 valleys (Fig. 7.7). This could mean that this second generation came before the G1 valleys were entirely filled with sediment. G2 has a mean direction towards the south and has widths, depths, and lengths that land neither on the upper nor lower end of the spectrum. Where the valleys in G1 were like each other, the valleys in G2 are diverse in size and shape. Three of the valleys end inside the study area without terminating in another valley; these are also the narrowest of the generation. The proposed ice front for G2 indicated ice retreat towards the north based on the mean orientation of the tunnel valleys (Fig. 7.9).

Generation 3 (G3) includes valleys from C2, C3, and C5 and is cut and/or overlain by both G4 and G5 (Figs. 7.7, 7.8). As a result of the generation being a mix of three different clusters, it is the most morphologically diverse of the six. Similarly to G2, the valleys are neither the widest, longest, deepest, nor the narrowest, shortest, or shallowest, and they have a mean direction towards the south-southwest. This mean direction is, however, heavily influenced by the presence of TV10, which deviates significantly (c. 50°) from the other valleys regarding orientations. The mean direction would be like that of G1 (southwest) without TV10. All G3 valleys are either cut short by other valleys or terminate on their own within the study area. One valley, TV10, comes to the centre of the area and branches into three smaller valleys right before terminating. This is a rare case where a large valley's termination is clearly mapped in this study. The proposed ice front for G3 indicates ice retreat towards the north based on the mean orientation of the tunnel valleys (Fig. 7.9).

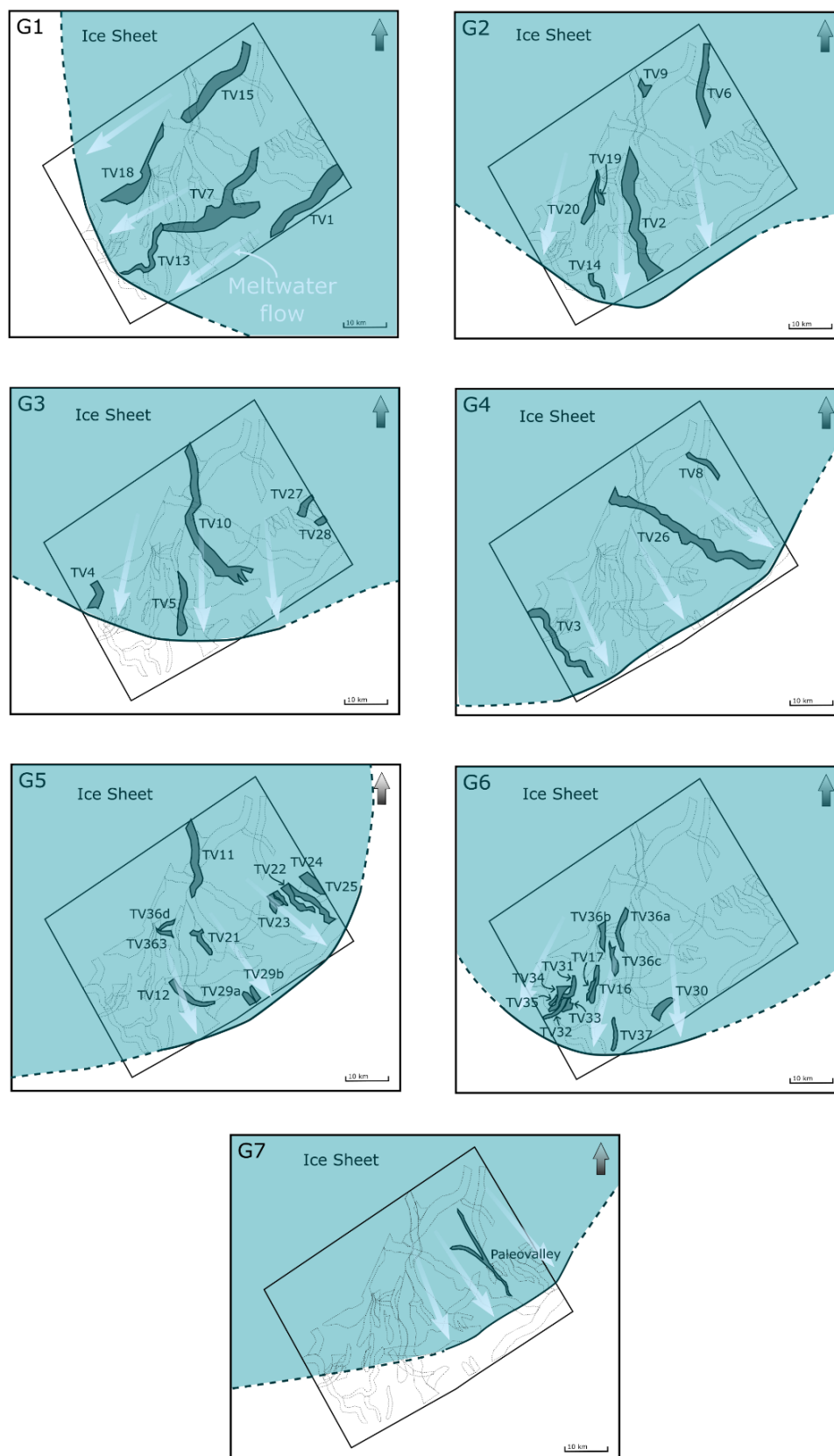


**Figure 7.9:** Tunnel valley generations with interpreted ice front placement during formation based on their orientations and occurrence within the SNII site. Solid line is supported by tunnel valley interpretations and stippled line is an interpreted continuation. The age of the tunnel valleys decreases from G1 to G7. Arrows show main meltwater flow direction.

Generation 4 (G4) only includes valleys from C3 and is cut and/or overlain by both younger generations, G5 and G6 (Figs. 7.7, 7.8). G4 has a mean direction towards the southeast and have the second-to-deepest incising valleys, which results in them cutting many older valleys. The amount of meandering in the valleys increases towards the south, as does the sinuosity value. This could indicate that the substrate to the south is different from that in the northern section of the study area. The proposed ice front for G4 indicates ice retreat towards the northwest based on the mean orientation of the tunnel valleys (Fig. 7.9).

Generation 5 (G5) includes valleys from both C2 and C4, although most valleys are from the latter (Fig. 7.8). G5 valleys are either cut and/or overlain by G6 valleys, both of which have significantly shallower incising, narrower, and shorter valleys than the four older generations (Fig. 7.7). The valleys generally come in pairs of two, are absent from the southwestern section of the study area, and have a mean direction towards the southeast. TV 11 sticks out regarding both width and length and is possibly a result of meltwater finding the easiest area to erode to be inside a multigenerational tunnel valley. Both the beginnings and the terminations of the valleys in G5 are either difficult to interpret and/or limited by the extent of the data. The proposed ice front for G5 indicates ice retreat towards the northwest based on the mean orientation of the tunnel valleys (Fig. 7.9).

Generation 6 (G6) only includes valleys from C5 and is cut and/or overlain by valleys within G6 (Figs. 7.7, 7.8). The G6 valleys are only present in the very southwestern part of the study area, are short and shallow, and have a mean direction towards the southwest. Valleys from this generation might also exist in the northern section of the study area, but the data quality is significantly lower, so these small valleys are more difficult to map. The G6 valleys have a similar morphology to that of the G5 valleys, but the beginnings and terminations are largely within the data extent and data resolution. The proposed ice front for G6 indicates ice retreat towards the northeast based on the mean orientation of the tunnel valleys (Fig. 7.9).

A possible seventh generation G7 can be discerned from the seabed surfaces (Fig. 7.1), where several shallow paleo valleys are visible as partially unfilled longitudinal depressions. These two to three connected valleys have similar directions to those of G5 (southeast) but differ morphologically as they are shallower and narrower. The proposed ice front for G7 indicates ice retreat towards the northwest based on the mean orientation of the tunnel valleys (Fig. 7.9).

## Seismic geomorphology from RMS amplitude time surfaces

RMS amplitude time surfaces can bring forth geological information regarding sediment's acoustic impedance and geomorphology, which can be used to interpret sediment properties like grain size and pore fill. RMS time surfaces for -436 ms TWT show the outline for the deepest G1 and G2 valleys, where several have areas of high amplitude values along the valley base that can indicate coarser sediments as these often have higher acoustic impedances than, for example, silt (Fig. 7.10F). On the same time slice, only in Figure 7.11F, a high RMS value area is visible in the southwestern part of the study area. This correlates with the meandering and anastomosing patterns in the valleys that incise this substrate, different from the straighter and singular valleys common in most other parts of the area. Along the eastern border of the SNII area, there is an area of very high RMS values, shaped as a lobe with a straight edge to the south and curved towards the north. This is present on time slices F, E, and D in Figure 7.10 and coincides with the location of TV29a and b, although it covers a larger area. Two high RMS value ovals with a diameter of ~4 km are visible on all time slices except B; these correlate to the locations of two salt diapirs (Fig. 7.10).

On time slices E and D (-380 ms and -332 ms, respectively), G1 and G2 are clearer, and the valley fill has higher RMS amplitudes in the entirety of the valleys (Figs. 7.10, 7.11). The difference from -380 ms to -332 ms is a change from high to lower RMS amplitudes in G3 and G4 that might reflect their infill, and a similar change in G1 and G2 where the deepest parts of the valleys become darker than the surrounding areas, indicating smaller grain sizes like silt and clay. Outlines of both younger generations, G5 and G6, are visible on both time slices E and D, though these might be multiples that show up deeper than the actual valley floors (Fig. 7.10). Possible shallow gas is visible as rounded closed areas in TV2, TV26, and TV11 on time slice D (Fig. 7.11). In both time slices E and D, the middle of the time slices has higher RMS values than the northeast and southwest (Fig. 7.10).

Fan-shaped objects ranging in size from 2 km to 5.6 km wide with high RMS amplitudes splay out over and inside several tunnel valleys. On the small side of the range is a fan shape exiting TV26 into TV1 (Fig. 7.10D). A larger fan shape is present at the terminating slope of TV10, which is 3.5 km wide and splays out from a relatively narrow apex point in comparison to the rest of TV10 up valley (Fig. 7.10D). The two widest fan-shaped objects spill over TV7 and TV15 the former is present at -332 ms (Fig. 7.10D) and the latter at -212 ms (Fig. 7.11C). The high RMS values might indicate coarser sediments, like sand and gravel, shallow gas, or both.

Abnormally high RMS values are also visible within TV26 and along the side of TV18 on the same time slice. This time depth corresponds to the base of the 'foundation zone'.

On time slice C, a bright area is present above TV7, possibly related to the fan shape to the east, and particularly high RMS values are visible above the salt diapirs, which could be salt caps that have higher reflectivity and cause a stark impedance contrast (Fig. 7.10). Potential lake deposits are present on time slices B and C, supported by very high RMS values that can reflect strong impedance contrasts from dried out clayey deposits (Fig. 7.10), similar to those found at the Dogger Bank (e.g. Emery et al., 2019). The potential lake is 5.3 km long and 1.8 km wide and situated along the strike of TV7 (Fig. 7.10). The G5 and G6 valleys are visible at -212 ms as either bright or dark, where the valleys in the southwestern area are the brightest and those in the eastern area the darkest. Many of the G6 valleys are not visible on any time slice and might possibly exist between two slices.

The -120 ms time slices are close to the seabed reflector and show overall high RMS values across both seismic datasets (Figs. 7.9, 7.10). Narrow, meandering channel features form a network that spans from the north to the south in the middle and eastern parts of the SNII site (Fig. 7.10B). Some of the channel-like features are darker, which could indicate that they have a low amplitude contrast-with the underlying mud-rich substrate. These are also wider than the channel features and thus might be unmapped tunnel valleys. One such structure corresponds to the paleo valleys defined on the seabed surface as part of G7 (Figs. 7.10B, 7.11B). Channel features are present between the potential lakes, connecting smaller round anomalies with the larger structure (Fig. 7.10B). Some of the larger valleys from G1 and G2 are visible on the shallow time slices (B and C) as dark areas, potentially due to their upper infill having a low impedance contrast to the lower infill (Figs. 7.10, 7.11).

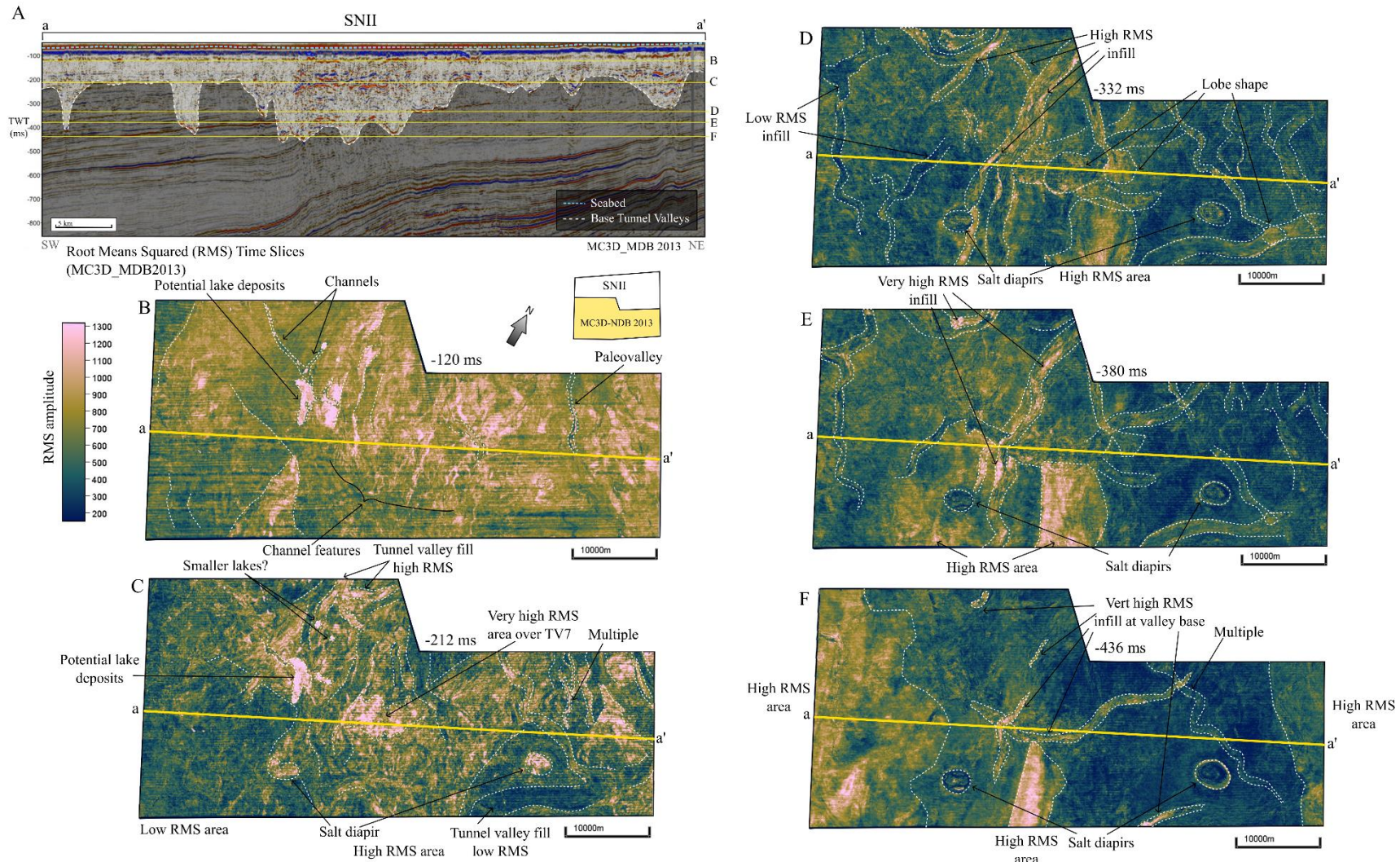


**Figure 7.10:** RMS amplitude time surfaces from MC3D\_MDB 2013. **A.** Seismic section showing the depths of all time slices in TWT and the interpreted seabed and base tunnel valleys surfaces. **B.** RMS time slice at -120 ms where seismic line a-a' is shown in yellow. **C.** RMS time slice at -212 ms. **D.** RMS time slice at -332 ms. **E.** RMS time slice at -380 ms. **F.** RMS time slice at -436 ms.

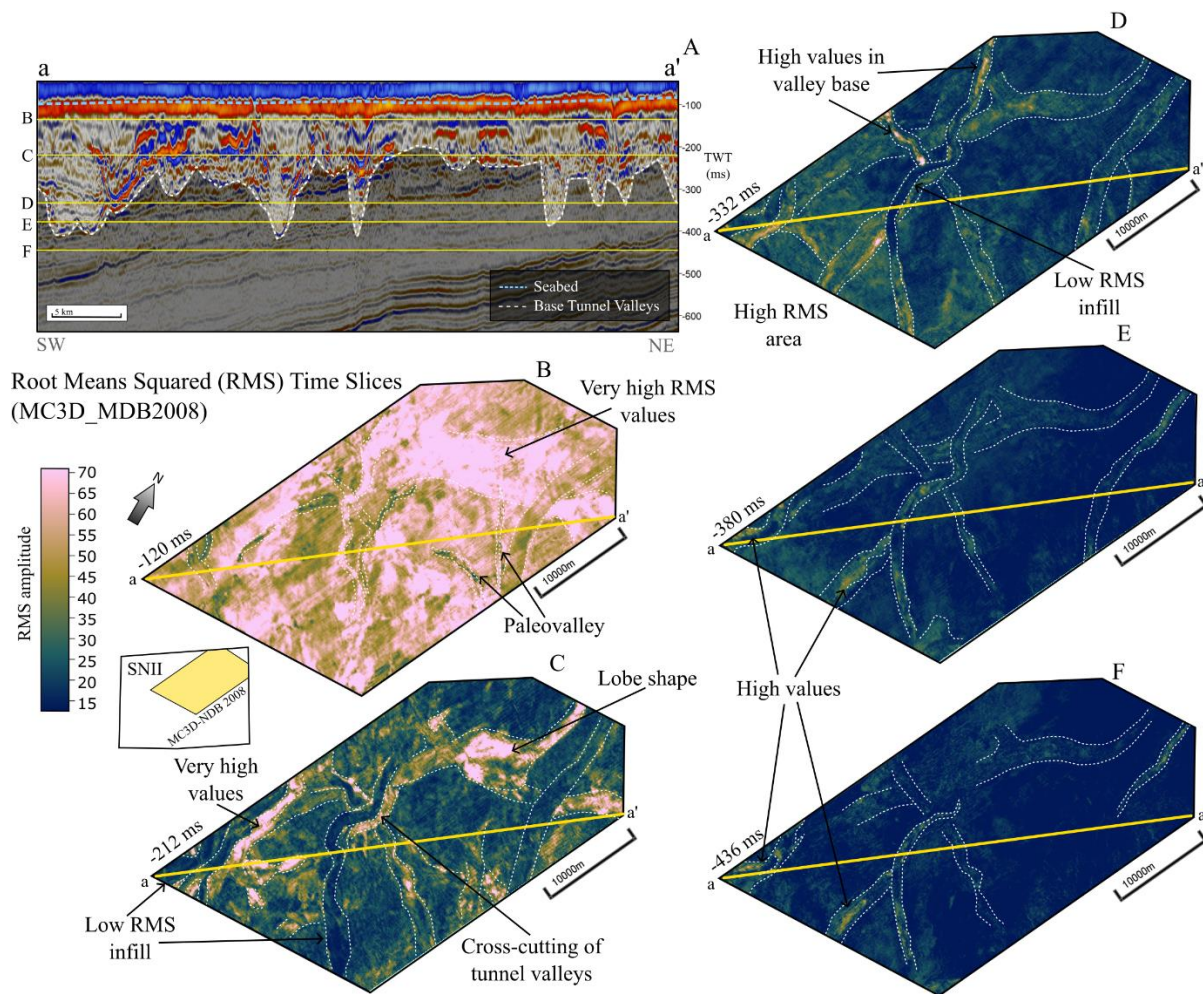


**Figure 7.11:** RMS amplitude time surfaces from MC3D\_MDB 2008 dataset. **A.** Seismic section showing the depths of all time slices in TWT and the interpreted seabed and base tunnel valleys surfaces. **B.** RMS time slice at -120 ms where seismic line a-a' is shown in yellow. **C.** RMS time slice at -212 ms. **D.** RMS time slice at -332 ms. **E.** RMS time slice at -380 ms. **F.** RMS time slice at -436 ms.



## Unmapped tunnel valleys

Several unmapped tunnel valleys are present within the SNII site due to data quality limitations. These have widths ranging from 0.5 km to 1.2 km and are often found above the seabed multiple (Fig. 7.12). These are in the same area of the stratigraphy as TV21 and TV36 and incise to depths of a maximum -200 ms. The unmapped valleys disappear and reappear throughout the dataset and likely exist as individual valleys like TV37 or as a network like TV31-35 (Fig. 7.3).

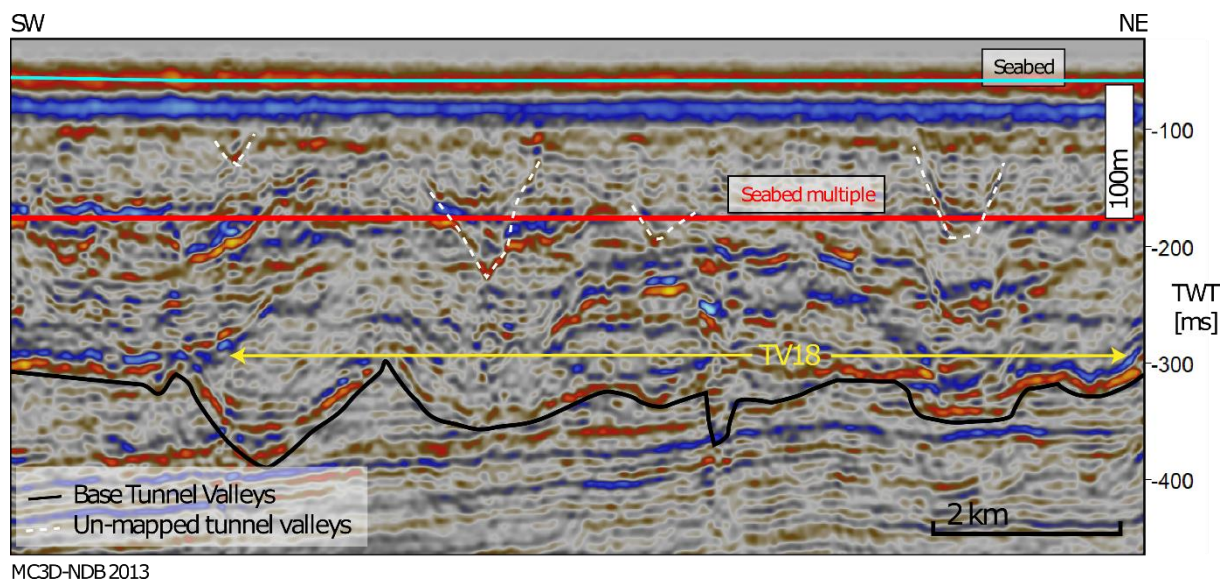


**Figure 7.12:** Seismic section showing examples of unmapped tunnel valleys (stippled white) over TV18 (Fig.7.3) along with the placement of the seabed multiple (red), Base tunnel valleys surface (black) and the seabed (light blue). The 'foundation zone' shown as the top 100m.

## Tunnel valley infill from seismic data

The resolution of the 3D seismic datasets used to map the tunnel valley generations is high enough to discern differences and similarities in the infill facies of the mapped tunnel valleys but might not capture the true complexity of the infill. Seismic sections along the thalwegs of all mapped tunnel valleys and some seismic sections perpendicular to the thalweg have been analysed.

All G1 valleys have reflectors with very high amplitudes, either along the base erosive surface or filling large parts of the valley, that can be indicative of shallow gas. The valleys to the very north and south have less continuous base reflectors than those in between, and several have a facies package with moderate amplitudes and a chaotic nature along the whole base of the valley that could be coarser sediments (Infill 1, Table 7.4). Two of the valleys have distinctive packages that dip, one with small dipping packages making up just one section of the valley, dipping towards the southwest, and one valley entirely filled with northward dipping packages (Infill 3, Table 7.4). Facies that include sub-horizontal continuous reflectors that onlap up-valley can be found in three of the G1 valleys (Infill 2, Table 7.4). The remainder of the valley infill is large and chaotic, with low to moderate amplitudes.

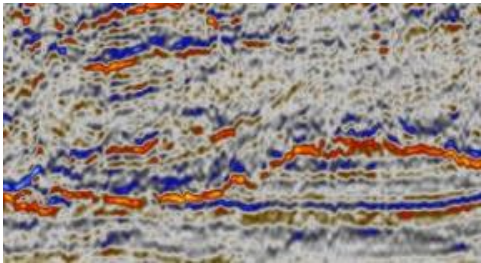
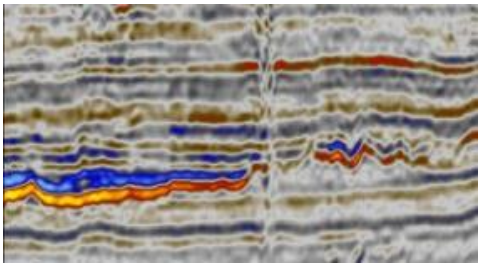
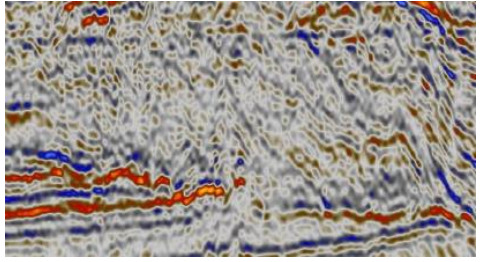
Similarly to G1, the G2 valleys either have base surfaces and/or infill with abnormally high amplitudes that can be an indication for shallow gas. There are also similarities in the dipping packages in the infill where the larger dipping reflectors do so towards the north, for example in TV 2 (Figure 7.11.b), and the smaller packages dip towards the south and cover smaller sections of the valleys (Infill 3, Table 7.4). Several valleys have the same facies along the base of the valleys as mentioned for G1 (Infill 1, Table 7.4), and most have chaotic infill except for TV20, where some sub-horizontal and continuous facies are present (Infill 2, Table 7.4). This package is visible along the valley base in TV2 (Fig. 7.4b). The same figure shows three cross-sections where the shape of the valley base clearly changes. In section c-c', the valley floor is flat with steep sides; in section d-d', the valley has a U-shape with a slightly flat base; and in section e-e', the valley is shaped like a V. The same pattern, a change from U-shape with a flat base to U-shape to V-shape, is present in many of the larger valleys within the SNII area. There is no clear pattern in the seismic character of the base of the G2 valleys.

The presence of shallow gas indicators is less common in the infill of G3 valleys, and their base reflectors are generally more difficult to discern from the substrate. Two of the valleys show dipping packages towards the north (Infill 3, Table 7.4), and the remaining valleys have

generally chaotic infill with no clear patterns in the infill. The valleys in G4 are very similar to those of G3, where one valley has some gas indicators of seismic anomalies, and another has some northward and southward dipping reflectors in the valley infill (Infill 3, Table 7.4). The G4 valleys have unclear valley bases and chaotic infill.

A clear pattern of low continuity and amplitude valley base reflectors and the same facies as mentioned in G1 and G2 covering the valley floor are present on both the G5 and G6 valleys (Infill 1, Table 7.4). Very few of the valleys in either of these generations show any signs of shallow gas, and three valleys have dipping reflectors towards the north (Infill 3, Table 7.4). Most of the valleys have chaotic infill, with only three of the valleys having sub-horizontal continuous reflectors that onlap up the valley (Infill 2, Table 7.4).

**Table 7.4:** Table summarising infill types identified in 3D seismic data in seismic sections along the thalweg of tunnel valleys.

Infill	3D seismic example	Seismic character	Interpretation
<i>Infill 1</i>		Chaotic, moderate to high amplitudes.	Coarse, non-layered sediment deposited by meltwater in pre- or sub-glacially.
<i>Infill 2</i>		Sub-horizontal, sub-parallel reflectors, moderate amplitudes, high continuity.	Interchanging between coarser and finer sediments deposited in quiet environments.
<i>Infill 3</i>		Dipping reflectors, often continuous throughs, with low to high amplitude chaotic packages between.	Fosets of different lithologies deposited in front of a receding ice sheet, either backfilling or outbuilding.

## Chapter 8 Discussion

The primary aim of this thesis is to map the tunnel valleys at the SNII site, assign them to distinct generations using tunnel-valley geomorphology analysis, and place the identified generations in the context of North Sea glacial history from the middle to late Pleistocene epoch. Objectives 1 through 4 are discussed in separate sub-chapters, where objective 5, comparison to previous studies, is incorporated. The four chapters will discuss tunnel valley occurrence and morphology, tunnel valley generations, and their formation. Lastly, all results are considered for implications for glacial history, geohazards, and seabed conditions.

### 8.1 Tunnel valley mapping and morphology

#### Tunnel Valley Mapping and Density

The SNII site is densely covered by tunnel valleys of varying sizes in a complex cross-cutting pattern, though visibly less complex after dividing the valleys into cluster generations. The occurrence of tunnel valleys outside the interpreted areas is unknown, but it is likely that the tunnel valley density outside SNII resembles that of the mapped valleys within SNII, due to the number of valleys that are cut short by the borders of the data. Of the mapped area (~2000 km<sup>2</sup>), approximately half is covered by tunnel valleys. Because of the lower quality of seismic data close to the seabed reflector and the seabed multiple, several smaller valleys remain unmapped (Fig. 7.12), thus it is likely that the actual percentage is higher than 50%. The unmapped valleys have similar incising depths and widths to the mapped tunnel valleys in G5 and G6 (0.5–1 km width, incising to TWT depths of -100 to -200 ms) (Fig. 7.12), and their occurrence in seismic data suggests an increase in the total number of tunnel valleys from 45 to ~60. This increases the density of tunnel valleys from 0.023 per km<sup>2</sup> to 0.030 per km<sup>2</sup>.

Ottesen et al. (2020) interpreted a total of 2297 tunnel valleys using both 3D seismic and high-resolution aeromagnetic data in the Central North Sea, where 2158 tunnel valleys were mapped using 3D seismic data covering an area of 110,000 km<sup>2</sup>. The result is a density of 0.02 tunnel valleys per km<sup>2</sup>. Compared to the mapped tunnel valleys in this thesis, there is a ~13% difference, and when including the unmapped valleys, ~33%. Kirkham et al. (2024) later mapped tunnel valleys in approximately the same areas as Ottesen et al. (2020), using a combination of improved 3D seismic data where some areas were additionally covered by HR3D seismic data. The result was a much higher density of tunnel valleys (0.037 per km<sup>2</sup>) compared to the previous study. When including high-resolution 3D seismic, the number of mapped tunnel valleys increased by 46%. Predating both studies by over two decades is the

work of Huuse & Lykke-Andersen (2000), who interpreted tunnel valleys in the Danish North Sea using 2D seismic data (Fig. 8.1). Visually, the density of mapped tunnel valleys in the Danish North Sea is much lower than that of the Norwegian and UK North Seas, except for the results from Salomonsen (1995) over parts of the Central Graben, which look to have a higher occurrence of tunnel valleys (Fig. 8.1). The “Area not mapped” is claimed to be almost free of tunnel valleys, which is interesting as it lies directly southeast from the SNII site and possibly within the path of the Elbe paleovalley (Fig. 8.1).

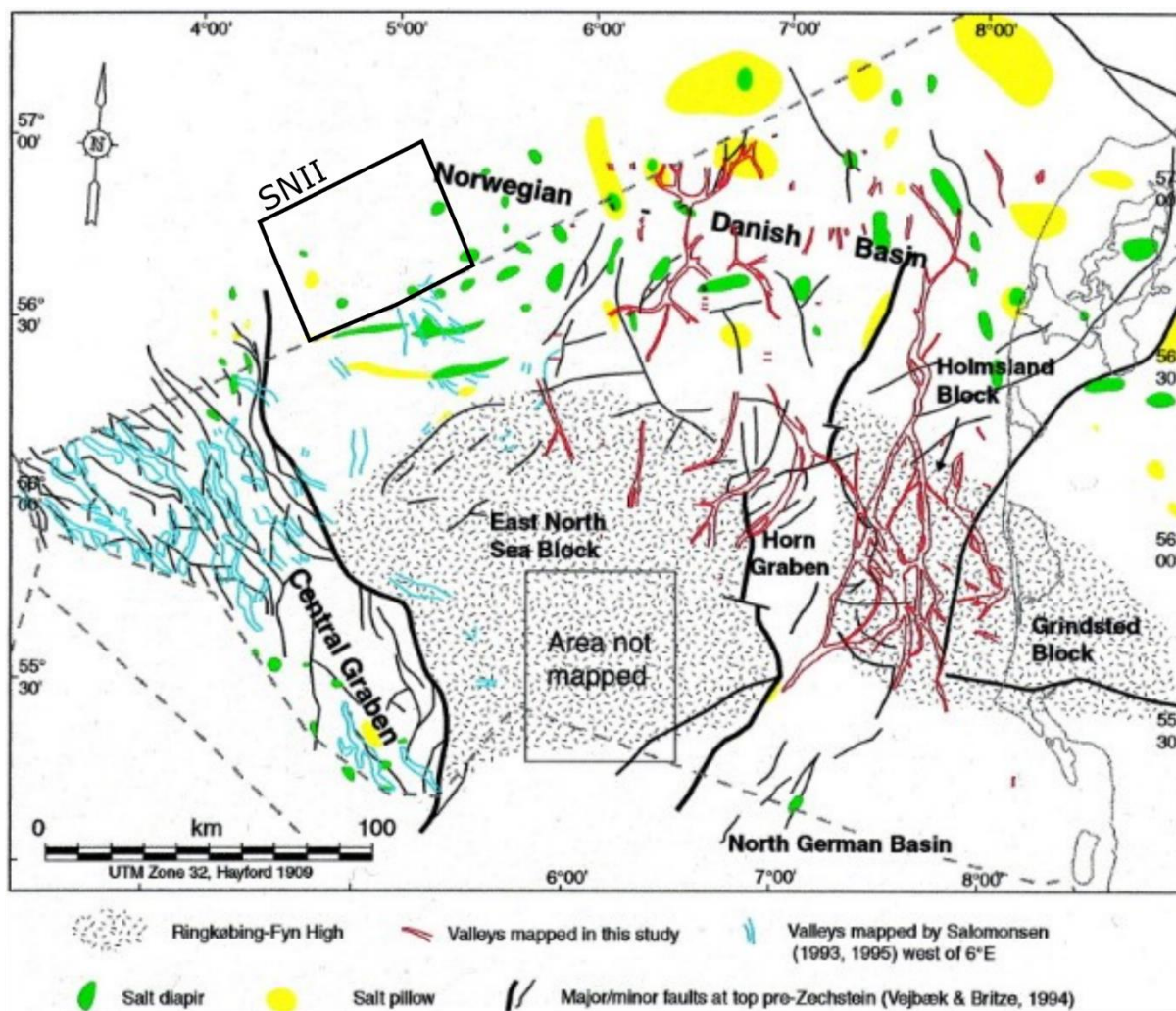


**Figure 8.1:** Map showing the tunnel valleys interpreted by (Huuse & Lykke-Andersen, 2000) in red and (Salomonsen, 1995) in blue. Figure modified from (Huuse & Lykke-Andersen, 2000).

There is a clear correlation between the resolution and dimensions of seismic data and the number of mapped tunnel valleys. Additionally, however, there seems to be a pattern where a higher density of tunnel valleys is present over the large grabens, the Central Graben, and the Southern Viking Graben. This could be due to a higher density of available exploration data,

and/or thicker Quaternary sediments (Fig. 4.1b), the latter of which is supported by Ottesen et al. (2020). The areas in which the British-Irish and Fennoscandian ice sheets coalesced also match these locations (Sejrup et al., 1994). This is further supported by a lower density of tunnel valleys further away from the central North Sea (Fig. 4.1a; Ottesen et al., 2020) and the knowledge that tunnel valleys often form along the borders of ice sheets (e.g. Huuse & Lykke-Andersen, 2000). A combination of data coverage and resolution, the occurrence of soft, unconsolidated sediments, and the location of the coalescence of large ice sheets is a plausible explanation for the distribution and preservation of tunnel valleys in the North Sea. As the SNII site is situated close to the coalescence point for the LGM (e.g. Bradwell et al., 2008; Graham et al., 2007; Hjelstuen et al., 2018; Sejrup et al., 2016), it makes sense that it has a higher density than that of, for example, the eastern Danish North Sea.

### Previous work in SNII

Hammer et al. (2016) mapped tunnel valleys from 3D seismic data in the Southern Norwegian North Sea in their study regarding a postglacial ‘lost land’ in the Doggerland of the Norwegian sector and its importance for human migration (Fig. 8.2). A minimum of five valleys were mapped within the SNII site, and several interpretations were extended outside the study area due to more available 3D seismic data. This further strengthens the interpretation of tunnel valleys in this thesis, in addition to providing more knowledge about the extent and orientations of surrounding mapped valleys. The mapped tunnel valleys are oriented increasingly westward towards the north and west of the SNII and increasingly southward to the southeast (Fig. 8.2).

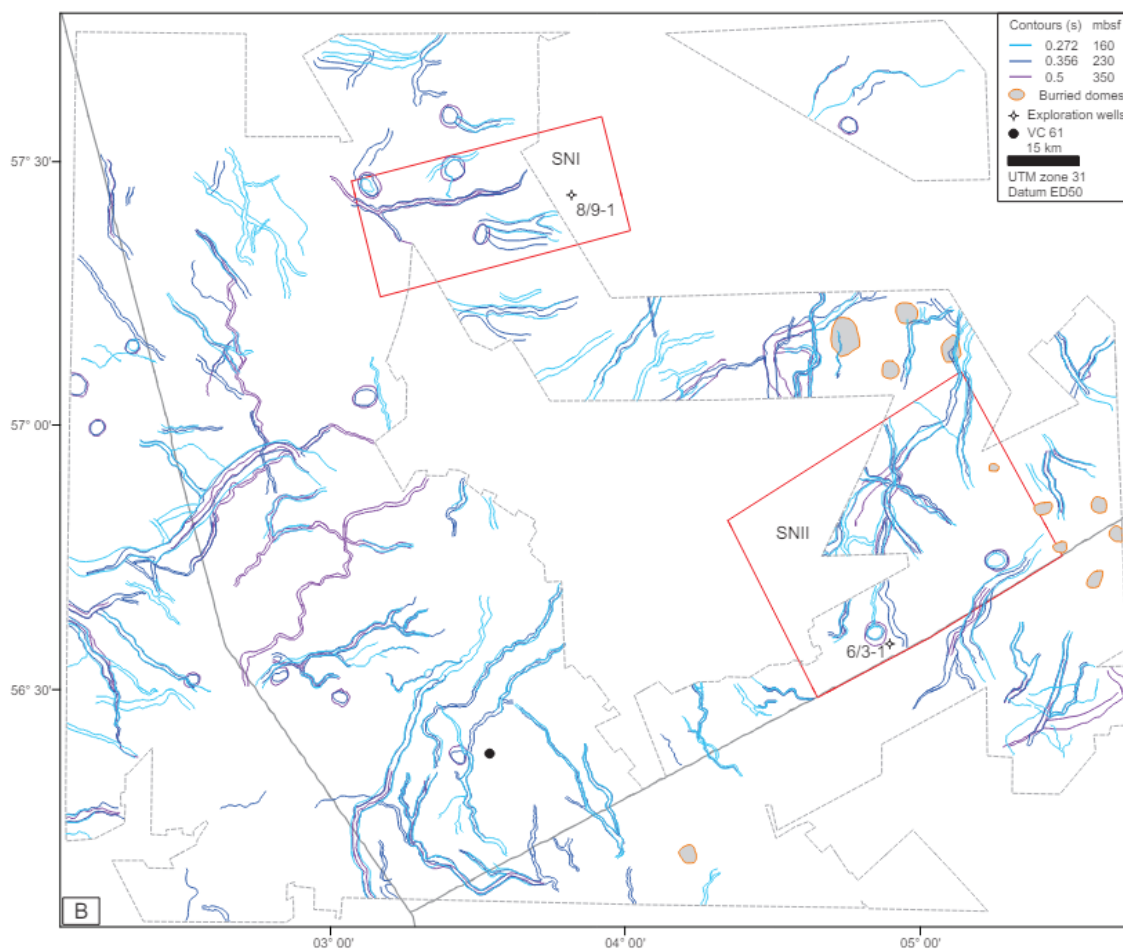


**Figure 8.2:** Tunnel valleys mapped by (Hammer et al., 2016) in the Southern Norwegian North Sea. Sørlige Nordsjø II (SNII), Sørlige Nordsjø I (SNI).

### Correlation to (Kristensen et al., 2007)

Southeast of the border between the Norwegian and Danish sectors, Kristensen et al. (2007) have interpreted 15 tunnel valleys and one shallow through conventional 3D seismic data over an area of comparable magnitude to the SNII. The shallow through is a large flat area, likely a secondary erosion surface above TV2. 15 tunnel valleys are significantly less than the number of valleys mapped in this thesis (45-60), which might be due to the available seismic data in this study having higher resolution or an actual increase in the density of tunnel valleys towards the north. The main difference being in the number of small valleys, supports the data quality being the differing factor, though this could also be explained by an actual decrease of smaller valleys caused by the Weichselian ice sheets not reaching this far south. When considering the high number of small unmapped tunnel valleys within the SNII area, the difference to the study area of Kristensen et al. (2007) becomes even bigger, thus the proposition regarding the Weichselian ice sheet is plausible.

The study area of Kristensen et al. (2007) slightly overlaps that of this thesis, making a direct correlation between eight tunnel valleys possible (Fig. 8.3). Of the tunnel valleys mapped in this thesis, ten cross into the study area of Kristensen et al. (2007) but are not mapped. For most of these, only the termination of the tunnel valley is present; thus, the lack of mapping could be due to less clear base reflectors for the tunnel valleys due to only shallow sections being imaged. It is likely that this specific limitation also applies to the mapping of tunnel valleys in this thesis, supported by four tunnel valleys mapped by Kristensen et al. (2007) that are missing.

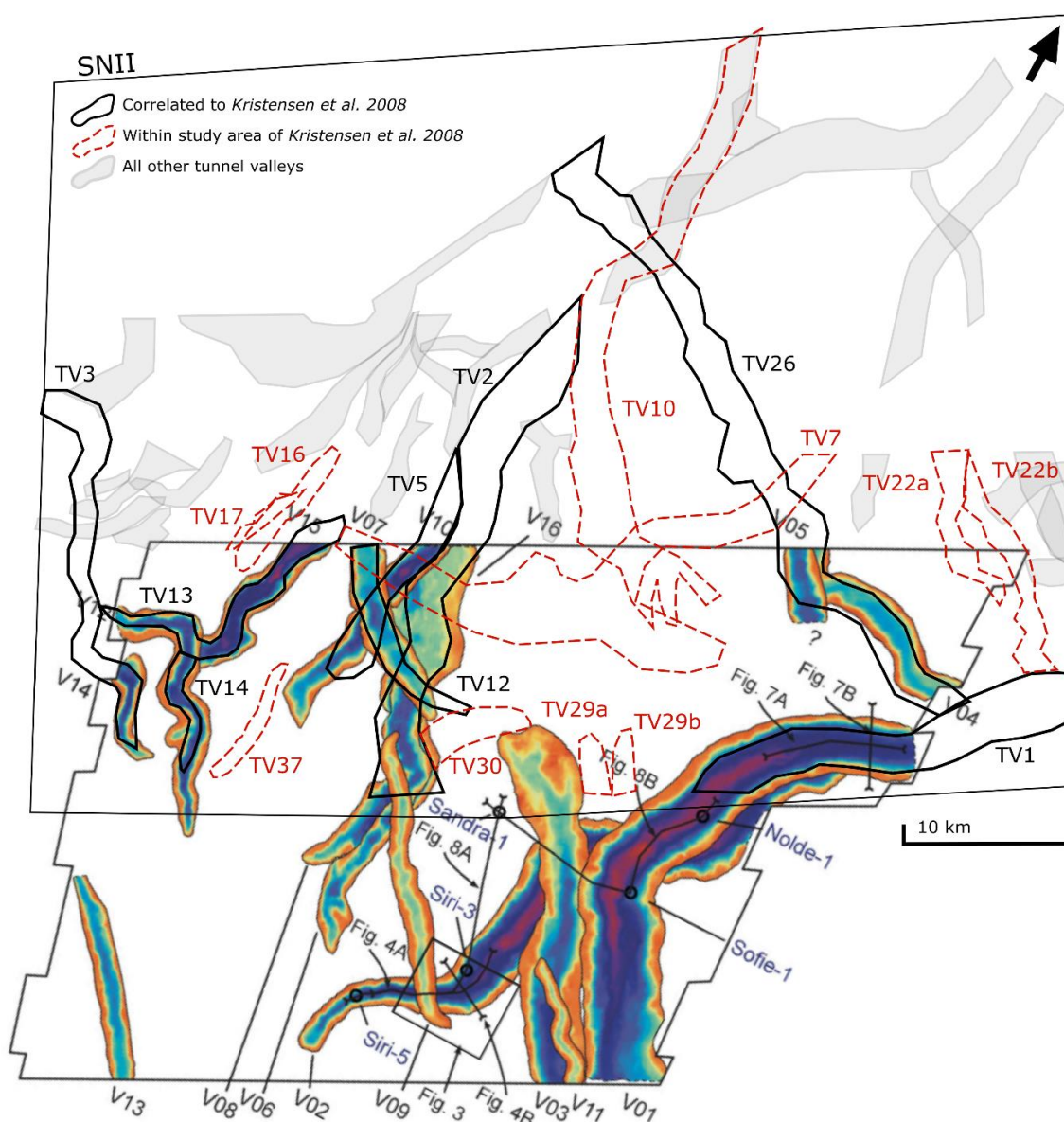


**Figure 8.3:** Correlation between mapped tunnel valleys in SNII from this thesis and that of (Kristensen et al., 2007). Tunnel valleys in black are directly correlated, tunnel valleys in red are within the correlation area but missing, and the rest of the mapped tunnel valleys of this thesis is in grey.



## Tunnel Valley Morphology

The morphology of the tunnel valleys in this thesis is within the range of those measured in previous studies. The widths of the tunnel valleys have been measured at their widest points; thus, it is likely that some of the valleys are narrower than the smallest measured width of 0.5 km. This is comparable to the minimum widths measured in most other areas of the North Sea, ranging from 0.2 km to 0.9 km (e.g. Kirkham et al., 2024; Kristensen et al., 2008; Lonergan et al., 2006; Ottesen et al., 2020; Stewart et al., 2013). The widest valley measures 2.8 km, which is similar to previously mapped valleys in the Central North Sea (e.g. Kirkham et al., 2024; Kristensen et al., 2008; Lonergan et al., 2006; Stewart et al., 2013), but smaller than the widest valleys mapped in the Danish and German sectors farther south, where some are 10 km wide (Lohrberg et al., 2020; Ottesen et al., 2020). Tunnel valleys with widths over 5 km are often assumed to be a result of other processes, for example, ice streams (e.g. Ghienne et al., 2007), though much is left undiscovered about these sub-glacial landforms; thus, their maximum widths should not be strictly limited yet.

The longest valley measured reaches 41 km, which is limited by the extent of the data at both the northern and southern ends, implying that the real length of the valley is longer. Several of the long valleys in the SNII site are limited by data extent and likely reach farther, supported by the correlation of valleys towards the south with mapped valleys by Kristensen et al. (2008), like, for example, TV1, which is correlated to V01 bends and continues much farther south. Huuse & Lykke-Andersen (2000) and Ottesen et al. (2020) have both measured valley lengths over 100 km in both the Danish and the Central North Sea, the latter up to 155 km. The widths and lengths of mapped tunnel valleys in this thesis and in previous studies indicate wider valleys in the Southern North Sea than in the Central and Northern North Sea; however, no patterns are visible for the lengths of them. This could be partially caused by many of the tunnel valleys in previous studies being limited by the extent of the data used for mapping.

The tunnel valleys in the SNII area are generally oriented north to south, ranging from NE-SW to NW-SE. This aligns with the knowledge available on the large Middle to Late Pleistocene ice sheets, their coalition in the middle of the North Sea, and their subsequent retreat and collapse towards the northeast and northwest. Most other previous studies on tunnel valleys in the North Sea report the same general direction (NE-SW and NW-SE) (Huuse & Lykke-Andersen, 2000; Kirkham et al., 2024; Kristensen et al., 2008; Lonergan et al., 2006; Ottesen et al., 2020; Stewart et al., 2013), except for Lohrberg et al. (2020), who measured orientations from East Northeast to West Northwest in the German sector.

Orientation measurements from tunnel valleys can be done in several different ways: i) a general orientation measurement along the entirety of the mapped tunnel valley; ii) calculating the mean orientation from several points collected along the reach of the tunnel valley; and iii) measuring several general orientations where there are abrupt changes in the direction of the tunnel valley. In this thesis, the i) method for measuring the orientations of the tunnel valleys is chosen due to their general direction being the most significant for ice sheet dynamics at a larger scale, as smaller oscillations in direction likely occurred during formation.

The maximum depth of incision in TWT and the relief of the thalweg are difficult morphological measurements to compare to previous studies, as methods of measurement vary. Huuse & Lykke-Andersen (2000) measured the maximum depths of tunnel valleys to be slightly deeper than 400 ms TWT (c. 350 mbsl) and more commonly 300-350 ms TWT (255-315 mbsl). The shallowest incising tunnel valleys mapped in this thesis reach 200 ms TWT (~180 mbsl) and the deepest incising is 522 ms TWT (~470 mbsl). This signifies that the valleys in the SNII site have a wider range of maximum depth, both shallower and deeper than that of the Danish North Sea. Less shallow valleys can be a result of Huuse & Lykke-Andersen (2000) use of 2D seismic data instead of 3D. The relief of the thalweg can be compared to where other studies refer to the size of internal sills. Huuse & Lykke-Andersen, (2000) measured internal sills up to 200 m, which is comparable to the maximum reliefs measured in this thesis. Two-way time depths of 233 ms are close to 215 m when converted using the velocity model. Sinuosity is also a measurement that is rarely specifically measured and is often rather talked about visually. There is, however, a clear trend where smaller (narrower, shorter, and shallower) tunnel valleys have lower sinuosity than larger (longer, wider, and deeper) tunnel valleys. This could hint at tunnel valleys becoming more sinuous when they are actively transporting meltwater for longer periods of time, assuming larger tunnel valleys require longer formation times. Limitations for all morphological measurements include resolution of seismic data, data extents, disturbance of the seabed multiple in the uppermost 200 ms TWT, disturbance of shallow hydrocarbons and gas chimneys, and uncertainties regarding the base erosional reflectors due to multiples from overlying tunnel valleys.

## 8.2 Tunnel valley generations

### K-means Clustering

When choosing which measurements to include in the k-means clustering, knowledge about the formation of tunnel valleys was considered. Three morphological measurements were included in the clustering analysis, one of which is orientation. Several previous works have theorised that tunnel valley orientation is perpendicular to the ice front and their longitudinal profile is parallel to ice retreat (e.g. Huuse & Lykke-Andersen, 2000; Praeg, 2003; Stewart et al., 2013). By extension, tunnel valleys of the same generation have the same general orientations, as they are created by the same ice sheet. This makes the tunnel valley orientations one of the most significant measurements to consider when dividing mapped tunnel valleys into groups (Kirkham et al., 2024; Stewart et al., 2013). The reason for this behaviour is that tunnel valleys are created with overpressure, where the meltwater wants to travel from high to low pressure areas, thus from under a thicker section of ice to the edge of the ice sheet (e.g. Huuse & Lykke-Andersen, 2000; Kristensen et al., 2008; Lonergan et al., 2006; Praeg, 2003). For smaller ice lobes, the main direction of meltwater flow could have greater variability across a larger area as opposed to a large ice lobe where the direct path between high and low pressure would be the same or very similar across a larger area (e.g. Kehew et al., 2012). Smaller icelobes can, for that reason, be a variable that weakens the strength of tunnel valley orientation as critical measurements for dividing them into generations.

The next measurement that is included in the clustering method is the relief of the thalweg, which correlates to size (width and depth) and, by extent, the overpressure. This is supported by tunnel valleys with smaller relief cutting through, and therefore younger than, tunnel valleys with larger reliefs in the results of this thesis. It is a possibility that deeper valleys with high internal relief are eroded under thicker ice sheets where there are higher pressure gradients, and smaller valleys with smaller internal relief are created where there are smaller pressure gradients. Relief becomes a measurement for both the size of a valley and the thickness of the ice sheet. This could indicate that the smaller valleys with smaller internal relief are created closer to the maximum border of the ice sheets. However, previous studies have included tunnel valleys with different internal reliefs in the same generations, making this specific measurement a potential limitation to comparison of generations across study areas (Kirkham et al., 2024; Kristensen et al., 2007). It is possibly also a weakness of this thesis, as the argument lacks sufficient support from previous work on tunnel valley generations.

The maximum depth of the thalweg is the third and final morphological measurement included in the clustering analysis. The reasoning for this is the notion that tunnel valleys of the same generation might incise to around the same maximum depth in the stratigraphy due to the area being filled with various sediments between ice sheet advances (e.g. Van Der Vegt et al., 2012). There are few, if any, instances where deeper tunnel valleys incise into shallower tunnel valleys in the results of this thesis, which further supports the inclusion of the maximum depth measurement. The minimum depth of the tunnel valley, the shoulders or shallowest section of the thalweg, was not used mainly due to data limitations, extent, and/or resolution. The seabed multiple disturbed the shoulders of many tunnel valleys in seismic imaging, making them challenging or impossible to define in most instances (Fig. 7.12).

The k-means clustering method removes much potential personal bias in dividing the tunnel valleys into similar groups but is heavily reliant on choosing the right measurements and the right number of groups to divide into. It is a great tool if these two things are chosen carefully, but different results can be achieved by adding or removing certain measurements and/or changing the number of clusters. One should refrain from including measurements in the analysis that are skewed by data extent and/or data quality, including lengths and widths (where the widest parts of the valleys often are at the valley shoulders, which in this case are disrupted by the seabed multiple). In this thesis, the number of clusters is chosen to be five due to the results from the cross-cutting relationships that displayed at least five levels of relative age.

Kristensen et al. (2007) proposed that one of the main criteria for tunnel valley generations was termination at approximately the same southward extent through the study area. This is not included in this thesis, and many of the mapped tunnel valleys have no clear end slope within the study area, nor is it included in many other studies on tunnel valley generations in the North Sea (e.g. Kirkham et al., 2024; Lonergan et al., 2006; Stewart et al., 2013). It is possible that this criterion is important for tunnel valley generations, though this is dependent on how a generation is defined. If a generation of tunnel valleys are valleys that form and emerge from ice coverage at the same time during ice retreat, it would be a significant criterion. In this thesis, one tunnel valley generation is defined as all tunnel valleys that are formed at around the same time by the same ice sheet, with no specifications around their terminations.

For future research on tunnel valley generations, it might be possible to measure how far south the terminations of the mapped tunnel valleys are and add it as a measurement in the clustering analysis along with orientation, resulting in groups of valleys that terminate around the same

southward extent and are oriented in the same direction. Another option could be that coordinates of southward extent could be marked in an x-y environment within a study site, where valleys with coordinates for their termination would be assigned to the same group. The valleys cut by the borders would get a null value for one axis and the highest value for the other axis; this way, they could be differentiated. It could be beneficial to add priority to the clustering method where the results of the termination and orientation analysis could be further analysed with the addition of max. depth and relief of thalweg to distinguish more specific generations within.

## Cross-cutting Relationships

Some cross-cutting relationships are not as certain as others due to limitations in interpretation and data resolution or quality. In some cases, it is challenging to discern which valley is cutting which, especially when both valleys have chaotic infill and weak base-valley reflectors. One example of this is the interpretation of TV13 and TV14 in this study, compared to the same valleys interpreted by Kristensen et al. (2007) (Fig. 8.2). The opposite cross-cutting relationship is chosen, indicating possible weak points for this method. There is more certainty regarding the relationship between the larger valleys, as both infill and valley-base reflectors are clearer farther down in the stratigraphy, likely due to the absence of the seabed multiple. The cross-cutting relationship between TV26 and TV1 is also opposite to that of Kristensen et al. (2007). In this thesis, the relationship between these two valleys is discerned by the relationships between time-depth surfaces in addition to a fan shaped anomaly visible on RMS inside TV1 that looks to originate from TV26 (Fig. 7.10D). This supports a relative age relationship where TV26 is younger than TV1. However, it is possible that TV26 also exists on the eastern side of TV1, but is less visible in seismic, and that the fan exiting TV26 is a result of a fluvial system that has developed on top of TV26. This would have significant consequences for the tunnel valley generations, as they are partly based on relative age. Shallow gas is also a challenge, as it disturbs some areas in which these valleys cross paths.

Kristensen et al. (2007) concluded with the same levels for the cross-cutting relationship hierarchy as in the SNII area. The correlations between valleys in this thesis and those in Kristensen et al. (2007) make it possible to discover a discrepancy in where the mapped valleys are placed from oldest to youngest. This indicates that both personal bias and data quality in the interpretation of the tunnel valley time depth surfaces seem to impact the results of the cross-cutting relationships drastically. The method is, however, useful together with other information on the valleys, although the relationships might skew an interpretation if followed too strictly where the relationship is weak or unclear. There are several unmapped valleys in the area that visibly overlay mapped valleys (Fig. 7.12), which could have added more certainty to the relationships.

Using cross-cutting relationships as the foundation for tunnel valley generations is a commonly used method, not only by Kristensen et al. (2007) but also in other studies from the North Sea (e.g. Kirkham et al., 2024; Ottesen et al., 2020; Stewart et al., 2013; Stewart & Lonergan, 2011). The method by Stewart (2009) involves using relative ages from cross-cutting stratigraphic

relationships as the basis for tunnel valley generations and including morphological data (orientation and stratigraphic depth) to aid where relative age is challenging to discern. This thesis follows a similar pattern but differs slightly in the choice of morphological measurements. Instead of using stratigraphic depth, the maximum depth of each valley, in addition to the relief of the valley thalweg, was used. This combination is comparable to stratigraphic depth; thus, the differing factor between the method by Stewart (2009) and that of this thesis is a higher influence of the morphology of tunnel valleys on the resulting generations. The use of machine learning is also a change from the original methodology and might have increased the level of objectivity in assigning the tunnel valleys.

## Number of Generations

Seven generations are interpreted in this thesis, including the six generations resulting from the clustering method and cross-cutting relationships (G1-G6) and one generation for the valleys with relief on the seabed time-depth surface (G7). Based solely on their cross-cutting relationships, a minimum of six generations of tunnel valleys in the SNII is plausible, including the G7. A maximum number of seven generations is, however, not confirmed due to the several smaller, unmapped valleys visible in seismic that have the potential to add another level to the relative age hierarchy of the cross-cutting relationships. If the termination criterion proposed by Kristensen et al. (2007) is applied to the results in this thesis, the determined generations would need to be divided into more generations to accommodate tunnel valley terminations, increasing the upper limit for the number of generations.

To compare the number of generations discovered in this thesis to that of previous studies, a selection of studies ranging in age from 1991 to recent is summarised in Table 8.1. Up until the twenty-first century, the number of generations in the Central and Southern North Seas has corresponded to the number of large glaciations (3). Likely due to data and methods improving, the number of interpreted generations has increased drastically to a maximum of ten generations in 2024 (Kirkham et al., 2024). The Central North Sea seems to have the highest recorded number of tunnel valley generations (Kirkham et al., 2024; Ottesen et al., 2020). It is plausible that this is partially due to higher coverage of quality seismic data from the oil and gas industry and/or a higher density of studies in this section. It could also be an indication of a higher frequency of overriding ice sheets in the Central North Sea. The notion of seven or more generations is repeatedly reported in literature from both the Danish and Central North Sea (UK and Norwegian sectors), which further supports the findings of seven generations in the Southern Norwegian North Sea (this thesis). The seven match the number proposed by the neighbouring/overlapping study by Kristensen et al. (2007). However, both the criteria used to define a generation as well as the grouping and relative age of tunnel valleys are contradictory. Seven or more tunnel valley generations in this area of the North Sea are highly supported by previous studies (Kirkham et al., 2024; Ottesen et al., 2020; Stewart et al., 2013; Stewart & Lonergan, 2011).



**Table 8.1:** Summary of a selection of previous studies on tunnel valley generations in the North Sea.

<b>Study</b>	<b>Gen.</b>	<b>Study area</b>
<i>Ehlers &amp; Wingfield (1991)</i>	3	Central and Southern North Sea (UK)
<i>Praeg (1996)</i>	3	Southern North Sea
<i>Lonergan et al. (2006)</i>	4	Central North Sea (UK)
<i>Kristensen et al. (2007)</i>	7	Danish North Sea
<i>Stewart &amp; Lonergan (2011)</i>	8	Central North Sea
<i>Moreau et al. (2012)</i>	4	Southern North Sea
<i>Stewart et al. (2013)</i>	3/7	Central North Sea (more South/more North)
<i>Ottesen et al. (2020)</i>	5/7	Central and Northern North Sea (more East/more West)
<i>Kirkham et al. (2024)</i>	10	Central North Sea

### 8.3 Tunnel valley formation based on infill facies

Wide and deeply incising valleys have up to three types of infill present, while smaller valleys (narrow and shallow) are often filled by one type of infill. The discernability of different infill types within tunnel valleys is highly reliant on seismic resolution, and studies like that of Kirkham et al. (2024) show that high-resolution 3D seismic datasets drastically improve the imaging of infill facies. Infill 1 is found across all generations of tunnel valleys, while Infill 2 and Infill 3 occur in the older generations.

Based on the types of infill observed within the mapped tunnel valleys in the SNII area, a subglacial depositional environment is interpreted for Infill 1 due to the findings described below. The seismic character and RMS values for the chaotic Infill 1 can indicate coarser sediments and possible diamicton, which could have been deposited as a product of two different erosional processes (Van Der Vegt et al., 2012). One is erosion by meltwater, especially plausible for V-shaped tunnel valley bases, where coarse sands and gravels are deposited at the base due to the flow strength being insufficient to move this grain size. The second process is erosion by ice, this being more likely for the valley bases with a wide U-shape, where subglacial till is deposited under the base of the ice sheet (e.g. Huuse & Lykke-Andersen, 2000; Jørgensen & Sandersen, 2006). Kirkham et al. (2024) have interpreted a similar type of infill (Type 7) and support a plausible subglacial depositional environment. However, though the deposition of subglacial tills may be possible in wide and shallow tunnel valleys, it is unlikely that the ice has reached the base of the narrower and deeply incising tunnel valleys (Huuse & Lykke-Andersen, 2000). Van Der Vegt et al. (2012) (and sources therein) suggest that these subglacial deposits can include both diamicton and coarser fluvial sediments, which are part of the primary infill of a tunnel valley.

The seismic character of Infill 2 includes near-horizontal layering, which is interpreted to be a result of deposition in still-standing water in a proglacial environment. A glaciolacustrine or glaciomarine origin is proposed for Infill 2, where water has accumulated in front of the receding ice sheet in an unfilled section of a tunnel valley or by a larger body of water after ice retreat (e.g. Kirkham et al., 2024; Kristensen et al., 2008). The seismic character changes between peaks and troughs and can indicate a shift in flow strength occurring due to an increased amount of meltwater, which resulted in a change in the grain size of the sediments. The heavily incised surfaces on top of this infill could represent fluvial systems in front of the receding ice sheet, potentially in a pro-glacial environment. In TV1, this facies transitions into

inclining packages of possible glacial outwash origin, like that proposed by Kristensen et al. (2008). Infill Type 1 and Type 5 from Kirkham et al. (2024) have similar seismic descriptions to those of Infill 2. A subglacial or proglacial to marine environment is suggested, and changes from sandy to clayey sediments explain the clear layering of reflectors (Kirkham et al., 2024). In the framework of Van Der Vegt et al. (2012), Infill 2 can be described as secondary infill, as it is not directly associated with tunnel valley formation.

Infill 3 is interpreted to have been deposited in two different environments, even though they have similar seismic characteristics. Where Infill 3 fills the entire valley (subtype one), a likely sub- or preglacial environment is proposed where the front of the ice sheet deposits foresets of varying grain sizes that dip in the direction of ice retreat. The second sub-type to Infill 2 (subtype two) is where it is present as slightly smaller foresets, often in the northern end of a tunnel valley, deposited by meltwater in a pre-glacial environment where the foresets are dipping away from ice retreat and filling the remainder of a valley (as mentioned accompanying Infill 2 in TV1). Infill 3 also presents with indications of fluvial systems on top of the infill, hinting to fluvial activity after deposition, possibly in a proglacial to terrestrial environment. One of the first to discover large dipping packages within tunnel valley infill was Praeg (2003), who interpreted them as a result of glaciofluvial backfilling. In the formational model proposed by Kristensen et al. (2008), both sub-types of Infill 3 are present along with Infill 2. Building on the glaciofluvial backfilling explanation from Praeg (2003), Kristensen et al. (2008) further proposed glaciohydraulic supercooling as an important part of the process. The large dipping packages can be placed in the primary infill category, and the smaller dipping packages as secondary infill, both in the framework from Van Der Vegt et al. (2012).

The direction in which the tunnel valley infill is analysed in seismic analysis can have implications for division into facies. A simple two-part infill interpretation is most evident when the infill is visualised in cross-sections perpendicular to the valley thalweg. These are often composed of one chaotic low-amplitude package and one moderate-amplitude package with some continuous reflectors (e.g. Huuse & Lykke-Andersen, 2000). However, this thesis and previous studies, including seismic sections along the valley thalweg, confirm that more information is needed about the geometries of these seismic facies. This is particularly useful when examining internal dipping packages for determining ice sheet retreat directions. RMS amplitude maps are a great method for extracting information about depositional environments. Three large, high RMS fan shapes are interpreted to be deposited as glacial outwash sediments partially filling the valleys as well as extending over the valley shoulders. This description is

similar to that of Type 2 infill from Kirkham et al. (2024), interpreted as highly homogeneous subaqueous or subaerial outwash.

The findings of this thesis support that of a time-transgressive tunnel valley formation, similar to that of Kristensen et al. (2008). The main method of excavation of a tunnel valley is credited to fluvial erosion, glacial erosion, or a combination of these under a receding ice sheet. This is evidenced by the changing shape of the valley base between a U- and a V-shape and the presence of subglacial tills and coarse fluvial deposits at the base of the valleys. Many smaller valleys are solely filled with these types of chaotic sediments, which indicates that they were close to entirely filled in by the time the ice had retreated. Glaciofluvial backfilling sediments directly overlay the base infill in many of the tunnel valleys, likely directly following the deposition of these. At the northern terminus of the tunnel valleys, glaciolacustrine and glaciomarine environments might have filled the remainder of the valleys, sometimes paired with proglacial deltas building out into the still-standing waters. Marine inundation often follows the retreat of large ice sheets, though this process is likely only preserved for the last event, as each ice sheet has eroded vast amounts of sediment for each passing (e.g. Cotterill et al., 2017 a; Petrie et al., 2024). Some of these sediments might, however, be preserved within some of the larger tunnel valleys with leftover relief after ice retreat (e.g. Kirkham et al., 2024).

## 8.4 Implications for North Sea glacial history, geohazards and seabed conditions for marine infrastructure

### North Sea glacial history

The oldest generation of tunnel valleys in the SNII area (G1) are of probable Elsterian age. No definite maximum age restraint is available for the tunnel valleys in the North Sea, but there is a consensus, supported by correlations to onshore records, that the deepest incising tunnel valleys in the North Sea are from MIS 12 (e.g. Huuse & Lykke-Andersen, 2000; Lohrberg et al., 2020; Lutz et al., 2009; Praeg, 2003). The G1 tunnel valleys are both cut and overlain by most of the younger generations, which further strengthens their relative age. The occurrence of large ice-marginal outwash fans on top of several of the valleys indicates a high sediment influx, which implies that the Elsterian ice sheet eroded vast amounts of sediment up-ice, which was subsequently transported to the ice margin. The general direction of ice retreat is towards the northeast, based on the orientations of the G1 tunnel valleys. Lonergan et al. (2006) (Central North Sea) and Lutz et al. (2009) (German North Sea) proposed that more than one of their mapped tunnel valley generations were created during the Elsterian based on their cross-cutting relationships and morphological similarities to previous well-known studies on tunnel valleys. A comparison between the Elsterian valleys in other studies and those in the SNII site shows a general agreement of wide and deep tunnel valleys (e.g. Huuse & Lykke-Andersen, 2000; Praeg, 2003), though the number of generations placed in MIS 12 is dissimilar. It is possible that more tunnel valley generations were created in the Danish North Sea due to its closer proximity to the Elsterian maximum extent.

The Saalian glaciation is characterised by multiple alternations between warm and cold periods (e.g. Batchelor et al., 2019), thus, four of the tunnel valley generations (G2-G5) are of proposed Saalian age. This is further supported by the main orientation of tunnel valley generations shifting significantly from NE-SW (G1) to N-S (G2 and G3). Which specific MIS the generations belong to cannot be determined in this thesis, but a MIS 10/8 age for G2 and G3, and a MIS 8/6 age for G4 and G5 are suggested. This is based on changes in the orientations of the tunnel valleys, where little to no change could signify a smaller readvance. The general orientation of the G6 valleys changes significantly from that of G4 and G5, thus G6 has a suggested Weichselian age. Due to the presence of unmapped valleys and paleo valleys with visible seabed relief, the G6 tunnel valleys are likely not from the Last Glacial Maximum (MIS 2). The proposed age for G6 for that reason is suggested to be MIS 4. The youngest of the

mapped tunnel valley generations in the SNII area is G7, which only includes the paleo valleys with seabed relief. A proposed age for G7 is MIS 2 (LGM), supported by the shallow depth of incision and lack of complete infill.

The generations with the best estimated formation ages are G1 and G7, placed as the oldest and youngest generations (MIS 12 and MIS 2, respectively), which corresponds to the conclusions of most previous work on tunnel valleys in the North Sea (e.g. Sejrup et al., 1994; Stewart et al., 2013; Stewart & Lonergan, 2011). All generations in between have less certainty and need specific geochronological dating to be confirmed. It is possible that even a small readvance of an ice sheet can create an entirely new set of tunnel valleys; thus, generations of valleys may not always correlate to a specific MIS, as previously favoured (Kirkham et al., 2024). The correlation to Kristensen et al. (2007) performed in Chapter 8.1 indicated a drastic decrease in narrow and shallow tunnel valleys from the SNII site to the Danish sector, further supported by a lack of valleys with these morphologies in the Southern North Sea in general. The extent of the Last Glacial Maximum is suggested to have extended to a position within the study area of Kristensen et al. (2007). Further research, including a detailed interpretation of narrow and shallow tunnel valleys in the areas to the south of the SNII site, is needed to confirm or disprove this interpretation.

The results of the generational analysis of tunnel valleys in the SNII site support the notion of a more complex glacial history of the North Sea than previously thought (e.g. Kirkham et al., 2024; Ottesen et al., 2020; Stewart et al., 2013). Additionally, there is evidence for deeper incising and wider tunnel valleys with more complex infill geometries where the maximum extent of the respective ice sheet is far away, like, for example, G1, G2, and G3. This could be due to higher overpressures caused by the tunnel valleys being situated under thicker ice closer to the centre of the ice sheet, as opposed to those created very close to the margin of smaller advances. The maximum extent of the respective ice sheets being further away could also result in a longer duration of high meltwater drainage during retreat, giving the valleys more time to form. The complex infill geometries might be a result of more accommodation space in the larger valleys and/or slower ice retreat with higher sediment supplies.

Maximum ice extents from Batchelor et al. (2019) for each MIS were introduced in Chapter 3.4, they cannot for the most part, be directly compared to the ice fronts proposed in this thesis due to their presentation of the ice front placement close to the SNII site. Despite this, the LGM position proposed by Batchelor et al. (2019) supports that of the G7 in this thesis, which further

strengthens this generation's age of ~20 ka. The G7 tunnel valleys are oriented towards the southeast, pointing towards the gap between the Dogger Bank to the southwest and the Jutland Bank to the southeast. Based on this fact, it is possible that the G7 tunnel valleys are related to a drainage pattern utilising this gap during the LGM (e.g. Hjelstuen et al., 2018; Petrie et al., 2024). The G4 and G5 tunnel valleys have a very similar general orientation to G7, which could hint to this gap being present during the Saalian (MIS 8/6). Further research on the gap between the Dogger and Jutland banks is essential for elucidating its geological significance in relation to drainage patterns during the middle to late Pleistocene and, by extension, the glacial history of the North Sea. Definite ages for the tunnel valleys in the North Sea lack, thus, future research regarding the direct dating of the tunnel valleys in the Central North Sea is proposed. Further, the many generations of tunnel valleys in the North Sea could be correlated to those present onshore NW Europe.

## Geohazards and seabed conditions

Two salt diapirs with diameters of ~4 km are present along the southeastern border of the study area. Evidence from seismic lines and RMS maps indicates potentially disturbed sediments above the salt structures and potential hydrocarbon migration paths along their flanks. Shallow gas, coupled with potential salt tectonic movement affecting the overlying sediments, makes the conditions above these structures potentially hazardous for seabed installations such as wind turbine foundations. Petrie et al. (2024) have mapped the area above these two salt diapirs as being high risk, further strengthening the notion that these areas should be considered when planning subsurface operations. This likely applies to all areas of the North Sea where salt structures exist close to the seabed.

Approximately half of the interpreted areas of the SNII site are covered by tunnel valleys, making these glacial structures the main facies of the area. Whereas several of the mapped tunnel valleys incise to depths of ~400 m, many exist inside the foundation zone (top 100 m) either partially, for example, shallow valley shoulders of large tunnel valleys, or completely. An argument can be made for tunnel valley shoulders being hazardous when close to the seabed, due to their potentially unstable nature. Many large tunnel valleys have steeply dipping valley sides that are found to slump after ice retreat (Kirkham et al., 2021, 2024). The shallow tunnel valleys are commonly filled with Infill 1, which is interpreted as diamicton or coarse-grained sediments. According to Petrie et al. (2024), these types of sediments pose a moderate risk to the safe installation and stability of turbine foundations. The complex infill patterns found in the larger Elsterian and Saalian tunnel valleys have no clear direct significance for seabed conditions as they exist below the foundation zone. Their potential for indirect contribution to geohazards related to hydrocarbon migration is, however, strongly supported (e.g. Huuse & Lykke-Andersen, 2000; Kirkham et al., 2024; Ottesen et al., 2020; Praeg, 2003).

21 of the 25 (84%) total pockmarks proposed by Petrie et al. (2024) using 2D lines fall within and/or along the margins of the tunnel valleys interpreted in this thesis (Fig. 8.4). Approximately 50% of the 21 correlating pockmarks are located along the margins of the valleys, hinting at a preferred hydrocarbon migration path along the valley base and sides (Fig. 8.4). The pockmarks primarily exist over tunnel valleys that incise deep into the underlying substrate, which include all tunnel valleys in G1 and some of the valleys in G2, G3, and G4. Of the six tunnel valleys with more than one associated pockmark, three are filled with continuous and layered infill type 2, and the remainder are filled with large dipping packages described in infill type 3. Where infill 2 is the main facies, the pockmarks are placed along the tunnel valley



margin, indicating that the hydrocarbons fail to migrate through these deposits. The opposite is true for infill type 3, where the pockmarks are placed in the middle of the valleys, which can be attributed to migration along the dipping packages. The valleys that correlate to pockmarks show seismic anomalies and high RMS values either along their base reflector or inside their infill or associated landforms, which can be an indication of shallow gas and support their role as hydrocarbon catchments and preferred migration paths. On the contrary, Kirkham et al. (2024) found no correlations between seabed pockmarks and mapped tunnel valleys in the

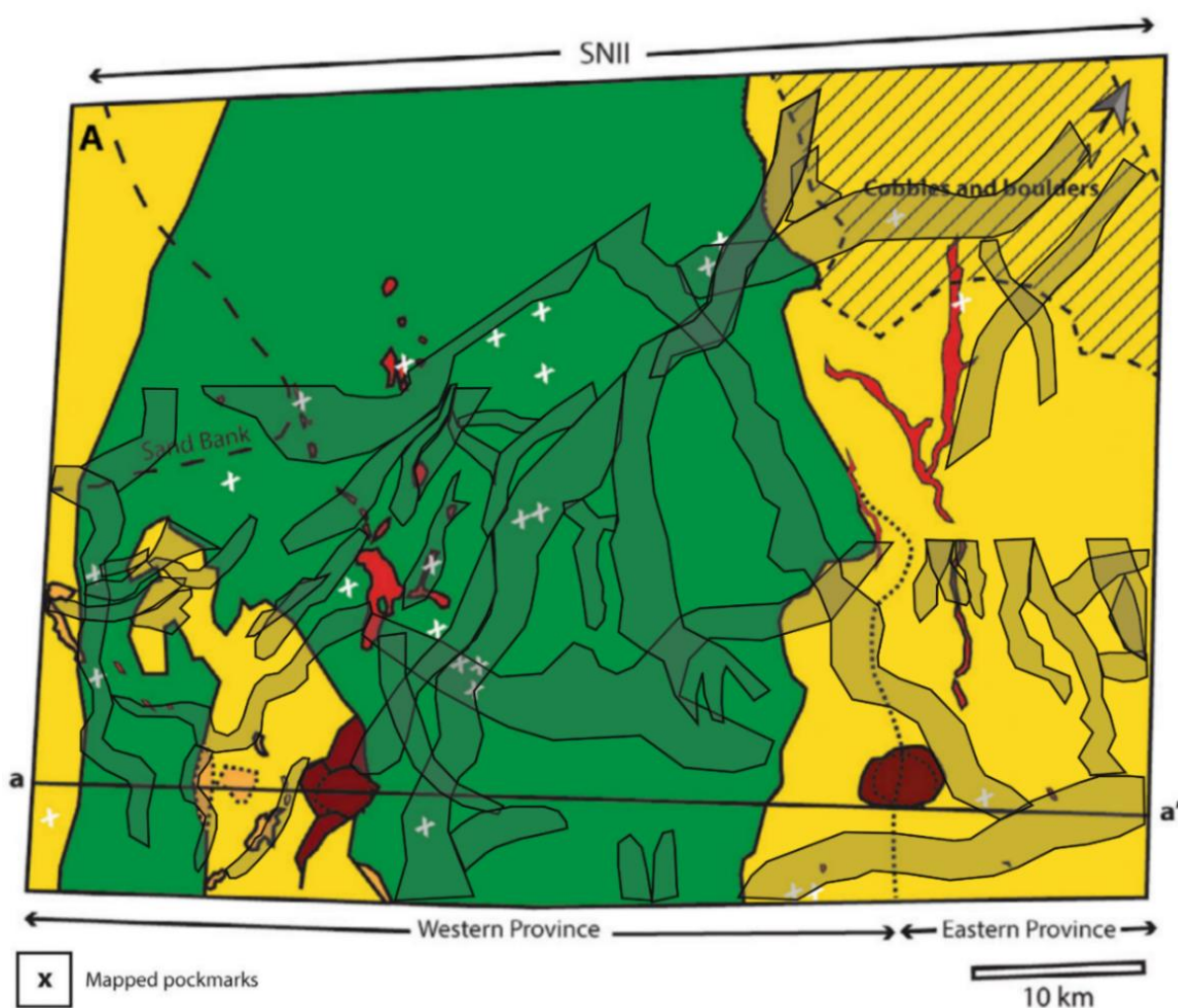


**Figure 8.4:** Mapped tunnel valleys displayed over risk map from Petrie et al. (2024), showing risk of installation challenges for wind turbine foundations. Low risk (green), medium risk (yellow, orange), high risk (red, dark red), proposed pockmarks on the seabed (white x). Notice how pockmarks correlate to tunnel valleys.

Central North Sea. This could be due to geographical variation, as Kirkham et al. (2024) worked across a considerably greater area than the SNII and focused on multiple smaller study sites. Close to the seabed are lake deposits and paleo valleys, both of which are recognised by Petrie et al. (2024) as potential challenging areas for seabed instalments.

This has important implications for the screening associated with CCS, where intact seals are important to keep the stored carbon trapped (e.g. Callow et al., 2021; Karstens & Berndt, 2015). The tunnel valleys can breach these seals during incision and/or are able to accumulate hydrocarbons and transport them along their tens of kilometres of longitudinal profiles (e.g. Lohrberg et al., 2020; Ottesen et al., 2020). The Hordaland group in this area is breached by salt diapirs and might also be incised by some of the deeper tunnel valleys. As the Hordaland group is rich with smectite, it is an effective seal (Løseth et al., 2003), and when broken, hydrocarbons may leak into the overlying structures, either along tunnel valleys and/or along the salt diapirs. The correlation to the proposed pockmarks from Petrie et al. (2024) further supports the importance of tunnel valley mapping in relation to hydrocarbon migration paths. Because of their deep incision depths and infill types, the older generations of tunnel valleys (Elsterian and Saalian) have the highest potential to have negative repercussions for CCS and marine installations that regard hydrocarbons.

The strata surrounding the tunnel valleys are likely composed of a variety of depositional environments, ranging from subglacial, glacial outwash, proglacial, and shallow marine (Cotterill et al., 2017 a). The third and fourth are potentially preserved inside some of the tunnel valleys of the deeper stratigraphy and in the very shallow section close to the seabed as remnants of the last deglaciation (Petrie et al., 2024). This can be due to the glacial history of the North Sea being characterised by large erosional events where ice sheets removed vast amounts of evidence from their preceding interglacials (Sejrup et al., 2005). Thus, it is plausible that areas of the North Sea where tunnel valleys are not the main facies include more subglacial and glacial outwash sediments as a substitute.

The sediments in the shallow subsurface where large ice sheets have passed are often glaciotectonized and highly heterogeneous because of overpressure and an oscillating ice front (Emery et al., 2019). Though areas with fewer tunnel valleys likely have fewer potential geohazards, these sites can still hold challenges for turbine foundations, such as those planned for the SNII offshore wind site, due to the presence of heterogeneous sediments with varying geotechnical properties (Petrie et al., 2024; Roy et al., 2023). Mapping the geology below the

foundation zone is relevant for regions with tunnel valleys, as there is evidence in this thesis suggesting they can impact seabed conditions in several ways. Most of the North Sea Plateau falls within this range. There are no tunnel valleys mapped within the Norwegian Channel (Ottesen et al., 2020), so offshore wind sites such as Utsira Nord do not need to account for them. Based on the previously mentioned interpretation for the extent of the LGM, areas south of the SNII site might be less complex and, by extension, less of a challenge for the planning and safety of marine infrastructure. Exceptions for this are areas like the Dogger Bank, where the shallow subsurface is extensively glaciotectonized (Emery et al., 2019).

## Chapter 9 Summary and conclusions

In this thesis, 45 tunnel valleys, with orientations ranging from NE-SW to NW-SE, lengths up to 41 km (full length restricted by data extent), widths up to 2.8 km, and incision depths up to ~400 m, have been mapped using 3D seismic data with the main aim of assigning them to distinct generations and placing them in the context of the North Sea glacial history. A combination of geomorphology analysis and cross-cutting relationships resulted in seven generations of tunnel valleys in the SNII site: G1 – five wide and deeply incising tunnel valleys oriented NE-SW with complex infill and ice-marginal fans spilling over the northern sections, with proposed Elsterian (MIS12) ages; G2 & G3 – six and five tunnel valleys with varied widths and lengths, deeply incising and oriented N-S with complex infill and a proposed Saalian (MIS10/8) age; G4 & G5 – three and 13 long and low sinuosity, and short and narrow tunnel valleys respectively, deeply incising and oriented NW-SE, with proposed Saalian (MIS 8/6) age; G6 – 12 narrow, short and shallow tunnel valleys with simple infill, oriented N-S and concentrated in southernmost section of SNII with a proposed Weichselian (MIS 4) age; G7 – two narrow paleo valleys with seabed relief, morphologically similar to tunnel valleys, orientation NW-SE with a proposed Weichselian (MIS 2, LGM) age. Definition of the different generations of tunnel valley formation are based on two separate methods: morphological analysis performed using machine learning to distinguish groups in the data; and cross-cutting relationships that divided the tunnel valleys into five levels of relative age.

The presence of a minimum of five (based solely on cross-cutting relationships) or seven (result when including geomorphology) tunnel valley generations in the shallow subsurface of the SNII sites indicates a complex and variable glacial history of the North Sea where up to four tunnel valley generations were created during the same glaciation. Large variations in the orientation of the ice fronts and a pattern indicating an increase in tunnel valley width, length, and infill complexity with age suggest that the North Sea ice sheets had varied retreat directions and differences in meltwater drainage patterns between advances. This is further supported by younger generations, which include more tunnel valleys than older generations. One can argue that the variability of the ice sheet dynamics along with the change in tunnel valley morphology indicates a relationship where tunnel valley size and density are dependent on their position in relation to the maximum extent of the ice sheet. This implies that the Elsterian tunnel valleys are longer and wider due to the maximum extent being much further south, and the opposite is true for the Weichselian tunnel valleys, which are narrow and short due to the LGM position

being close to the SNII site. A higher density of tunnel valleys is present at the SN2 site compared to the average of the North Sea Plateau, as the Quaternary sediments are thickest here, and the Pleistocene ice sheets coalesced here in the Central North Sea.

Analysis of 3D seismic data indicates three types of tunnel valley infill: Infill 1 – diamicton, gravels, or glacial till deposited in a subglacial environment; Infill 2 – layered sediments with alternating grain sizes deposited in a glaciolacustrine or glaciomarine environment; Infill 3 – two subtypes of dipping ‘clinoform’ structures: a smaller subtype interpreted as outwash sediments in an ice-marginal or proglacial environment, and a larger subtype deposited by glaciofluvial backfilling in an ice-marginal environment. Time-transgressive tunnel valley formation is supported by the environments of these infill facies, where Infill 1 is deposited during the erosion of the tunnel valley, the larger subtype of Infill 3 is deposited when the ice margin passes the tunnel valley, and Infill 2 and the smaller subtype of Infill 3 are deposited after the ice margin has passed and left some of the valley unfilled.

In addition to researching how tunnel valleys relate to the North Sea's glacial history and the significance of their infill geometries for tunnel valley formation, this thesis evaluates geohazards and seabed conditions relevant to marine installations. Partially filled paleo valleys, buried lake sediments, potentially unstable areas above salt diapirs, and the shoulders of large, buried tunnel valleys can all pose challenges when planning and executing safe and stable seabed installations in the SNII area.

A key finding is the coincidence of tunnel valleys and pockmarks where 84% of the mapped pockmarks in the SNII site lie above tunnel valleys. This indicates that tunnel valleys affect hydrocarbon migration by creating permeable conduits through otherwise low-permeable deposits. Complex tunnel valley networks cover most of the North Sea Plateau; thus, the knowledge from this thesis can be applied to future offshore wind sites where tunnel valleys are the main facies. Understanding of tunnel valleys increase in relevance as the effort to decarbonise the energy industry persists, due to their implications for not only the glacial history of the North Sea but additionally the safety and stability of marine installations and successful monitoring of CO<sub>2</sub> storage.

# Bibliography

- Anell, I., Thybo, H., & Rasmussen, E. (2012). A synthesis of Cenozoic sedimentation in the North Sea. *Basin Research*, 24(2), 154–179. <https://doi.org/10.1111/j.1365-2117.2011.00517.x>
- Batchelor, C. L., Margold, M., Krapp, M., Murton, D. K., Dalton, A. S., Gibbard, P. L., Stokes, C. R., Murton, J. B., & Manica, A. (2019). The configuration of Northern Hemisphere ice sheets through the Quaternary. *Nature Communications*, 10(1), 3713. <https://doi.org/10.1038/s41467-019-11601-2>
- Batchelor, C. L., Ottesen, D., & Dowdeswell, J. A. (2017). Quaternary evolution of the northern North Sea margin through glacial debris-flow and contourite deposition. *Journal of Quaternary Science*, 32(3), 416–426. <https://doi.org/10.1002/jqs.2934>
- Beets, D. J., Meijer, T., Beets, C. J., Cleveringa, P., Laban, C., & Van der Spek, A. J. F. (2005). Evidence for a Middle Pleistocene glaciation of MIS 8 age in the southern North Sea. *Quaternary International*, 133, 7–19.
- Bjørlykke, K. (2015). Mudrocks, Shales, Silica Deposits and Evaporites. In K. Bjørlykke (Ed.), *Petroleum Geoscience* (pp. 217–229). Springer Berlin Heidelberg. [https://doi.org/10.1007/978-3-642-34132-8\\_6](https://doi.org/10.1007/978-3-642-34132-8_6)
- Boulton, G., & Hagdorn, M. (2006). Glaciology of the British Isles Ice Sheet during the last glacial cycle: Form, flow, streams and lobes. *Quaternary Science Reviews*, 25(23–24), 3359–3390. <https://doi.org/10.1016/j.quascirev.2006.10.013>
- Boulton, G. S. (1986). Push-moraines and glacier-contact fans in marine and terrestrial environments. *Sedimentology*, 33(5), 677–698. <https://doi.org/10.1111/j.1365-3091.1986.tb01969.x>
- Boyd, R., Scott, D. B., & Douma, M. (1988). Glacial tunnel valleys and Quaternary history of the outer Scotian shelf. *Nature*, 333(6168), 61–64.
- Bradwell, T., Stoker, M. S., Golledge, N. R., Wilson, C. K., Merritt, J. W., Long, D., Everest, J. D., Hestvik, O. B., Stevenson, A. G., Hubbard, A. L., Finlayson, A. G., & Mathers, H. E. (2008). The northern sector of the last British Ice Sheet: Maximum extent and demise. *Earth-Science Reviews*, 88(3–4), 207–226. <https://doi.org/10.1016/j.earscirev.2008.01.008>
- Brown, E. J., Rose, J., Coope, R. G., & Lowe, J. J. (2007). An MIS 3 age organic deposit from Balglass Burn, central Scotland: Palaeoenvironmental significance and implications for the timing of the onset of the LGM ice sheet in the vicinity of the British Isles. *Journal of Quaternary Science*, 22(3), 295–308. <https://doi.org/10.1002/jqs.1028>
- Callow, B., Bull, J. M., Provenzano, G., Böttner, C., Birinci, H., Robinson, A. H., Henstock, T. J., Minshull, T. A., Bayrakci, G., Lichtschlag, A., Roche, B., Yilo, N., Gehrman, R., Karstens, J., Falcon-Suarez, I. H., & Berndt, C. (2021). Seismic chimney characterisation in the North Sea – Implications for pockmark formation and shallow gas migration. *Marine and Petroleum Geology*, 133, 105301. <https://doi.org/10.1016/j.marpetgeo.2021.105301>

- Cameron, T. D. J., Crosby, A., Balson, P. S., Jeffrey, D. H., Lott, G. K., & Bulat, J. (1992). *United Kingdom offshore regional report: The geology of the southern North Sea*. HMSO British Geological Survey.
- Cameron, T. D. J., Stoker, M. S., & Long, D. (1987). The history of Quaternary sedimentation in the UK sector of the North Sea Basin. *Journal of the Geological Society*, *144*(1), 43–58. <https://doi.org/10.1144/gsjgs.144.1.0043>
- Carr, S. J. (2004). The North Sea basin. In *Quaternary glaciations—extent and chronology: Part I: Europe* (pp. 261–270). Elsevier.
- Carr, S. J., Holmes, R., Van Der Meer, J. J. M., & Rose, J. (2006). The Last Glacial Maximum in the North Sea Basin: Micromorphological evidence of extensive glaciation. *Journal of Quaternary Science*, *21*(2), 131–153. <https://doi.org/10.1002/jqs.950>
- Carrivick, J. L., & Tweed, F. S. (2013). Proglacial lakes: Character, behaviour and geological importance. *Quaternary Science Reviews*, *78*, 34–52. <https://doi.org/10.1016/j.quascirev.2013.07.028>
- Cartelle, V., Barlow, N. L. M., Hodgson, D. M., Busschers, F. S., Cohen, K. M., Meijninger, B. M. L., & Van Kesteren, W. P. (2021). Sedimentary architecture and landforms of the late Saalian (MIS 6) ice sheet margin offshore of the Netherlands. *Earth Surface Dynamics*, *9*, 1399–1421.
- Clark, C. D., Hughes, A. L. C., Greenwood, S. L., Jordan, C., & Sejrup, H. P. (2012). Pattern and timing of retreat of the last British-Irish Ice Sheet. *Quaternary Science Reviews*, *44*, 112–146. <https://doi.org/10.1016/j.quascirev.2010.07.019>
- Clark, P. U., Archer, D., Pollard, D., Blum, J. D., Rial, J. A., Brovkin, V., Mix, A. C., Piasias, N. G., & Roy, M. (2006). The middle Pleistocene transition: Characteristics, mechanisms, and implications for long-term changes in atmospheric pCO<sub>2</sub>. *Quaternary Science Reviews*, *25*(23–24), 3150–3184. <https://doi.org/10.1016/j.quascirev.2006.07.008>
- Cotterill, C., Phillips, E., James, L., Forsberg, C. F., Tjelta, T. I., Carter, G., & Dove, D. (2017 a). The evolution of the Dogger Bank, North Sea: A complex history of terrestrial, glacial and marine environmental change. *Quaternary Science Reviews*, *171*, 136–153.
- Cotterill, C., Phillips, E., James, L., Forsberg, C., & Tjelta, T. I. (2017 b). How understanding past landscapes might inform present-day site investigations: A case study from Dogger Bank, southern central North Sea. *Near Surface Geophysics*, *15*(4), 403–414. <https://doi.org/10.3997/1873-0604.2017032>
- Davies, B. J. (2008). *British and Fennoscandian Ice-Sheet interactions during the quaternary*. Durham University.
- Davies, B. J., Roberts, D. H., Bridgland, D. R., Cofaigh, C. Ó., & Riding, J. B. (2011). Provenance and depositional environments of Quaternary sediments from the western North Sea Basin. *Journal of Quaternary Science*, *26*(1), 59–75. <https://doi.org/10.1002/jqs.1426>
- Davison, S. (2004). Reconstructing the last Pleistocene (Late Devensian) glaciation on the continental margin of Northwest Britain. *University of Edinburgh*.
- Deegan, C. E., & Scull, B. J. (1977). A standard lithostratigraphic nomenclature for the central and northern North Sea, in Institute of Geological Sciences Report. In *NPD Bulletin X*.

- DNV. (2023). *Energy transition Norway*. Det Norske Veritas.
- Doré, A. G. (1992). The Base Tertiary Surface of southern Norway and the northern North Sea. In *Norsk Geologisk Tidsskrift* (Vol. 72, pp. 259–256). [https://www.geologi.no/images/NJG\\_articles/NGT\\_72\\_3\\_Spec\\_Issue.pdf#page=41](https://www.geologi.no/images/NJG_articles/NGT_72_3_Spec_Issue.pdf#page=41)
- Dowdeswell, J. A., & Ottesen, D. (2013). Buried iceberg ploughmarks in the early Quaternary sediments of the central North Sea: A two-million year record of glacial influence from 3D seismic data. *Marine Geology*, 344, 1–9. <https://doi.org/10.1016/j.margeo.2013.06.019>
- Dürst Stucki, M., Reber, R., & Schlunegger, F. (2010). Subglacial tunnel valleys in the Alpine foreland: An example from Bern, Switzerland. *Swiss Journal of Geosciences*, 103, 363–374.
- Ehlers, J. (1990). Reconstructing the dynamics of the North-west European Pleistocene ice sheets. *Quaternary Science Reviews*, 9(1), 71–83. [https://doi.org/10.1016/0277-3791\(90\)90005-U](https://doi.org/10.1016/0277-3791(90)90005-U)
- Ehlers, J., & Gibbard, P. L. (2004). *Quaternary glaciations-extent and chronology: Part I: Europe*. Elsevier.
- Ehlers, J., Gibbard, P. L., & Hughes, P. D. (2018). Quaternary glaciations and chronology. In *Past glacial environments* (pp. 77–101). Elsevier.
- Ehlers, J., & Linke, G. (1989). The origin of deep buried channels of Elsterian age in Northwest Germany. *Journal of Quaternary Science*, 4(3), 255–265.
- Ehlers, J., & Wingfield, R. (1991). The extension of the Late Weichselian/Late Devensian ice sheets in the North Sea Basin. *Journal of Quaternary Science*, 6(4), 313–326. <https://doi.org/10.1002/jqs.3390060406>
- Eidvin, T., Jansen, E., Rundberg, Y., Brekke, H., & Grogan, P. (2000). The upper Cainozoic of the Norwegian continental shelf correlated with the deep sea record of the Norwegian Sea and the North Atlantic. *Marine and Petroleum Geology*, 17(5), 579–600. [https://doi.org/10.1016/S0264-8172\(00\)00008-8](https://doi.org/10.1016/S0264-8172(00)00008-8)
- Eidvin, T., & Rundberg, Y. (2001). Late Cainozoic stratigraphy of the Tampen area (Snorre and Visund fields) in the northern North Sea, with emphasis on the chronology of early Neogene sands. *Norwegian Journal of Geology/Norsk Geologisk Forening*, 81(2).
- Elverhøi, A., Hooke, R. LeB., & Solheim, A. (1998). Late Cenozoic erosion and sediment yield from the Svalbard–Barents Sea region: implications for understanding erosion of glacierized basins. *Quaternary Science Reviews*, 17(1–3), 209–241. [https://doi.org/10.1016/S0277-3791\(97\)00070-X](https://doi.org/10.1016/S0277-3791(97)00070-X)
- Emery, A. R., Hodgson, D. M., Barlow, N. L. M., Carrivick, J. L., Cotterill, C. J., & Phillips, E. (2019). Left High and Dry: Deglaciation of Dogger Bank, North Sea, Recorded in Proglacial Lake Evolution. *Frontiers in Earth Science*, 7, 234. <https://doi.org/10.3389/feart.2019.00234>
- Equinor. (2009). *Closer look at Peon*. <https://www.equinor.com/news/archive/2009/07/23/CloserLookAtPeon>



- Eschard, R., Abdallah, H., Braik, F., & Desaubliaux, G. (2005). The Lower Paleozoic succession in the Tassili outcrops, Algeria: Sedimentology and sequence stratigraphy. *First Break*, 23(10).
- Everest, J., Bradwell, T., & Golledge, N. (2005). Subglacial landforms of the Tweed Palaeo-Ice stream. *Scottish Geographical Journal*, 121(2), 163–173.
- Faleide, J. I., Bjørlykke, K., & Gabrielsen, R. H. (2015). Geology of the Norwegian Continental Shelf. In K. Bjørlykke (Ed.), *Petroleum Geoscience* (pp. 603–637). Springer Berlin Heidelberg. [https://doi.org/10.1007/978-3-642-34132-8\\_25](https://doi.org/10.1007/978-3-642-34132-8_25)
- Faleide, J. I., Kyrkjebø, R., Kjennerud, T., Gabrielsen, R. H., Jordt, H., Fanavoll, S., & Bjerke, M. D. (2002). Tectonic impact on sedimentary processes during Cenozoic evolution of the northern North Sea and surrounding areas. *Geological Society, London, Special Publications*, 196(1), 235–269. <https://doi.org/10.1144/GSL.SP.2002.196.01.14>
- Fichler, C., Henriksen, S., Rueslaatten, H., & Hovland, M. (2005). North Sea Quaternary morphology from seismic and magnetic data: Indications for gas hydrates during glaciation? *Petroleum Geoscience*, 11(4), 331–337.
- Frahm, L., Hübscher, C., Warwel, A., Preine, J., & Huster, H. (2020). Misinterpretation of velocity pull-ups caused by high-velocity infill of tunnel valleys in the southern Baltic Sea. *Near Surface Geophysics*, 18(6), 643–657. <https://doi.org/10.1002/nsg.12122>
- Galon, R. (1965). Some new problems concerning subglacial channels. *Geographia Polonica*, 6, 19–28.
- Gatliff, R. W., Richards, P. C., Smith, K., Graham, C. C., McCormac, M., & Smith, N. J. P. (1994). *United Kingdom Offshore Regional Report: The geology of the central North Sea* (Vol. 5). HMSO British Geological Survey.
- Ghienne, J. F., & Deynoux, M. (1998). Large-scale channel fill structures in Late Ordovician glacial deposits in Mauritania, western Sahara. *Sedimentary Geology*, 119(1–2), 141–159.
- Ghienne, J.-F., Le Heron, D. P., Moreau, J., Denis, M., & Deynoux, M. (2007). The Late Ordovician glacial sedimentary system of the North Gondwana platform. *Glacial Sedimentary Processes and Products*, 295–319.
- Golledge, N. R., Finlayson, A., Bradwell, T., & Everest, J. D. (2008). The last glaciation of shetland, north atlantic. *Geografiska Annaler: Series A, Physical Geography*, 90(1), 37–53. <https://doi.org/10.1111/j.1468-0459.2008.00332.x>
- Gottsche, C. (1897). Die tiefsten glacialablagerungen der gegend von Hamburg. *Vorläufige Mittheilung, Mittheilungen Der Geographischen Gesellschaft in Hamburg*, 13, 131–140.
- Graham, A., Lonergan, L., & Stoker, M. S. (2009). Seafloor glacial features reveal the extent and decay of the last British Ice Sheet, east of Scotland. *Journal of Quaternary Science*, 24(2), 117–138. <https://doi.org/10.1002/jqs.1218>
- Graham, A., Lonergan, L., & Stoker, M. (2007). Evidence for Late Pleistocene ice stream activity in the Witch Ground Basin, central North Sea, from 3D seismic reflection data. *Quaternary Science Reviews*, 26(5–6), 627–643. <https://doi.org/10.1016/j.quascirev.2006.11.004>

- Graham, A., Stoker, M. S., Lonergan, L., Bradwell, T., & Stewart, M. A. (2011). Chapter 21—The Pleistocene Glaciations of the North Sea Basin. In J. Ehlers, P. L. Gibbard, & P. D. Hughes (Eds.), *Developments in Quaternary Sciences* (Vol. 15, pp. 261–278). Elsevier. <https://doi.org/10.1016/B978-0-444-53447-7.00021-0>
- Hall, A. M., & Bent, A. J. A. (1990). The limits of the last British ice sheet in northern Scotland and the adjacent shelf. *Quaternary Newsletter*, 61, 2–12.
- Hammer, Ø., Planke, S., Hafeez, A., Hjelstuen, B. O., Faleide, J. I., & Kvalø, F. (2016). Agderia – a postglacial lost land in the southern Norwegian North Sea. *Norwegian Journal of Geology*, 96(1), 43–60. <https://doi.org/10.17850/njg96-1-05>
- Hirst, J. P. P., Benbakir, A., Payne, D. F., & Westlake, I. R. (2002). Tunnel valleys and density flow processes in the upper Ordovician glacial succession, Illizi Basin, Algeria: Influence on reservoir quality. *Journal of Petroleum Geology*, 25(3), 297–324.
- Hjelstuen, B. O., Nygård, A., Sejrup, H. P., & Hafliðason, H. (2012). Quaternary denudation of southern Fennoscandia – evidence from the marine realm. *Boreas*, 41(3), 379–390. <https://doi.org/10.1111/j.1502-3885.2011.00239.x>
- Hjelstuen, B. O., Sejrup, H. P., Valvik, E., & Becker, L. W. M. (2018). Evidence of an ice-dammed lake outburst in the North Sea during the last deglaciation. *Marine Geology*, 402, 118–130. <https://doi.org/10.1016/j.margeo.2017.11.021>
- Holmes, R. (1997). Quaternary stratigraphy: The offshore record. In *Reflections on the Ice Age in Scotland* (pp. 72–94). Scottish Natural Heritage.
- Hubbard, A., Bradwell, T., Golledge, N., Hall, A., Patton, H., Sugden, D., Cooper, R., & Stoker, M. (2009). Dynamic cycles, ice streams and their impact on the extent, chronology and deglaciation of the British–Irish ice sheet. *Quaternary Science Reviews*, 28(7–8), 758–776. <https://doi.org/10.1016/j.quascirev.2008.12.026>
- Huuse, M., & Lykke-Andersen, H. (2000). Overdeepened Quaternary valleys in the eastern Danish North Sea: Morphology and origin. *Quaternary Science Reviews*, 19, 1233–1253.
- Huuse, M., Lykke-Andersen, H., & Michelsen, O. (2001). Cenozoic evolution of the eastern Danish North Sea. *Marine Geology*, 177(3–4), 243–269. [https://doi.org/10.1016/S0025-3227\(01\)00168-2](https://doi.org/10.1016/S0025-3227(01)00168-2)
- Jackson, C. A.-L., & Stewart, S. A. (2017). Composition, Tectonics, and Hydrocarbon Significance of Zechstein Supergroup Salt on the United Kingdom and Norwegian Continental Shelves. In *Permo-Triassic Salt Provinces of Europe, North Africa and the Atlantic Margins* (pp. 175–201). Elsevier. <https://doi.org/10.1016/B978-0-12-809417-4.00009-4>
- Jentzsch, A. (1884). Über die Bildung der preussischen Seen. *Zeitschrift Der Deutschen Geologischen Gesellschaft*, 699–702.
- Johnson, H., Richards, P. C., Long, D., & Graham, C. C. (1993). *United Kingdom Offshore Regional Report: The geology of the northern North Sea*. HM Stationery Office.

- Jørgensen, F., & Sandersen, P. B. E. (2006). Buried and open tunnel valleys in Denmark—Erosion beneath multiple ice sheets. *Quaternary Science Reviews*, *25*(11–12), 1339–1363. <https://doi.org/10.1016/j.quascirev.2005.11.006>
- Karstens, J., & Berndt, C. (2015). Seismic chimneys in the Southern Viking Graben – Implications for palaeo fluid migration and overpressure evolution. *Earth and Planetary Science Letters*, *412*, 88–100. <https://doi.org/10.1016/j.epsl.2014.12.017>
- Kehew, A. E., Piotrowski, J. A., & Jørgensen, F. (2012). Tunnel valleys: Concepts and controversies — A review. *Earth-Science Reviews*, *113*(1–2), 33–58. <https://doi.org/10.1016/j.earscirev.2012.02.002>
- King, E. L. (2001). *A glacial origin for Sable Island: Ice and sea-level fluctuations from seismic stratigraphy on Sable Island Bank, Scotian Shelf, offshore Nova Scotia*. Natural Resources Canada, Geological Survey of Canada, 2001-D19, 18 p.
- Kirkham, J. D., Hogan, K. A., Larter, R. D., Games, K., Huuse, M., Stewart, M. A., Ottesen, D., Arnold, N. S., & Dowdeswell, J. A. (2021). Tunnel valley infill and genesis revealed by high-resolution 3-D seismic data. *Geology*, *49*(12). <https://doi.org/10.1130/G49048.1>
- Kirkham, J. D., Hogan, K. A., Larter, R. D., Self, E., Games, K., Huuse, M., Stewart, M. A., Ottesen, D., Le Heron, D. P., Lawrence, A., Kane, I., Arnold, N. S., & Dowdeswell, J. A. (2024). The infill of tunnel valleys in the central North Sea: Implications for sedimentary processes, geohazards, and ice-sheet dynamics. *Marine Geology*, *467*, 107185. <https://doi.org/10.1016/j.margeo.2023.107185>
- Kluiving, S. J., Aleid Bosch, J. H., Ebbing, J. H. J., Mesdag, C. S., & Westerhoff, R. S. (2003). Onshore and offshore seismic and lithostratigraphic analysis of a deeply incised Quaternary buried valley system in the Northern Netherlands. *Journal of Applied Geophysics*, *53*(4), 249–271. <https://doi.org/10.1016/j.jappgeo.2003.08.002>
- Kristensen, T. B., Huuse, M., Piotrowski, J. A., & Clausen, O. R. (2007). A morphometric analysis of tunnel valleys in the eastern North Sea based on 3D seismic data. *Journal of Quaternary Science: Published for the Quaternary Research Association*, *22*(8), 801–815.
- Kristensen, T. B., Piotrowski, J. A., Huuse, M., Clausen, O. R., & Hamberg, L. (2008). Time-transgressive tunnel valley formation indicated by infill sediment structure, North Sea – the role of glaciohydraulic supercooling. *Earth Surface Processes and Landforms*, *33*(4), 546–559. <https://doi.org/10.1002/esp.1668>
- Krohn, C. F., Larsen, N. K., Kronborg, C., Nielsen, O. B., & Knudsen, K. L. (2009). Litho- and chronostratigraphy of the Late Weichselian in Vendsyssel, northern Denmark, with special emphasis on tunnel-valley infill in relation to a receding ice margin. *Boreas*, *38*(4), 811–833.
- Kubala, M., Bastow, M., Thompson, S., Scotchman, I. C., & Øygard, K. (2003). Geothermal regime, petroleum generation and migration. In *The millennium atlas: Petroleum geology of the central and Northern North Sea*, 289–315. [https://www.researchgate.net/publication/313711828\\_Geothermal\\_regime\\_petroleum\\_generation\\_and\\_migration](https://www.researchgate.net/publication/313711828_Geothermal_regime_petroleum_generation_and_migration)

- Lamb, R. M., Harding, R., Huuse, M., Stewart, M., & Brocklehurst, S. H. (2018). The early Quaternary North Sea Basin. *Journal of the Geological Society*, *175*(2), 275–290. <https://doi.org/10.1144/jgs2017-057>
- Le Heron, D. P. (2007). Late Ordovician glacial record of the Anti-Atlas, Morocco. *Sedimentary Geology*, *201*(1–2), 93–110.
- Le Heron, D., Sutcliffe, O., Bourgig, K., Craig, J., Visentin, C., & Whittington, R. (2004). Sedimentary architecture of Upper Ordovician tunnel valleys, Gargaf Arch, Libya: Implications for the genesis of a hydrocarbon reservoir. *GeoArabia*, *9*(2), 137–160.
- Lee, J. R., Busschers, F. S., & Sejrup, H. P. (2012). Pre-Weichselian Quaternary glaciations of the British Isles, The Netherlands, Norway and adjacent marine areas south of 68°N: Implications for long-term ice sheet development in northern Europe. *Quaternary Science Reviews*, *44*, 213–228. <https://doi.org/10.1016/j.quascirev.2010.02.027>
- Lidmar-Bergström, K., Elvhage, C., & Ringberg, B. (1991). Landforms in Skåne, South Sweden: Preglacial and glacial landforms analysed from two relief maps. *Geografiska Annaler: Series A, Physical Geography*, *73*(2), 61–91.
- Livingstone, S. J., Ó Cofaigh, C., Evans, D. J. A., & Palmer, A. (2010). Sedimentary evidence for a major glacial oscillation and proglacial lake formation in the Solway Lowlands (Cumbria, UK) during Late Devensian deglaciation. *Boreas*, *39*(3), 505–527. <https://doi.org/10.1111/j.1502-3885.2010.00149.x>
- Lohrberg, A., Schwarzer, K., Unverricht, D., Omlin, A., & Krastel, S. (2020). Architecture of tunnel valleys in the southeastern North Sea: New insights from high-resolution seismic imaging. *Journal of Quaternary Science*, *35*(7), 892–906. <https://doi.org/10.1002/jqs.3244>
- Lonergan, L., Maidment, S. C. R., & Collier, J. S. (2006). Pleistocene subglacial tunnel valleys in the central North Sea basin: 3-D morphology and evolution. *Journal of Quaternary Science*, *21*(8), 891–903. <https://doi.org/10.1002/jqs.1015>
- Løseth, H., Nygård, A., Batchelor, C. L., & Fayzullaev, T. (2022). A regionally consistent 3D seismic-stratigraphic framework and age model for the Quaternary sediments of the northern North Sea. *Marine and Petroleum Geology*, *142*, 105766. <https://doi.org/10.1016/j.marpetgeo.2022.105766>
- Løseth, H., Wensaas, L., Arntsen, B., & Hovland, M. (2003). Gas and fluid injection triggering shallow mud mobilization in the Hordaland Group, North Sea. *Geological Society, London, Special Publications*, *216*(1), 139–157. <https://doi.org/10.1144/GSL.SP.2003.216.01.10>
- Lutz, R. K., Gaedicke, C., Reinhardt, L., & Winsemann, J. (2009). Pleistocene tunnel valleys in the German North Sea: Spatial distribution and morphology. *Zeitschrift Der Deutschen Gesellschaft Für Geowissenschaften*, *160*(3), 225–235. <https://doi.org/10.1127/1860-1804/2009/0160-0225>
- Madsen, V. (1921). Terrainformerne på Skovbjerg Bakkeø. *Danmarks Geologiske Undersøgelse IV. Række*, *1*(12), 1–24.

- Mangerud, J. (2004). Ice sheet limits in Norway and on the Norwegian continental shelf. In *Developments in Quaternary Sciences*, 2, 271–294. [https://doi.org/10.1016/S1571-0866\(04\)80078-2](https://doi.org/10.1016/S1571-0866(04)80078-2)
- Martin, C. J., Morley, A. L., & Griffiths, J. S. (2017). Chapter 1 Introduction to engineering geology and geomorphology of glaciated and periglaciated terrains. *Geological Society, London, Engineering Geology Special Publications*, 28(1), 1–30. <https://doi.org/10.1144/EGSP28.1>
- Mix, A. (2001). Environmental processes of the ice age: Land, oceans, glaciers (EPILOG). *Quaternary Science Reviews*, 20(4), 627–657. [https://doi.org/10.1016/S0277-3791\(00\)00145-1](https://doi.org/10.1016/S0277-3791(00)00145-1)
- Moreau, J., Ghienne, J.-F., Le Heron, D. P., Rubino, J.-L., & Deynoux, M. (2005). 440 Ma ice stream in North Africa. *Geology*, 33(9), 753–756.
- Moreau, J., Huuse, M., Janszen, A., Van Der Vegt, P., Gibbard, P. L., & Moscariello, A. (2012). The glaciogenic unconformity of the southern North Sea. *Geological Society, London, Special Publications*, 368(1), 99–110. <https://doi.org/10.1144/SP368.5>
- Moscariello, A. (1996). *Quaternary geology of the Geneva bay (Lake Geneva, Switzerland): Sedimentary record, palaeoenvironmental and palaeoclimatic reconstruction since the last glacial cycle*. Section des Sciences de la Terre, Université de Genève. <https://doi.org/10.13097/archive-ouverte/unige:97752>
- Moscariello, A., Azzouni, H., Hulver, M., Alain, J., & Rubino, J.-L. (2008). New insights on the sedimentology and stratigraphy of the glaciogenic Late Ordovician Sanamah Member, Wajid Sandstone Formation, southwest Saudi Arabia. *GEO 2008*, cp-246-00250. <https://doi.org/10.3997/2214-4609-pdb.246.253>
- Muzhingi, I. (2020). K-Means clustering made simple. *Oxford Protein Informatics Group*. <https://www.blopig.com/blog/2020/07/k-means-clustering-made-simple/>
- Norwegian Government. (2022, December 6). *Press Statement: Regjeringen går videre i sin satsing på havvind*. <https://www.regjeringen.no/no/aktuelt/regjeringen-gar-videre-i-sin-satsing-pa-havvind/id2949762/>
- Nygård, A., Sejrup, H. P., Haflidason, H., & Bryn, P. (2005). The glacial North Sea Fan, southern Norwegian Margin: Architecture and evolution from the upper continental slope to the deep-sea basin. *Marine and Petroleum Geology*, 22(1–2), 71–84. <https://doi.org/10.1016/j.marpetgeo.2004.12.001>
- Ottesen, D., Dowdeswell, J. A., & Bugge, T. (2014). Morphology, sedimentary infill and depositional environments of the Early Quaternary North Sea Basin (56°–62°N). *Marine and Petroleum Geology*, 56, 123–146. <https://doi.org/10.1016/j.marpetgeo.2014.04.007>
- Ottesen, D., Rise, L., Andersen, E. S., Bugge, T., & Eidvin, T. (2009). Geological evolution of the Norwegian continental shelf between 61°N and 68°N during the last 3 million years. In *Norwegian Journal of Geology*, 89, 251–265.

- Ottesen, D., Stewart, M., Brønner, M., & Batchelor, C. L. (2020). Tunnel valleys of the central and northern North Sea (56°N to 62°N): Distribution and characteristics. *Marine Geology*, 425, 106199. <https://doi.org/10.1016/j.margeo.2020.106199>
- Ottesen, D., Stokes, C. R., Bøe, R., Rise, L., Longva, O., Thorsnes, T., Olesen, O., Bugge, T., Lepland, A., & Hestvik, O. B. (2016). Landform assemblages and sedimentary processes along the Norwegian Channel Ice Stream. *Sedimentary Geology*, 338, 115–137. <https://doi.org/10.1016/j.sedgeo.2016.01.024>
- Patrino, S., Kombrink, H., & Archer, S. G. (2022). Cross-border stratigraphy of the Northern, Central and Southern North Sea: A comparative tectono-stratigraphic megasequence synthesis. *Geological Society, London, Special Publications*, 494(1), 13–83. <https://doi.org/10.1144/SP494-2020-228>
- Peck, V. L., Hall, I. R., Zahn, R., Elderfield, H., Grousset, F., Hemming, S. R., & Scourse, J. D. (2006). High resolution evidence for linkages between NW European ice sheet instability and Atlantic Meridional Overturning Circulation. *Earth and Planetary Science Letters*, 243(3–4), 476–488. <https://doi.org/10.1016/j.epsl.2005.12.023>
- Petrie, H. E., Eide, C. H., Hafliðason, H., Brendryen, J., & Watton, T. (2024). An integrated geological characterization of the Mid-Pleistocene to Holocene geology of the Sørliche Nordsjø II offshore wind site, southern North Sea. *Boreas*, 53(2), 186–226. <https://doi.org/10.1111/bor.12647>
- Piotrowski, J. A. (1994). Tunnel-valley formation in northwest Germany—Geology, mechanisms of formation and subglacial bed conditions for the Bornhöved tunnel valley. *Sedimentary Geology*, 89(1–2), 107–141.
- Praeg, D. (1996). *Morphology, stratigraphy and genesis of buried MidPleistocene tunnel valleys in the southern North Sea*. University of Edinburgh.
- Praeg, D. (2003). Seismic imaging of mid-Pleistocene tunnel-valleys in the North Sea Basin—High resolution from low frequencies. *Journal of Applied Geophysics*, 53(4), 273–298. <https://doi.org/10.1016/j.jappgeo.2003.08.001>
- Rappol, M., Haldorsen, S., Jørgensen, P., JM van der Meer, J., & MP Stoltenberg, H. (1989). Composition and origin of petrographically-stratified thick till in the northern Netherlands and a Saalian glaciation model for the North Sea basin. *Mededelingen van de Werkgroep Voor Tertiaire En Kwartaire Geologie*, 26(2), 31–64.
- Rea, B. R., Newton, A. M. W., Lamb, R. M., Harding, R., Bigg, G. R., Rose, P., Spagnolo, M., Huuse, M., Cater, J. M. L., Archer, S., Buckley, F., Halliyeva, M., Huuse, J., Cornwell, D. G., Brocklehurst, S. H., & Howell, J. A. (2018). Extensive marine-terminating ice sheets in Europe from 2.5 million years ago. *Science Advances*, 4(6), eaar8327. <https://doi.org/10.1126/sciadv.aar8327>
- Rise, L. (2004). Mid-Pleistocene ice drainage pattern in the Norwegian Channel imaged by 3D seismic. *Quaternary Science Reviews*, 23(23–24), 2323–2335. <https://doi.org/10.1016/j.quascirev.2004.04.005>

- Rise, L., & Rokoengen, K. (1984). Surficial sediments in the Norwegian sector of the North Sea between 60°30' and 62°N. *Marine Geology*, 58(3–4), 287–317. [https://doi.org/10.1016/0025-3227\(84\)90206-8](https://doi.org/10.1016/0025-3227(84)90206-8)
- Roy, S., Andrews, E. D., Fox, A., Michel, G., Mangal, J., Rezaeifar, M., Thusyanthan, I., & Trindade, L. (2023). Shallow Gas and Associated Seabed Features: A Primary Geohazard for Offshore Wind Installations. *NSG2023 1st Conference on Sub-Surface Characterisation for Offshore Wind, 2023*, 1–5. <https://doi.org/10.3997/2214-4609.202320126>
- Salomonsen, I. (1995). Origin of a deep buried valley system in Pleistocene deposits of the eastern central North Sea. *Danmarks Geologiske Undersøgelse Serie C*, 12, 7–19. <https://doi.org/10.34194/seriec.v12.7106>
- Salomonsen, I., & Jensen, K. A. (1994). Quaternary erosional surfaces in the Danish North Sea. *Boreas*, 23(3), 244–253. <https://doi.org/10.1111/j.1502-3885.1994.tb00946.x>
- Scourse, J. D., Ansari, M. H., Wingfield, R. T. R., Harland, R., & Balson, P. S. (1998). A Middle Pleistocene shallow marine interglacial sequence, Inner Silver Pit, southern North Sea: Pollen and dinoflagellate cyst stratigraphy and sea-level history. *Quaternary Science Reviews*, 17(9–10), 871–900.
- Scourse, J. D., Haapaniemi, A. I., Colmenero-Hidalgo, E., Peck, V. L., Hall, I. R., Austin, W. E. N., Knutz, P. C., & Zahn, R. (2009). Growth, dynamics and deglaciation of the last British–Irish ice sheet: The deep-sea ice-rafted detritus record. *Quaternary Science Reviews*, 28(27–28), 3066–3084. <https://doi.org/10.1016/j.quascirev.2009.08.009>
- Sejrup, H. P., Aarseth, I., Ellingsen, K. L., Reither, E., Jansen, E., Løvlie, R., Bent, A., Brigham-Grette, J., Larsen, E., & Stoker, M. (1987). Quaternary stratigraphy of the fladen area, central North Sea: A multidisciplinary study. *Journal of Quaternary Science*, 2(1), 35–58. <https://doi.org/10.1002/jqs.3390020105>
- Sejrup, H. P., Aarseth, I., Hafliðason, H., Løvlie, R., Bratten, Å., Tjøstheim, G., Forsberg, C. F., & Ellingsen, K. L. (1995). Quaternary of the Norwegian Channel: Glaciation history and palaeoceanography. *Norsk Geologisk Tidsskrift*, 75(2–3), 65–87.
- Sejrup, H. P., Clark, C. D., & Hjelstuen, B. O. (2016). Rapid ice sheet retreat triggered by ice stream debuttressing: Evidence from the North Sea. *The Geological Society of America*, 44(5), 355–358. <https://doi.org/10.1130/G37652.1>
- Sejrup, H. P., Hafliðason, H., Aarseth, I., King, E., Forsberg, C. F., Long, D., & Rokoengen, K. (1994). Late Weichselian glaciation history of the northern North Sea. *Boreas*, 23(1), 1–13. <https://doi.org/10.1111/j.1502-3885.1994.tb00581.x>
- Sejrup, H. P., Hjelstuen, B. O., Torbjørn Dahlgren, K. I., Hafliðason, H., Kuijpers, A., Nygård, A., Praeg, D., Stoker, M. S., & Vorren, T. O. (2005). Pleistocene glacial history of the NW European continental margin. *Marine and Petroleum Geology*, 22(9–10), 1111–1129. <https://doi.org/10.1016/j.marpetgeo.2004.09.007>
- Sejrup, H. P., King, E. L., Aarseth, I., Hafliðason, H., & Elverhøi, A. (1996). Quaternary erosion and depositional processes: Western Norwegian fjords, Norwegian Channel and North

- Sea Fan. *Geological Society, London, Special Publications*, 117(1), 187–202. <https://doi.org/10.1144/GSL.SP.1996.117.01.11>
- Sejrup, H. P., Larsen, E., Hafliðason, H., Berstad, I. M., Hjelstuen, B. O., Jonsdottir, H. E., King, E. L., Landvik, J., Longva, O., Nygård, A., Ottesen, D., Raunholm, S., Rise, L., & Stalsberg, K. (2003). Configuration, history and impact of the Norwegian Channel Ice Stream. *Boreas*, 32(1), 18–36. <https://doi.org/10.1080/03009480310001029>
- Sejrup, H. P., Larsen, E., Landvik, J., King, E. L., Hafliðason, H., & Nesje, A. (2000). Quaternary glaciations in southern Fennoscandia: Evidence from southwestern Norway and the northern North Sea region. *Quaternary Science Reviews*, 19(7), 667–685. [https://doi.org/10.1016/S0277-3791\(99\)00016-5](https://doi.org/10.1016/S0277-3791(99)00016-5)
- Sejrup, H. P., Nygård, A., Hall, A. M., & Hafliðason, H. (2009). Middle and Late Weichselian (Devensian) glaciation history of south-western Norway, North Sea and eastern UK. *Quaternary Science Reviews*, 28(3–4), 370–380. <https://doi.org/10.1016/j.quascirev.2008.10.019>
- Shackleton, N. J. (1969). The last interglacial in the marine and terrestrial records. *Proceedings of the Royal Society of London. Series B. Biological Sciences*, 174(1034), 135–154. <https://doi.org/10.1098/rspb.1969.0085>
- Shaw, J., Piper, D. J. W., Fader, G. B. J., King, E. L., Todd, B. J., Bell, T., Batterson, M. J., & Liverman, D. G. E. (2006). A conceptual model of the deglaciation of Atlantic Canada. *Quaternary Science Reviews*, 25(17–18), 2059–2081.
- Smith, L. N. (2004). Late Pleistocene stratigraphy and implications for deglaciation and subglacial processes of the Flathead Lobe of the Cordilleran Ice Sheet, Flathead Valley, Montana, USA. *Sedimentary Geology*, 165(3–4), 295–332.
- Stackebrandt, W. (2009). Subglacial channels of Northern Germany—a brief review. *Zeitschrift Der Deutschen Gesellschaft Fur Geowissenschaften*, 160(3), 203.
- Stewart, F. S. (1991). Reconstruction of the eastern margin of the late Weichselian Ice Sheet in northern Britain. *Annexe Thesis Digitisation Project 2016 Block 7*.
- Stewart, M. A. (2009). *3D seismic analysis of Pleistocene tunnel valleys in the Central North Sea*. Imperial College London (University of London).
- Stewart, M. A., & Lonergan, L. (2011). Seven glacial cycles in the middle-late Pleistocene of northwest Europe: Geomorphic evidence from buried tunnel valleys. *Geology*, 39(3), 283–286. <https://doi.org/10.1130/G31631.1>
- Stewart, M. A., Lonergan, L., & Hampson, G. (2013). 3D seismic analysis of buried tunnel valleys in the central North Sea: Morphology, cross-cutting generations and glacial history. *Quaternary Science Reviews*, 72, 1–17. <https://doi.org/10.1016/j.quascirev.2013.03.016>
- Stoker, M. S. (1995). The influence of glacial sedimentation on slope-apron development on the continental margin off Northwest Britain. *Geological Society, London, Special Publications*, 90(1), 159–177. <https://doi.org/10.1144/GSL.SP.1995.090.01.10>
- Stoker, M. S., Balson, P. S., Long, D., & Tappin, D. R. (2011). *An overview of the lithostratigraphical framework for the Quaternary deposits on the United Kingdom*



- continental shelf: British Geological Survey report RR/11/003*. British Geological Survey. 44pp.
- Stoker, M. S., & Bent, A. (1985). Middle Pleistocene glacial and glaciomarine sedimentation in the west central North Sea. *Boreas*, 14(4), 325–332. <https://doi.org/10.1111/j.1502-3885.1985.tb00920.x>
- Stoker, M. S., Hitchen, K., & Graham, C. C. (1993). *The geology of the Hebrides and West Shetland shelves, and adjacent deep-water areas*. HMSO.
- Stoker, M. S., & Holmes, R. (1991). Submarine end-moraines as indicators of Pleistocene ice-limits off northwest Britain. *Journal of the Geological Society*, 148(3), 431–434. <https://doi.org/10.1144/gsjgs.148.3.0431>
- Stoker, M. S., Leslie, A. B., Scott, W. D., Briden, J. C., Hine, N. M., Harland, R., Wilkinson, I. P., Evans, D., & Arduş, D. A. (1994). A record of late Cenozoic stratigraphy, sedimentation and climate change from the Hebrides Slope, NE Atlantic Ocean. *Journal of the Geological Society*, 151(2), 235–249. <https://doi.org/10.1144/gsjgs.151.2.0235>
- Stoker, M. S., Long, D., & Fyfe, J. A. (1985). *A revised Quaternary stratigraphy for the central North Sea*, 17(2), 35p.
- Toucanne, S., Zaragosi, S., Bourillet, J. F., Gibbard, P. L., Eynaud, F., Giraudeau, J., Turon, J. L., Cremer, M., Cortijo, E., Martinez, P., & Rossignol, L. (2009). A 1.2Ma record of glaciation and fluvial discharge from the West European Atlantic margin. *Quaternary Science Reviews*, 28(25–26), 2974–2981. <https://doi.org/10.1016/j.quascirev.2009.08.003>
- Underhill, J. R., & Richardson, N. (2022). Geological controls on petroleum plays and future opportunities in the North Sea Rift Super Basin. *AAPG Bulletin*, 106(3), 573–631. <https://doi.org/10.1306/07132120084>
- Ussing, N. V. (1903). *Om Jyllands hedesletter og teorierne for deres dannelse* (Vol. 2). Oversigt over det Kongelige Danske Videnskabernes Selskabs Forhandlinger.
- Van Der Vegt, P., Janszen, A., & Moscariello, A. (2012). Tunnel valleys: Current knowledge and future perspectives. *Glaciogenic Reservoirs and Hydrocarbon Systems*, 1(368), 75–97. <https://doi.org/10.1144/SP368.13>
- Wingfield, R. T. R. (1990). The origin of major incisions within the Pleistocene deposits of the North Sea. *Marine Geology*, 91(1–2), 31–52. [https://doi.org/10.1016/0025-3227\(90\)90131-3](https://doi.org/10.1016/0025-3227(90)90131-3)
- Wingfield, R. T. R. (1989). Glacial incisions indicating Middle and Upper Pleistocene ice limits off Britain. *Terra Nova*, 1(6), 538–548. <https://doi.org/10.1111/j.1365-3121.1989.tb00430.x>
- Woldstedt, P. (1922). Studien an Rinnen und Sanderflächen in Norddeutschland. *Zeitschrift Der Deutschen Geologischen Gesellschaft*, 130–133.
- Woodland, A. W. (1970). The buried tunnel-valleys of east Anglia. *Proceedings of the Yorkshire Geological Society*, 37(4), 521–578. <https://doi.org/10.1144/pygs.37.4.521>
- Worsley, D., Johansen, R., & Kristensen, S. E. (1988). The Mesozoic and Cenozoic succession of Tromsøflaket. In *NPD Bulletin*, 4, 65 pp.

- Yin, Q. Z., & Berger, A. (2010). Insolation and CO<sub>2</sub> contribution to the interglacial climate before and after the Mid-Brunhes Event. *Nature Geoscience*, 3(4), 243–246. <https://doi.org/10.1038/ngeo771>
- Ziegler, P. A. (1975). The Geological Evolution of the North Sea Area in the Tectonic Framework of North Western Europe. *Norges Geologiske Undersøkelse*, 316, 1–27.
- Ziegler, P. A. (1990). Collision related intra-plate compression deformations in Western and Central Europe. *Journal of Geodynamics*, 11(4), 357–388. [https://doi.org/10.1016/0264-3707\(90\)90017-O](https://doi.org/10.1016/0264-3707(90)90017-O)

# Appendices

## Appendix 1: K-means Clustering

### Step 1:

```
import pandas as pd
from sklearn.preprocessing import StandardScaler
import numpy as np
import matplotlib.pyplot as plt
from sklearn.cluster import KMeans
```

### Step 2:

```
excel_file = "Documents\MASTER\Masterprosjekt\Python\TV_stats.xlsx"
data = pd.read_excel(excel_file, sheet_name='Sheet2')
```

```
numerical_columns = ['Width', 'DepthVar', 'Direction', 'MaxDepth']
X = data[numerical_columns]
```

```
scaler = StandardScaler()
X_scaled = scaler.fit_transform(X)
```

### Step 3:

```
n_clusters = 5

kmeans = KMeans(n_clusters=n_clusters, random_state=42)
kmeans.fit(X_scaled)
```

```
data['Cluster'] = kmeans.labels_
```

### Step 4:

```
cluster_centers = scaler.inverse_transform(kmeans.cluster_centers_)
cluster_df = pd.DataFrame(cluster_centers, columns=numerical_columns)
print("Cluster Centers:")
print(cluster_df)
```

Step 5:

```
plt.figure(figsize=(12, 8))
for cluster_id in data['Cluster'].unique():
    cluster_data = data[data['Cluster'] == cluster_id]
    plt.scatter(cluster_data['MaxDepth'], cluster_data['Direction'], label=f'Cluster {cluster_id}')

    plt.scatter(267.357, 209.642, s=50, c='k', marker='o')
    plt.scatter(461.400, 222.000, s=50, c='k', marker='o')
    plt.scatter(453.400, 135.000, s=50, c='k', marker='o')
    plt.scatter(354.076, 163.615, s=50, c='k', marker='o')
    plt.scatter(254.444, 128.222, s=50, c='k', marker='o')

plt.xlabel('MaxDepth')
plt.ylabel('Direction')
plt.title('Clusters of Valleys')
plt.legend()

for i in range(len(data)):
    jitter = np.random.uniform(-1, 1) # Adjust the jitter range as needed
    plt.text(data['MaxDepth'].iloc[i] + jitter, data['Direction'].iloc[i] + jitter, data['TV'].iloc[i],
    fontsize=8)

plt.show()
```